MPHIL

The Interpretation of Fouling Data from a Stirred Batch Cell

Harris, Jonathan

Award date:
2014

Awarding institution:
University of Bath

The Interpretation of Fouling Data from a Stirred Batch Cell

Jonathan Simon Harris

A Thesis Submitted for the Degree of Master of Philosophy

University of Bath

Department of Chemical Engineering

October 2014

Abstract

This thesis is based upon work using the stirred batch cell fouling rig at the University of Bath to collect fouling data and investigate the fouling of calcium carbonate and of two crude oils. Research aims were to discover the conditions under which a single crude oil would foul, and to see whether a fouling deposit could be removed by increasing shear stresses exerted by the cylindrical stirrer in the rig. The key purpose of this research was to attempt to record a negative fouling rate and then interpolate between positive and negative fouling rates in order to find the conditions at which the fouling rate would be zero. In conducting the research, a number of issues presented themselves, providing noteworthy observations and new avenues of investigation. The first crude ('crude 19') would not foul in the rig, even when temperatures were raised to very high levels. The second crude ('crude 21') also initially would not foul, but did foul once a significant proportion of the light ends of the crude were flashed. Initial problems with crude 21 led to an investigation into heat transfer inside the rig with the oil, resulting in a number of findings that have been presented in this thesis. These include the observation that nucleate boiling was occurring in the rig, and the impacts of this finding have been discussed. Data was collected to measure the effect of wall temperature and stirrer speed on fouling rate for crude 21 and the activation energy was found using an Arrhenius plot. Five fouling removal tests were completed and the results were mixed, with some evidence for removal observed, but also several inconclusive results sets. It was, therefore, not possible to record a negative fouling rate and hence use the apparatus to predict the fouling threshold.

Acknowledgements

I extend my gratitude to my supervisor Professor B. Crittenden for his guidance and suggestions.

I thank both Dr M. Yang at the University of Bath and Dr A. Smith at the Heat Transfer Research, Inc. (HTRI) for their help and contribution of simulations to this thesis.

Additionally, thanks are due to HTRI for sponsoring my studies, providing the oils for this thesis and for all their advice, time and discussions.

I also express my appreciation to Dr H. Goodyear for her help with editing this thesis.

Lastly, I thank my wife for her love, support and help, and dedicate this thesis to her.

Contents

List of Figures

List of Tables

List of Acronyms

CH	Cartridge Heater
CFD	Computational Fluid Dynamics
ESDU	Engineering Sciences Data Unit
HTC	Heat Transfer Coefficient
HTRI	Heat Transfer Research, Inc.
NSO	Nitrogen, Sulfur, and Oxygen
RMM	Relative Molecular Mass
ST	Surface Temperature
TEMA	Tubular Exchanger Manufacturers Association

List of Nomenclature

Symbol	Description	SI Units
a	Dimensionless Constant	-
A	Heat Transfer Area	m^2
A_{III}	Dimensionless Group of Constants	-
b	Dimensionless Constant	-
B_{III}	Dimensionless Group of Constants	-
C'	Dimensionless Constant	-
C_f	Fanning Friction Factor	-
C_p	Specific Heat Capacity	J/kg°C
D	Agitator Cup Diameter	m
d_o	Outside Tube Diameter	m
d_i	Inside Pipe Diameter	m
F_t	Temperature Correction Factor	-
E_a	Activation Energy of the Crude Oil	J/mol
g	Acceleration Due to Gravity	m/s^2
G	Parameter Fitted to the Data	m^2K/J
h	Heat Transfer Coefficient	$W/m^{2}°C$
h_o	Outside Fluid Film Heat Transfer Coefficient	$W/m^{2}°C$
h_{od}	Shell Side Fouling Layer Heat Transfer Coefficient	$W/m^{2}°C$
h_{id}	Tube Side Fouling Layer Heat Transfer Coefficient	$W/m^{2}°C$
k	Thermal Conductivity	W/m°C
k_w	Thermal Conductivity of the Tube Wall Material	W/m°C
k_f	Foulant Thermal Conductivity	W/m°C
m	Mass Flow Rate	kg/h
N	Stirrer Speed	RPS
Pr	Prandtl Number	-
q	Heat Flux	W/m^2
Q	Heat Transfer	W
Re	Reynolds Number	-
R_f	Fouling Resistance	$m^{2}˚K/W$
t_1	Inlet Temperature of the Cold Stream	°C
t_2	Outlet Temperature of the Cold Stream	°C
t	Time	s
T_m	Log Mean Temperature Difference	°C
T_s	Tube Surface Temperature	°C
T_1	Inlet Temperature of the Hot Stream	°C
T_2	Outlet Temperature of the Hot Stream	°C
T_b	Bulk Temperature	°C
T_f	Film Temperature	°C

Symbol	Description	SI Units
T_w	Wall Temperature	°C
T_{wb}	Wall Temperature at Thermocouple *b*	°C
T_{wm}	Wall Temperature at Thermocouple *m*	°C
u	Fluid Velocity	m/s
U	Heat Transfer Coefficient	$W/m^2°C$
U_o	Overall Heat Transfer Coefficient of a Tube	$W/m^2°C$
α	Dimensionless Constant	-
β	Volumetric Expansion Coefficient	-
β'	Dimensionless Constant	-
η	Dynamic Viscosity	Pa/s
γ	Dimensionless Constant	-
μ	Fluid Viscosity	Ns/m^2
μ_w	Fluid Viscosity at the Wall	Ns/m^2
v	Kinematic Viscosity	m^2/s
ρ	Density	kg/m^3
τ	Shear Stress	Pa

CHAPTER 1

1 Introduction

1.1 Background and Context for Research

Heat exchanger fouling in the crude oil preheat train of distillation units on petroleum oil refineries is an issue that is under heavy scrutiny globally, with research being conducted on all aspects of its cause, effects and mitigation. Indeed, heat exchanger fouling is a huge problem experienced in chemical processes worldwide, estimated to cost as much as 0.25% of the gross national product of modern industrialised countries (Engineering Sciences Data Unit (ESDU), 2005). Heat exchanger fouling results in extra costs to a system in three different ways:

1. Additional operating costs to heat the fluids up to the required temperature; this could be the cost of extra steam in a heat exchanger, fuel in a furnace or the increased pressure drop across exchangers resulting in greater pump, and thus energy, usage.
2. Increased capital cost to pay for fouling prevention systems, new heat exchangers and resultant installation costs.
3. Loss of revenue caused by shutdown; if a plant needs to shut down or reduce output in order to replace or clean a heat exchanger then potential profit is being lost for every second it is not operating at usual capacity.

One of the most costly, and thus heavily investigated types of fouling, is the fouling by crude oil of the preheat train heat exchangers of a petroleum refinery. These are a set of exchangers that heat the crude oil feed to the atmospheric distillation column from ambient temperature to around 220°C. These exchangers are heated by waste energy from the product steams of the distillation column. A diagram of a typical preheat train is shown in Figure 1. When these exchangers become fouled their outlet temperature falls and the lost energy has to be made up by combusting costly natural gas in the furnace. The total worldwide cost of crude oil fouling of the preheat train alone was estimated to be as high as US$4.5 billion in 1995 (ESDU, 2005). It is, therefore, of paramount importance that the fouling caused by crude oil is understood as best as possible so that methods of mitigating it can be found.

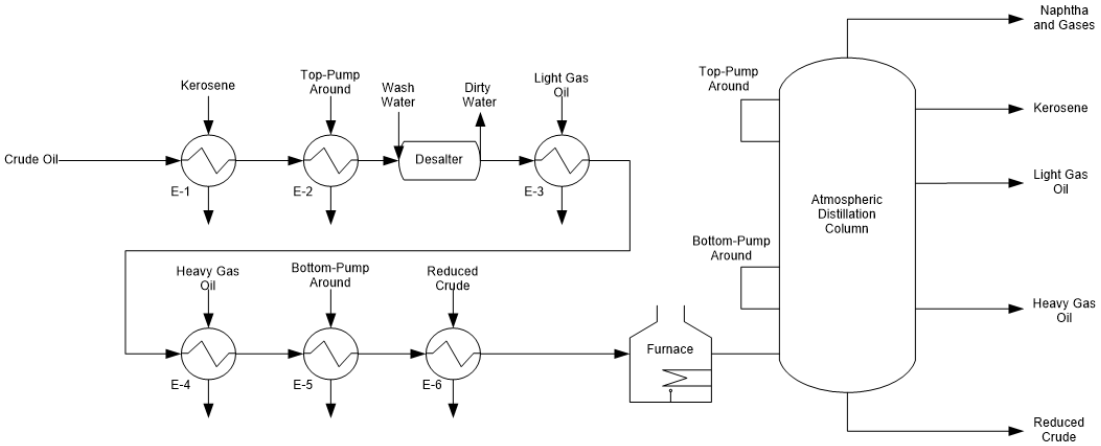

Figure 1: A typical crude oil distillation preheat train (Panchal and Huangfu, 2000)

Another problematic type of fouling is due to calcium carbonate crystallisation when fresh water is used to cool hot streams. Fouling of cooling water exchangers is costly because it causes production loss, increased pumping power requirements, frequent cleaning and maintenance, as well as extra capital costs due to oversizing exchangers or purchasing spares. These costs are a particular problem because cooling water exchangers are so commonplace in industry; they are often present in high numbers and large in size, causing costs associated with fouling to quickly mount up.

The fouling of heat exchangers is something that has been researched extensively over the past 50 years, but there is still much that is not fully understood about many of the different fouling types. This is because fouling is difficult to recreate in a laboratory environment as there are so many factors that can affect the fouling process and therefore working out which variables are important can be difficult. Additionally, fouling is typically a very slow process that is difficult to track as changes over even large periods of time are extremely small.

There are several key designs of fouling test rig that have been developed and used over the years, each recreating the desired fouling conditions in various ways:

- Tubular: the fouling fluid recirculates through tubes and fouls either a heated test section of the pipe, or an annular heater inserted inside the pipe (Bennett *et al.*, 2009).
- Modified autoclave: fluid flows over a heated annular test section held within a piece of tubing inside an autoclave reactor; fouling builds up on the annular heater (Kuru and Panchal, 1997).
- Stirred batch: fluid is rotated at high speeds in a stirred batch reactor around a heated finger on which fouling forms (Eaton and Lux, 1984).

The work conducted in this project uses the stirred batch reactor fouling rig at the University of Bath, built as a modification of the unit first designed and built by Eaton and Lux (1984), detailed by Young *et al.* (2009). The rig has been used to research a number of fouling topics since it was built including the characterisation of fouling deposits (Young *et al.*, 2009), the fouling induction period (Yang *et al.*, 2009), fouling thresholds (Yang *et al.*, 2011), and enhance surfaces (Yang *et al.*, 2013). The rig is capable of producing fouling deposits at a much quicker rate than alternatives such as the tubular fouling rigs – around 10 hours, versus several weeks for the latter. This is advantageous as it enables experimentation and research of varying conditions over a much shorter period of time. However, conditions in the rig are different to those in tubular rigs, both in terms of flow types and temperature. Moreover, whereas most rigs are designed to test either fresh water fouling or crude oil fouling, the University of Bath rig is capable of being used to investigate both.

1.2 Research Aims and Objectives

The aim of this thesis is to use the stirred batch cell fouling rig to find and investigate the fouling conditions for a crude oil. Initially the temperature and shear stress conditions required for a deposit to form are to be found, before measuring the effect of changing them on the fouling rate. The overall aim is to investigate the fouling threshold of the oil by seeing if it is possible to remove a fouling deposit by raising the stirrer speed and therefore the shear stress sufficiently so that a negative fouling rate can be measured. The threshold at which the fouling rate is zero is to be estimated by interpolating between positive and negative fouling rates.

The objectives of this study are:

- To carry out initial calcium carbonate fouling tests in order to get the rig up and running and to fix any rig problems.
- To find a wall temperature (T_w) under which the test crude oil will foul.
- To measure the fouling rate of the oil at various T_ws and stirrer speeds.
- To see if it is possible to raise the stirrer speed sufficiently to enable a negative fouling rate to be measured.
- To interpolate between positive and negative fouling rates to find the fouling threshold conditions.

1.3 Introduction Summary and Thesis Outline

This thesis investigates the problematic issue of fouling in crude oil preheat train exchangers, feeding into the atmospheric distillation columns of oil refineries. The research is conducted using the stirred batch cell fouling rig at the University of Bath and the key aim of the work is to use it to create fouling conditions for a crude oil, and then see if a fouling deposit can be removed if the shear stress forces are raised sufficiently. This research builds on, and furthers, the initial research into fouling removal first presented by Yang *et al.* (2011). The outline of this thesis is as follows: firstly, in Chapter 2, an extensive literature review is conducted, grounding this work in existing research and theories. In Chapter 3, the stirred batch cell is introduced, and how it has been utilised in the past, before the research methodology in outlined in Chapters 4 and 5. Findings are then presented, analysed and discussed in Chapters 6–9. Finally, conclusions and implications are given in Chapter 10.

CHAPTER 2

2 Literature Review

This chapter provides a review and evaluation of existing literature on fouling. It investigates all aspects of the different types of fouling, with particular emphasis on calcium carbonate and crude oil fouling. The fundamentals of heat transfer are additionally presented, so that the implications of fouling, and the ways in which fouling can be analysed are better understood. A full review of the different test rig designs used in fouling research is also undertaken. The chapter is then summarised.

2.1 Fundamentals of Heat Transfer

Heat exchangers are pieces of equipment that transfer heat from one process stream to another. The primary purpose of a heat exchanger is either to cool or heat a stream. This can be to vaporise a liquid, condense a gas or simply to utilise energy that would otherwise have been wasted. The most common types of heat exchangers are shell and tube, and plate and frame. Shell and tube exchangers function by flowing one process stream through tubes, and the other stream around the tubes (contained within a shell); heat is transferred through the tube walls. Plate and frame exchangers comprise of many layers of corrugated metal plates, forming chambers for the two fluids to flow through and transfer heat between.

The basic heat transfer equation is: [1]

$$Q = UA\Delta T_{lm}$$

(Sinnott *et al.*, 2005)

Where Q is the total heat transferred (W);

U is the overall heat transfer coefficient (HTC); this represents the heat that will be transferred between two different process streams per unit area and degree of temperature. This is dependent on both what the flow streams are (i.e. water, light oils, heavy oils) and the type of heat exchanger (W/m^2°C);

A is the heat transfer area, in the case of shell and tube heat exchangers this is the total surface area of the tubes (m^2);

T_{lm} is the log mean temperature difference and is a function of the inlet and outlet temperatures of the hot and cold streams (°C).

It is calculated from: [2]

$$\Delta T_{lm} = \frac{(T_1 - t_2) - (T_2 - t_1)}{ln\frac{(T_1 - t_2)}{(T_2 - t_1)}}$$

(Sinnott *et al.*, 2005)

Where T_1 is the inlet temperature of the hot stream (ºC);

T_2 is the outlet temperature of the hot stream (ºC);

t_1 is the inlet temperature of the cold stream (ºC);

t_2 is the outlet temperature of the cold stream (ºC).

Whilst rough estimations of the HTC of a heat exchanger can be made using the basic heat transfer equation, realistically it is dependent on many more factors than are accounted for in this equation. More accurate calculations of the HTC are based upon the principle that for heat to be transferred from a hot to a cold fluid in a heat exchanger, the heat must first travel through several heat resistant layers. There are five principal layers; these are shown in Figure 2.

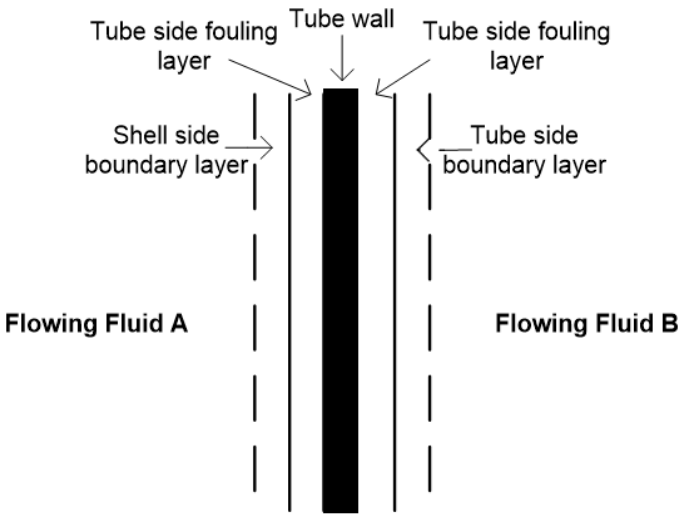

Figure 2: A diagram of the different heat transfer resistant boundary layers across a tube wall of a heat exchanger

Each of these layers resists heat transfer to different extents and depends on different factors:

- The boundary layer heat transfer terms are dependent on the hot and cold side fluid properties: their flow rate, temperature, viscosity, heat capacity, thermal conductivity and density.
- The fouling layer term is dependent on the heat transfer resistance of the foulant material.
- The tube wall term is dependent on the heat transfer resistance of the tube material.

The overall HTC for the tubes of a heat exchanger can be calculated using the formula below. Each of the terms in the equation represents one of the heat transfer layers explained above: [3]

$$\frac{1}{U_o} = \frac{1}{h_o} + \frac{1}{h_{od}} + \frac{d_o \ln(\frac{d_o}{d_i})}{2k_w} + \frac{d_o}{d_i}\frac{1}{h_{id}} + \frac{d_o}{d_i}\frac{1}{h_i}$$

(Sinnott *et al.*, 2005)

Where U_o is the overall HTC of a tube (W/m^2°C);

h_o is the outside fluid film HTC (W/m^2°C);

h_{od} is the shell side fouling layer HTC (W/m^2°C);

d_o is the outside tube diameter (m);

d_i is the pipe diameter (m);

k_w is the thermal conductivity of the tube wall, dependent on the material it is made from (W/m°C);

h_{id} is the tube side fouling layer HTC (W/m^2°C).

This more complex method of calculation enables the estimation of the HTC of an exchanger based upon the dimensions of its internals (such as tube diameter, pitch and material) and the exact properties of the liquid flowing through it.

2.2 Fouling of Heat Exchangers

Fouling is the deposition of solid material onto the heat transfer surface of a heat exchanger. This layer does not conduct heat well, so reduces the overall HTC of the surface it is on (Sinnott *et al.*, 2005). Over the lifespan of a heat exchanger, the gradual build-up of this fouling layer causes a continual reduction of the heat exchanger's HTC. This causes its effectiveness to drop, reducing its cold side outlet temperature and increasing its hot side outlet temperature over time (Müller-Steinhagen, 2000).

During the design of heat exchangers, the fouling that occurs with use is accounted for in the design equations, through the use of fouling factors, typically those by The Tubular Exchanger Manufacturers Association (TEMA) (Müller-Steinhagen, 2000). These factors mean that heat exchangers are typically oversized, and will have an excess heat transfer area. However, designing exchangers with an excess surface can sometimes make the problem worse, because it reduces the flow rate through the exchanger which often increases the deposition rate (ESDU, 2005).

2.3 Calculating Fouling Resistance

The fouling resistance build-up on a heat transfer surface can be measured as a change in its HTC.

R_f is therefore calculated as: [4]

$$R_f = \frac{1}{U_{t1}} - \frac{1}{U_{to}}$$

Where U_{t1} is the HTC at time 1 (W/m^2°C);

U_{t0} is the HTC at time 0 (W/m^2°C).

Substituting in the basic heat transfer equation this becomes: [5]

$$R_f = \frac{T_{st1} - T_b}{Q/A} - \frac{T_{st0} - T_b}{Q/A}$$

Where T_{st1} is the surface temperature (ST) at time 1 (°C);

T_b is the bulk temperature (°C);

T_{st0} is the ST at time 0 (°C).

However, as the T_b remains the same, the equation can be simplified to: [6]

$$R_f = \frac{T_{st1} - T_{st0}}{Q/A}$$

This is particularly useful as it gives the fouling resistance as a function of change in the ST.

2.4 Fouling Types

Fouling can be classified into several different types:

- Crystallisation fouling: where inorganic salts precipitate out of the fluid and deposit on the tube wall. This occurs when a degree of super saturation is reached, caused either by increasing the fluid temperature above the super saturation limit, or the salt concentration increasing above the solubility limit by evaporation (Hasson, 1981).
- Particulate fouling: where particulates that are suspended in the bulk fluid attach to the heat transfer surface. This can occur either by particulates settling out under gravity and sticking to the tube wall (sedimentation fouling) or diffusion to the surface by mass transport and attachment by electrostatic forces (Sheikholeslami and Watkinson, 2013). These particulates may already be present in the fluid, as products of chemical reactions in the fluid, crystals formed by super saturation, or corrosion products (Gudmundson, 1981).
- Chemical reaction fouling: where a chemical reaction occurs within the bulk fluid, the thermal boundary layer, or on the tube surface itself, depositing the products of the reaction on the tube wall (Garrett-Price *et al.*, 1985). The tube wall material is not involved in the reaction. This occurs when soluble precursors present in the fluid react to form an insoluble foulant. However, sometimes precursors may not initially be present in the fluid, but instead form in the heat exchanger from reactants within it. As either the reactants, precursors or foulant must get to the tube wall for fouling to occur, mass transport is a very important step in chemical reaction fouling (Watkinson and Wilson, 1997).
- Corrosion fouling: where the heat transfer surface reacts with the fluid, forming corrosion products such as iron sulfide on the surface (Somerscales, 1981). Often particles are formed from the corrosion reaction, which are transported downstream where they can cause particulate fouling (Epstein, 1983). There are often many different chemical reactions occurring side by side in corrosion fouling so it is often difficult to work out exactly what is causing it (Yépez, 2005).

- Biological fouling: there are two different types of biofouling: micro and macro. Microbiological fouling is the deposition and growth of microorganisms on the heat transfer surface. Macro biofouling is the attachment of macroorganisms such as clams or mussels (Pugh *et al.*, 2009). Microorganisms require a warm environment and nutrients in order to grow whereas macroorganisms typically require a layer of microorganisms to build up before they will attach (Charaklis, 1981).

Within a heat exchanger one or many of these types of fouling may be occurring at any time during operation, dependent on the nature of the fluid. Almost all fluids will cause at least some fouling within a heat exchanger but the extent of this fouling is governed by the process conditions. The conditions with the biggest effect on fouling propensity are the fluid velocity and the temperature (both bulk and surface) (Deshannavar *et al.*, 2010).

2.5 General Fouling Mechanisms

Epstein (1983) split the process of fouling into five distinct sub-processes or mechanisms:

- Initiation is the time period before fouling actually begins, and the fouling conditions established. Examples of things that may be happening here are the formation of crystal nucleation sites, the conditioning of the surface, or the formation of concentration, velocity or temperature gradients.
- Transport is where the reactant, fouling precursor or foulant particles or ions are transported from the bulk to the heat transfer surface.
- Attachment is where the foulant itself attaches to the heat transfer surface, by either van der Waals forces or electrostatic forces.
- Transformation is where the deposited foulant undergoes physical or chemical reactions, often referred to as ageing. An example of this is where organic foulant degrades to form coke, or inorganic crystal size decreases due to dehydration.
- Removal is where deposited foulant particles are removed and return back into the bulk fluid. This can be caused by erosion due to shear forces, dissolution, or chemical reaction. This is argued to be the least understood of all the mechanisms (Pugh *et al.*, 2009).

2.6 Crude Oil Fouling Mechanisms

Fouling in the crude preheat train of exchangers is the focus of this thesis, so it is this fouling that warrants discussion. There are four different types of fouling that occur in the preheat train: chemical fouling, inorganic fouling, corrosion fouling and particulate fouling (Wiehe, 2006). Each of these fouling types occurs to different extents in refineries, dependent on the crude oil being processed. Variance in crude type, where it was extracted from and by what method, affects the chemical and particulate content of the crude, which therefore affects its fouling potential (ESDU, 2005). An example of a heat exchanger fouled by crude oil can be seen in Figure 3.

Figure 3: Crude oil fouling on the tubes of a heat exchanger (MERUS Oil and Gas, 2013)

2.6.1 Chemical Reaction Fouling by Asphaltene Degradation

The most common cause of fouling in the crude oil preheat train is due to the degradation of the asphaltene molecules within the crude oil and their resultant deposition onto the tube walls. This is a form of chemical reaction fouling. The mechanism by which this occurs is described below.

Asphaltene molecules are a heavy fraction of crude oil, and are comprised of a variety of different components, predominantly polar aromatics, naphthenic aromatics, heteroatoms, and trace metals (Asomaning, 1997). Asphaltenes are defined as n-Pentane insoluble polar molecules. Within crude oil, asphaltenes generally occur in micellar form. In these micelles the asphaltenes are at the centre, and the outer layer surrounding them is made up of resins. Crude oil also contains paraffinic components; when these come into contact with the resinous shell of the micelle, they can cause the micelle to break apart and be removed. This process is called a destabilisation reaction and it causes the asphaltene molecules to come out of solution in the oil. The free asphaltene molecules then rapidly bond together with other asphaltenes to form agglomerations, because they are polar molecules.

This process is depicted below in Figure 4. The destabilisation reaction typically occurs in the bulk of the oil in the tubes (ESDU, 2005).

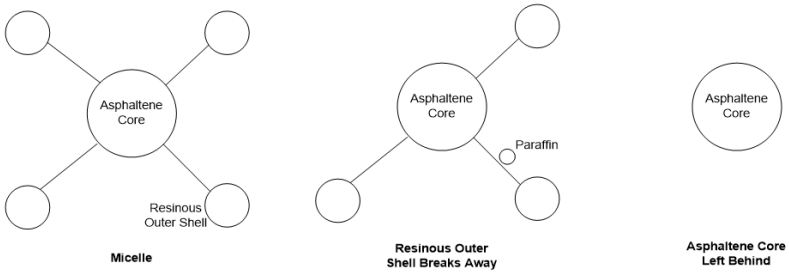

Figure 4: A diagram of the destabilisation of an asphaltene micelle (Wiehe, 2006)

After asphaltenes have agglomerated, they migrate towards the tube wall of the heat exchanger where they are eventually adsorbed by the tube metal surface. The asphaltenes are transported to the tube surface by diffusion, the rate of which is dependent on the

difference in concentration between the bulk and the surface (Epstein, 1983). Once adsorbed to the tube wall, asphaltenes degrade to a dehydrogenated, carbon build up. This chemical reaction fouling is dependent on the temperature of the heat transfer surface, with the rate of fouling having an Arrhenius type dependency on it: [7]

$$\frac{dR_f}{dt} = G \exp(\frac{-E_{act}}{RT_S})$$

(Crittenden *et al.*, 1992)

Where R_f is the fouling resistance (m^2°K/W);

t is the time (s);

T_s is the tube ST (°C);

G is a pre-exponential factor fitted to the data;

E_{act} is the activation energy of the crude oil (kJ/mol).

It is of note that both the rate of destabilisation of asphaltenes, as well as their rate of breakdown to carbon once bonded to the tube wall, are favoured in this way by temperature increase (Crittenden *et al.*, 1992). The degradation reaction can occur in either the boundary layer between the wall and the bulk fluid, or on the tube surface itself. Depending on where this reaction occurs, the activation energy is controlled by either the film temperature, or the wall ST (surface temperature) respectively (Asomaning, 1997).

2.6.2 Inorganic Fouling

Inorganic fouling of heat exchangers due to the presence of salt or hydrogen sulfide in the crude oil is the second most common form of fouling after that due to asphaltene (ESDU, 2005). As most crude oil comes from deposits or wells below the sea bed, small amounts of saltwater naturally mix in with the crude, either in the well itself, or during extraction. It is this salt that can foul the heat exchanger surfaces. This occurs when the water molecules in crude oil evaporate, leaving behind solid crystalline salt (ESDU, 2005; Wiehe, 2006).

Knowledge on the specifics of saline fouling and the exact mechanisms by which it occurs is limited and little is written about it in all sources found. This is because worldwide far more research has been done on organic fouling, which is perhaps because the inorganic content of feed crude oil is less controllable than the organic content (Wiehe, 2006).

Saline fouling occurs mostly in the exchangers before the desalter unit, which removes almost all of the salt. The exchangers downstream experience some slight saline fouling, though it is dwarfed by the asphaltene fouling. Inorganic fouling deposition has been found in investigations to grow at a linear rate in heat exchangers (Silva *et al.*, 2005).

2.6.3 Corrosion Fouling

Corrosion fouling is a prevalent form of fouling in the first two heat exchangers of the preheat train (Lemke, 1999). The fouling layer is made up of iron sulfide; the mechanism that leads to the formation of iron sulfide is as follows:

- Sulfur is released when aromatic sulfides in the crude break down during asphaltene fouling.
- The sulfur reacts in the bulk liquid to form hydrogen sulfide.
- This hydrogen sulfide then reacts with the iron in the tubes to form iron sulfide.

(ESDU, 2005).

The iron sulfide forms as a fouling layer on the pipes, the corrosion of the pipe wall also increases surface roughness, which makes it easier for other forms of fouling particulates to deposit (Wiehe, 2006). It is not well known how significantly this contributes to overall fouling corrosion compared to saline or asphaltene fouling, or how levels of corrosion vary in the different exchangers of the preheat train. However, in high temperature laboratory fouling tests such as the stirred batch cell, fouling deposits have been found to contain as much as 50% iron sulfide, suggesting that it plays a large part in overall fouling (Young *et al.*, 2009).

2.6.4 Particulate Fouling

Particulate fouling has been found to occur in the crude oil preheat train when insoluble suspended particulates that are sometimes present in crude oil either adhere to the tube walls, or settle out under gravity. Examples of such particulates are sand, precipitated asphaltenes, waxes and gums (Escobedo and Mansoori, 2010).

2.7 Factors Affecting Fouling

There are many factors that influence the rate of crude oil fouling deposition. Of these, the most important variables are the fluid velocity, the crude type (and mixing) and the ST of the tubes, though there are other things that can affect it such as tube roughness and material (Crittenden *et al.*, 1992).

2.7.1 Velocity

Increasing fluid velocity generally decreases the fouling rate. This is because firstly the HTC is increased, causing a reduction in the tube T_w, thereby reducing fouling. Secondly, the forces of the liquid flow shears off particulates from the tube wall, reducing its build-up (ESDU, 2005). It is important to note that in some cases an increase in flow velocity leads to an increase in the fouling rate. This occurs when the reactions that occur on the tube wall are mass transfer dependent; in this case a velocity increase raises the mass transfer rate and thus increases fouling rate. Crittenden *et al.* (2009) found that in these cases, whilst the fouling rate increases with velocity to a point, eventually the effect of shear will become

stronger than that of increased mass transfer, and the fouling rate will begin to decrease with further velocity increase. This behaviour was observed in both Maya Crude and fouling due to styrene polymerisation (Crittenden and Kolaczkowski, 1987).

2.7.2 T_w

The effect of T_w on the rate of fouling formation was explained in Chapter 2.6.1.

2.7.3 T_b

The T_b is also known to affect the formation rate of fouling deposits in the bulk fluid, but it is still not fully understood exactly how it affects fouling deposition rates. Storm *et al.* (1996) found that a drop in T_b can increase the fouling rate by increasing the temperature driving force. Asomaning (1997) meanwhile found that a drop in T_b can reduce fouling because the Reynolds number of the liquid is increased, which reduces the thickness of the thermal boundary layer and thus reaction rate. The effects of a variation in T_b is one of the biggest weaknesses in current knowledge of crude fouling. The reason for this is because in many models, the T_b is assumed to be constant. Realistically, however, there will be fluctuations in T_b as the crude flows through the many exchangers in the preheat train (Deshannavar *et al.*, 2010). More research is needed on this topic.

2.7.4 Crude Oil Instability

Whilst the destabilisation of asphaltene is generally driven by temperature, there are cases where asphaltenes can be fundamentally insoluble with the crude oil itself. In this case they will naturally precipitate out. This can also occur when different varieties of crude are mixed together (Wiehe, 2006). The oil incompatibility model is used to predict insolubility of asphaltenes based upon the heptane and toluene content of the crude oil (ESDU, 2005).

2.8 Calcium Carbonate Fouling

Fouling by calcium carbonate happens because it is an inverse solubility salt. Crystallisation fouling occurs by salt precipitation when a degree of super saturation is reached (Mwaba *et al.*, 2006). This is caused by increasing the temperature above the super saturation limit, or the salt concentration increasing above the solubility limit by evaporation (Pääkönen *et al.*, 2012). Super saturation caused by temperature often takes place because of a large difference between the temperature of the bulk fluid, and the heat transfer ST. This is often represented by the super saturation ratio, *S*, which is the ratio of the concentration in the bulk to the saturation concentration (Mullin, 2001).

Crystallisation fouling can only start to occur when nuclei, seeds or embryos are present. The induction phase of crystallisation fouling is where stable nuclei start to form and crystal growth begins which generally occurs on the heat transfer surface itself, though it can also occur in the bulk fluid (Zhao and Chen, 2013). Once these nuclei have been created on, or

adhered to the heat transfer surface they can start to grow, and the fouling layer will build up. As with most other types of fouling this fouling process can be mass transfer (diffusion) controlled, or (crystallisation) reaction controlled. The rate of mass transfer of ions to the heat transfer surface is dependent on the concentration driving force, which is represented by the following equation: [8]

$$\frac{dm}{dt} = k_d A(c - c_i)$$

(Zhao and Chen, 2013)

Where *m* is the mass deposited per unit area;

c is the concentration of ions in the bulk fluid;

c_i is the concentration of ions on the heat transfer surface;

k_d is a mass transfer coefficient.

The rate of [crystallisation] reaction represents the crystallisation process itself and can be described by the following equation: [9]

$$\frac{d_m}{d_t} = k_r A(c_i - c)^g$$

(Zhao and Chen, 2013)

Where k_r is the crystal growth rate constant;

g is an index that is dependent on the number of types of ions involved in the reaction (Konak, 1974).

2.9 Factors Affecting Calcium Carbonate Fouling

2.9.1 Heat Transfer ST

Crystallisation fouling increases with temperature, because super saturation is dependent on the temperature. Temperature increases both the heat transfer surface crystal precipitation, as well as the bulk fluid crystal precipitation. As with crude oil fouling, the rate of crystallisation has an Arrhenius dependency on temperature. Mass transfer coefficients in both the diffusion and reaction equations shown above increase linearly with temperature, increasing fouling (Krause, 1993).

Increasing the temperature of the heat transfer surface also has an effect on the crystal structure. Increased ST, usually caused by increased heat flux, creates smaller and harder to remove crystals (Bansal and Muller-Steinhagen, 1993). There are also several different forms (also called polymorphs) of calcium carbonate crystals: calcite, aragonite and vaterite (Wray and Daniels, 1957). Calcite is the most thermodynamically stable and often is formed at room temperature (Zhao and Chen, 2013). Vaterite, by comparison, is the least stable.

Aragonite will transform to calcite at raised temperatures (Sheikholeslami, 2000), whilst vaterite is metastable and readily transforms to calcite and aragonite. Calcite crystals are roughly hexagonal in shape, whereas aragonite crystals are sharp, needle like crystals. Finally, vaterite crystals are roughly spherical (Reeder, 1983). Calcium carbonate fouling is largely made up of calcite and aragonite crystals, with very little vaterite typically formed.

2.9.2 Velocity

As flow velocity through a heat exchanger is increased, the effect it has on the fouling rate changes. At low velocities the controlling fouling mechanism is mass transfer; thus increasing the velocity increases the fouling rate. Eventually, however, the effect of the shear forces caused by increased velocity, removing fouling particulates will become more prevalent than the increased mass transfer rate and it becomes reaction controlled. Therefore, the fouling rate will drop with further increase in velocity. In addition, at low velocities, ST has a significant effect on fouling, whilst at higher velocities, temperature has little effect (Pääkönen *et al.*, 2012).

Yang *et al.* (2002) performed some experiments to see if intermittently increasing the velocity through an exchanger could remove any fouling. They found that it was only possible to remove crystals during the induction phase when the crystals are weaker; thereby extending the induction phase. Consequently, it was not possible to remove any crystals once a foulant layer had built up (Yang *et al.*, 2002).

2.9.3 Bulk Precipitation

Pääkönen *et al.* (2012) found by conducting fouling experiments using filters that crystals formed in the bulk fluid strongly contribute to the fouling rate of the heat transfer surface. This happens by a mixture of these crystals providing a higher number of nucleation sites for crystals to form, as well as attaching to the surface itself (particulate fouling). Changing the T_b does not have a significant effect on the fouling rate, though Pääkönen *et al.* (2012) found that increasing it changed the bulk crystal deposition mechanism from crystallisation to particulate. This, they observed, slightly weakened the foulant layer, which they felt could be attributed to particulate foulant crystals being larger and less strongly bonded to the heat transfer surface.

2.9.4 pH

An increase in pH has been found to increase calcium carbonate fouling, by decreasing its solubility (Augustin and Bohnet, 2001). pH has also been found to impact the morphology of the crystals produced, with pHs of 10-12 favouring aragonite crystals, and pHs below this favouring calcite (Tai and Chen, 1998).

2.10 Fouling Models

A large proportion of the research into crude oil fouling in recent years has centred on mathematical modelling and prediction, each author adding their own variations to the previous models (Crittenden and Kolaczkowski, 1987; Ebert and Panchal, 1995; Polley *et al.*, 2002; Yeap *et al.*, 2004). This is because if fouling can be accurately predicted, based upon the operating conditions of exchangers, it can hopefully be mitigated by designing exchangers to operate at low, or zero fouling conditions.

One of the first attempts at modelling generic fouling of heat exchangers was done by Kern and Seaton (1959), based upon the key principle of:

Fouling Rate = Rate of Deposition – Rate of Removal

The various crude oil fouling models are fundamentally based upon this initial model, but represent the deposition and removal terms in varying ways. The key differences between them are the processes involved in fouling which they take into account. For example, some models just represent the reaction stage of fouling, whilst others include the mass transfer of foulant particles to the tube wall, as well as the reaction stage. It is important to note that most models are based upon single crude types and, therefore, the constants in their equations cannot be used to predict fouling by other crude varieties. Additionally, all of the fouling models currently published only represent chemical reaction fouling, and not any other type.

2.10.1 Early Models

The first general oil chemical reaction fouling model to be developed was that by Nelson (1934) who investigated fouling rate and the effect the thermal boundary layer and velocity has on it. Later, Crittenden and Kolaczkowski (1979) also attempted to model hydrocarbon fouling, representing both the mass transfer of fouling precursors to and from the tube wall, and the chemical reaction itself. This model was later modified so as to include a back diffusion term (Crittenden and Kolaczkowski, 1987). However, this was criticised by Epstein (1994) as he believed for back diffusion to be possible at time zero, a finite concentration of foulant would be required at the surface, which would be difficult to explain. Epstein (1994) thus developed a model of his own based upon the concept that the rate of chemical reaction fouling was dependent on the residence time of the foulant fluid at the surface. The greater the residence time, the greater the probability of a particle sticking due to the chemical reaction occurring. In the model, the main driving force for mass transfer of the foulant from the bulk to the surface was based upon the difference between the bulk and surface concentration. [10]

$$\frac{dR_f}{dt} = \frac{m\Phi}{k_f \rho_f}$$

Where R_f is the fouling resistance in the exchanger (m^2ºK/W);

t is the time (s);

φ is deposition mass flux (kg m^2/h);

m is the stoichiometric factor;

k_f is the foulant thermal conductivity (W/mºK);

ρ_f is the foulant density (kg/m^2).

[11]

$$\Phi = \frac{c_b}{\left(\frac{k' Sc^{\frac{2}{3}}}{u(j_f)^{\frac{1}{2}}}\right) + \left(\frac{k'' \rho u^2 j_f}{\mu \exp\left(\frac{-E}{RT_{so}}\right) C_s^{n-1}}\right)}$$

Where k' and k'' are constants;

c_b is the bulk concentration (kg/m^3);

c_s is the surface concentration (kg/m^3);

Sc is the Schmidt number;

j_f is the friction factor;

ρ is the fluid density (kg/m^3);

n is the order of reaction.

In this equation, the first part of the denominator ($m\varphi$) represents the mass transfer of the foulant; the second part ($k_f \rho_f$) represents the reaction and deposition of it. Whilst this model proved a very good fit to the styrene polymerisation chemical reaction fouling, it is not possible to apply it to crude oil fouling. This is because several of the terms in the equation, such as the attachment term order of reaction, are specific to styrene, but are not known for crude oil which is so chemically complex and varied (Crittenden *et al.*, 2009).

2.10.2 Threshold Models

Due to the complexity of the chemistry and interactions in crude oil chemical reaction fouling, there has been little advancement in the detailed modelling of it since Crittenden and Epstein's initial models (Bott *et al.*, 2001). In 1995, Ebert and Panchal proposed a new concept for predicting crude oil fouling called the fouling threshold model.

2.10.2.1 The Fouling Threshold

The key idea behind the fouling threshold is that fouling has typically been found to be most predominantly controlled by tube/film temperature and flow velocity. Ebert and Panchal (1997) concluded the following from analysing a set of coking data by Scarborough *et al.* (1979):

- Fouling will increase with film/tube temperature.
- Fouling will decrease as flow velocity is increased.

In particular, fouling will only begin once a threshold temperature has been exceeded, and that fouling will cease occurring once a high enough velocity is reached. These are the threshold conditions.

The Ebert and Panchal (1995) model assumes that the asphaltene degradation reaction (forming coke) is the primary cause of fouling and occurs in the thermal boundary layer (Deshannavar *et al.*, 2010). The first term in the equation represents the deposition of foulant by mass transfer (this represents the deposition term in the Kern and Seaton (1959) basic model of fouling). The model also assumes that the removal of foulant is caused by the shearing away of particles by the turbulent forces created by the bulk flow (Polley *et al.*, 2002). This is the removal term in the Kern and Seaton (1959) model. The equation of the model is: [12]

$$\frac{dR_f}{dt} = \alpha Re^{\beta'} \exp\left(-\frac{E}{RT_f}\right) - \gamma\tau_w$$

(Ebert and Panchal, 1995)

Where α, β' and γ are constants;

E is the activation energy (kJ/mol);

T_f is the film temperature (°C);

T_w is the shear stress (Pa).

Ebert and Panchal (1995) successfully fitted this model to Scarborough *et al.*'s (1979) data. Each of the dimensionless constants in the equation is specific to each crude and must be determined graphically when the model is used. This does, however, allow the model to be used to compare fouling propensity of different crudes (Wilson *et al.*, 2005).

The threshold concept and models, such as Ebert and Panchal, have generated considerable interest from both academics and industry, because it offers several key advantages:

- The left hand side of the equation can be set to zero in order to determine velocity and film temperatures at which fouling will not occur (Polley *et al*., 2002).
- It offers a more reliable method for designing exchangers compared to the traditional method of oversizing them using TEMA fouling factors (Wilson *et al.*, 2005), which have long been considered inaccurate.
- It enables a method by which heat exchanger networks could be better designed or retrofitted (Wilson *et al.*, 2005).

Ebert and Panchal (1997) later modified the initial model to include the Prandtl number so as to take into account crude oil thermal conductivity and specific heat. Later Panchal *et al*. (1999) and Asomaning *et al*. (2000) made estimations of the parameters in the equation using crude oil fouling data from a high pressure autoclave fouling unit giving:

[13]

$$\frac{dR_f}{dt} = \alpha Re^{\beta} Pr^{-0.33} \exp\left(-\frac{E}{RT_f}\right) - \gamma\tau_w$$

2.10.2.2 Polley et al.'s Model

Polley *et al.* (2002) were the next to modify the Ebert and Panchal (1995) model and made the following changes to it:

- The Reynolds number exponent in the equation was changed from -0.66 to -0.8 as they argued this is more applicable to the turbulent flow in heat exchanger tubes.
- The temperature used in the exponential term was changed to the T_w instead of the film temperature. They suggested this would give a better fit, as the method by which Ebert and Panchal (1995) estimated the film temperature was suspect.
- The shear stress term in the right hand side of the equation was replaced with $Re^{0.8}$. This they suggested would be better because when deposit formation has not yet occurred, the removal mechanism is more likely to be mass transfer driven as opposed to shear stress driven. A velocity term such as *Re* is therefore better at representing the mass transfer.

Polley *et al.* (2002) fitted this model to a set of fouling data published by Knudsen *et al.* (1999). Whilst they had to make many assumptions in estimating the physical properties of the crude oil in the data set, they found that the model both fitted the data well and predicted the threshold temperatures better than the Ebert and Panchal (1995) model could:

[14]

$$\frac{dR_f}{dt} = \alpha Re^{-0.8} Pr^{-0.33} \exp\left(-\frac{E}{RT_s}\right) - \gamma Re^{0.8}$$

Where T_s is the ST (°C).

2.10.2.3 Yeap et al.'s Model

In 2004, Yeap *et al.* modified Epstein's (1983) chemical reaction fouling model by adding a number of dimensionless parameters, as well as a suppression term to it in order to form a threshold model. Yeap *et al.* tried several suppression terms and found that by adding a mass transfer term, like Polley *et al.* (2002) had done, gave the best results.

The model also takes into account more velocity dependent process variables than the Ebert and Panchal (1995)/Polley *et al.* (2002) models and can therefore vary its velocity dependency by varying the B_{III} term. This enables situations whereby the fouling rate increases with velocity, such as those found by Crittenden and Kolaczkowski (1987), to be modelled. If, however, this is not the case the B_{III} term can be increased and the model will reduce to a similar form of Polley *et al.*'s (2002) model (Yeap *et al.*, 2004).

The modified Epstein (1983) model is: [15]

$$\frac{dR_f}{dt} = \frac{A_{III} C_f u T_s^{\frac{2}{3}} \rho^{\frac{2}{3}} \mu^{-\frac{4}{3}}}{1 + B_{III} u^3 \left(C_f^2\right) \rho^{\frac{5}{3}} \mu^{-\frac{7}{3}} T_s^{\frac{2}{3}} \exp\left(\frac{E}{RT_s}\right)} - C_{III} u^{0.8}$$

(Yeap *et al.*, 2004)

Where C_f is the Fanning friction factor;

A_{III} and B_{III} represents a group of constants;

μ is the dynamic viscosity (kg/m s);

u is the mean velocity (m/s);

C_{III} is a dimensionless constant.

Yeap *et al.* (2004) developed and tested the model using both the data used to develop the previous models (Scarborough *et al.*, 1979; Knudsen *et al.*, 1999; Panchal *et al.*, 2009) and some unpublished refinery data they obtained. They used this data to compare the new model with the Ebert and Panchal (1995) and Polley *et al.* (2002) models, and found the new model gave the best fit. Yeap *et al.* (2004) in agreement with Bories and Patreaux (2004) found that the fouling in exchangers operating at lower temperatures could not be accurately modelled by the Ebert and Panchal (1995) or Polley *et al.* (2002) models. They, however, found that the modified Epstein model provided significantly more accurate prediction of fouling under these conditions, though there was still significant error.

2.10.3 Deriving Constants in Models

As mentioned previously, each time a model is used, the constants in the equation must be recalculated to fit the data set. This procedure is done by non–linear regression, either graphically by curve fitting (Yang *et al.*, 2011) or computationally using software such as Sigma-Plot™ (Yeap *et al.*, 2004) or FOULING™ (Costa *et al.*, 2013). Indeed, great care should be taken when calculating these parameters, as poor estimation can produce very different, incorrect model fits even when the model itself is reasonable (Costa *et al.*, 2013).

2.10.4 Data Use in Models

It is of note that many of these models were developed using laboratory scale equipment to simulate the flow of oil through heated pipes, like in a heat exchanger. This is often done under enhanced conditions (i.e. higher temperatures than in a real preheat train), and with a recirculating flow of oil to speed up the process. These methods do not necessarily represent perfectly what actually occurs in real life pre-heat trains for a number of reasons:

- The composition of a recirculating flow of crude oil under high temperatures may vary over time.
- The fouling precursors may be used up over time.
- Corrosion products present in refineries may not be present.

- Different flow geometries are used compared to industrial preheat exchangers.
- Varying operating pressures compared to industry.

(Asomaning *et al.*, 2000; Deshannavar *et al.*, 2010).

However, these are all only opinions currently and very little research into these conclusions is currently available in public literature. Scrutiny should therefore always be applied when assessing models in the literature, or when applying any models to actual refinery exchangers.

2.10.5 Fitting Models to Refinery Data

There has been limited investigation into applying these models to real refinery data recently, so as to prove the accuracy and applicability of them. Some of these investigations are detailed below.

Bories and Patreaux (2004) investigated the change in heat transfer due to fouling of all the exchangers in the preheat train of a crude refinery over time. This was done by on-line measurement of the flows in and out of the exchangers over a period of 30 months, with readings taken once per day. Over this time the exchangers were cleaned three times. The HTC of each exchanger was calculated from the recorded data using the formula:

[16]

$$Q = UAF_t\Delta T_{LM}$$

Where F_t is the temperature correction factor.

The variation in the HTC over time was then used to track the fouling build-up using the typical fouling resistance calculation. The fouling levels recorded in the exchangers were then compared to the fouling predicted in the system by the Ebert and Panchal (1995) threshold model.

The results of this work concluded that whilst the fouling levels recorded were slightly under those predicted, they did fit the model well. It is also concluded that for the first few exchangers in the train, where very little fouling occurs (and the fouling is largely inorganic salt deposition), the model does not apply.

Asomaning *et al.* (2000) also attempted to apply the Ebert and Panchal (1995) threshold model to a set of refinery data they collected by installing ‘heating blocks’ to the inlet and outlet of a set of heat exchangers in a refinery. These monitored the heat flux, fluid and ST and the HTC. Conversely they found that the Ebert and Panchal (1995) model did not accurately predict the fouling occurring, and very few of their data points matched the model predictions.

In the testing of their new model Yeap *et al.* (2004) applied it to several sets of unpublished refinery data they obtained, though details of where they were from or what information they contained was not disclosed. They found that their model gave a good match to some of the data sets, but not to others. They attributed the likely cause of this to be the inevitable varying quality of the data.

2.11 Fouling Test Rigs

Laboratory scale equipment has been used extensively over the past 30 years to investigate fouling. In that time many different types of unit have been designed and used to test a variety of different types of fouling, under a wide range of operating conditions. The key advantages of laboratory scale fouling test rigs compared to on-line fouling investigation are:

- Precise operating conditions can be set and varied.
- Good access to fouling deposits is possible so that they can be inspected and tested.
- Heat transfer area shape and material can be varied in any way desired.
- Some designs allow fouling reduction devices such as HiTRAN inserts to be incorporated and used.
- They allow the fluid being tested to be analysed before and after use.
- They enable the composition of the test fluid to be controlled and varied.

(Young *et al.*, 2009).

The specific designs of fouling laboratory equipment vary greatly depending on the industrial situation they are trying to recreate; some are meant to recreate the conditions in a shell and tube heat exchanger, whilst others plate and frame. Varying operating condition requirements in order to produce fouling also adds to the differences between rigs. For example, crude oil fouling occurs at far higher temperatures and pressures than crystallisation fouling. The various different designs of fouling test rigs for crude oil and crystallisation are now detailed.

2.11.1 Crude Oil Fouling Rigs

2.11.1.1 Tubular-Externally Heated Test Section

Externally heated tubular fouling tests rig are designed to recreate the fouling in a single tube of a heat exchanger. They function by recirculating crude oil though a single pipe, with a similar diameter to that in a heat exchanger. In order to control and test fouling they have a small heated test section whereby the outside of the tube is heated to a temperature high enough to cause fouling over a specified length. The ST of the fouled area is measured by the insertion of thermocouples close to the tube surface. As fouling builds up on the heated test section, the ST recorded by the thermocouples will increase and therefore fouling can

be tracked. Examples of such equipment can be seen in Bennett *et al.* (2009) and Crittenden *et al.* (2009). In these two examples the rigs both had two heated test sections, enabling validation of the results by collecting two fouling rates at the same time. Test runs on tubular rigs typically take from a week to a month to form a significant, measurable fouling deposit. Externally heated tubular rigs can be operated at flow rates, turbulence structures, T_bs, STs, and heat fluxes of typical industrial heat exchangers (Crittenden *et al.*, 2009). However, a drawback of them is that it is difficult to reach the deposit for examination without cutting out a section of pipework (Bennett *et al.*, 2009; Crittenden *et al.*, 2009).

2.11.1.2 Tubular-Annular

Annular test rigs recirculate the crude oil inside a single tube, in a similar manner to the other type of tubular rig; however instead of the tube wall being heated, there is a heated fouling probe held inside the tube. As the crude flows over the probe, the flow pattern becomes annular. Fouling on the probe is monitored by thermocouples within it, close to the heat transfer surface. The most popular fouling probe that is used is the Heat Transfer Research, Inc. (HTRI) probe, which has a 101.6mm long heated section, with four thermocouples embedded 90° apart to measure the ST change on all sides of the probe (Saleh *et al.*, 2005; Srinivasan and Watkinson, 2005; Bennett *et al.*, 2009). Like the other type of tubular rig, they can be operated at similar temperatures, flow rates and pressures to industrial exchangers. However, the main criticism of them is that the flow geometry/pattern is different to a tube in an industrial exchanger and this may affect the applicability of results (Asomaning *et al.*, 2000).

2.11.1.3 Stirred Batch

The stirred batch cell fouling rig was first developed by Eaton and Lux (1984); they wanted to make a compact fouling device that could produce test runs in less than 48 hours. The unit consists of a vessel with a heated metal finger secured centrally to the bottom of it. Surrounding the finger is a downwards facing metal cup that rotates the crude around it. The idea is that the metal finger represents the heat transfer surface of a heat exchanger, and the rotating fluid represents the effect of crude flowing through one. The heated finger itself consisted of a metallic housing, with an electric heater held inside it and a thermocouple between the two to monitor fouling build up.

Later, Young *et al.* (2009) built an upgraded stirred batch cell, modifying the problems in the original design and its experimental methodology. Firstly, thermocouples were housed inside the metallic housing itself, so as to bring them closer to the heat transfer surface and gain more accurate readings. Secondly, in the original design, the shear forces caused by the rotation of the fluid were not estimated in any way. Therefore, a computational fluid dynamics package was used to estimate them (Yang *et al.*, 2009). Finally, fouling build up was estimated with an emphasis on the mass of the fouling deposit produced. However,

Young *et al.* (2009) concluded that this was not an appropriate method because the deposit is not uniform across the length of the heat transfer surface. Therefore, fouling rate dR_f/dt was used as the predominant fouling analysis, though Proscan 2000 optical scanning was also used to analyse the varying thickness of the deposit.

In the stirred batch cell rig, it is very easy to remove the heated finger after a fouling run and inspect/remove the fouling deposit compared to tubular rigs. In addition, crude oils being investigated can easily have their chemistry changed by adding things like asphaltenes or iron to see their effect on fouling (Yang *et al.*, 2009). The heat transfer surfaces' material and shape can be also changed to investigate their affect (Yang *et al.*, 2013). The biggest disadvantage is that the flow pattern is dramatically different to that inside a tubular heat exchanger, far more so than the other rig types.

2.11.1.4 Modified Autoclave

Kuru and Panchal (1997) developed a modified autoclave fouling unit at the Argonne National Laboratory. The aim was to make a portable fouling experiment, similar to that of Eaton and Lux (1984), but with a flow pattern more similar to that of a tubular heat exchanger. Their unit was essentially an autoclave, which had a vertically mounted tube fitted inside it, containing a 76.2mm heated test section, as well as an impeller in its upper section. Rotation of the impeller drove the crude oil up through the tube and across the test section. As with the other rigs, fouling was monitored using thermocouples housed within the test section. This unit type has the same problems as some of the others: it has potentially limited applicability due to the difference in flow geometry; especially as it is essentially an annular test rig, held inside a batch reactor.

2.11.2 Crystallisation Fouling Rigs

2.11.2.1 Plate Test Rigs

Several workers have produced rigs where a test fluid flows between heated metal plates in order to recreate the conditions of an industrial plate and frame exchanger. Pääkönen *et al.* (2012) flowed a test fluid though two 0.1m x 0.2m flat stainless steel plates held vertically 15mm apart from each other. The plates were heated electrically using Ohmic heaters to ensure constant heat flux. Fouling was monitored using thermocouples embedded in the heated metal surface. Andritsos and Karabelas (2003) used a small scale plate and frame heat exchanger containing only six plates to investigate the effect of particulates on fouling. They tracked the fouling process by monitoring the increase in pressure drop across the unit. These kinds of investigations are particularly useful as the plates can easily be dismantled and removed so that the fouling deposit can be inspected under the microscope in order to examine the crystal structures (Pääkönen *et al.*, 2012).

2.11.2.2 Tubular Rigs

Albert *et al.* (2011) investigated the crystallisation fouling of calcium sulphate in a test rig comprising of a tube held inside another tube, with the hot fluid on the inside, and cold cooling water on the outside. The change in the HTC and hence fouling of the whole unit was then tracked by monitoring the change in outlet temperatures. The fouling on the inside of the tubes was inspected using an endoscope. Hasan *et al.* (2012) looked into the effect of using turbulence generators to increase shear and reduce fouling. This was done by using a tank to flow a hot Na_2SO_4 solution in a channel across a tube containing a flow of cooling water. Na_2SO_4 fouling then built up on the outside of the pipe. The fouling rate was monitored using thermocouples embedded inside the pipe wall. In order to raise turbulence and shear, different shaped flow disrupters were held in place in front of the tube.

2.11.2.3 Stirred Batch

Young *et al.*'s (2009) stirred batch reactor rig described above has also been used to carry out crystallisation fouling experiments. The test fluid is simply changed to solutions of Ca_2SO_4 or $CaCO_3$ and the unit operated at lower temperatures and pressures (Yang *et al.*, 2013).

2.12 Fouling Mitigation

There are a variety of ways that fouling levels can be reduced in the crude heat exchangers. Below, the key methods and ideas are explained.

2.12.1 Mitigation by Process Control

Fouling build-up is controlled by the fluid velocity and the ST of the tubes. These can be manipulated to reduce fouling. One way this can be achieved is to monitor velocity through the exchangers to ensure it does not decrease over time (Yeap *et al.*, 2004).

2.12.2 Mitigation by Inserts

Many fouling mitigation technologies function by inserting long metal shapes inside the tubes themselves. When crude flows through the tubes and therefore the inserts, turbulence is increased, reducing fouling. Some inserts also move by the force of the crude flow, causing abrasion of the fouling deposit. The three main technologies available are SPIRELF, TURBOTAL and HiTRAN inserts (ESDU, 2005).

2.12.2.1 HiTRAN

HiTRAN inserts are a flexible matrix of wire loops held together by a core. They are made with a diameter slightly larger than the tube it is inserted into, so that the loops are compression fitted and always in contact with the tube walls. When crude flows through HiTRAN inserts they create a greater amount of mixing and turbulence around the tube wall compared to a plain tube, which should reduce fouling (ESDU, 2005).

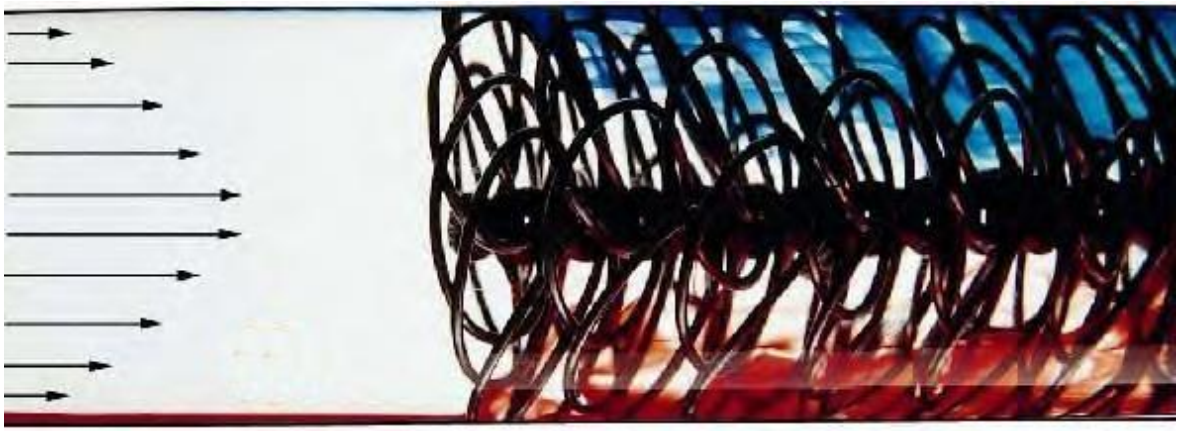

Figure 5: A HiTRAN insert inside a tube (ESDU, 2005)

Their effectiveness in the removal of crude fouling is discussed in the literature, with debate as to when and whether they should be used. Crittenden *et al.* (1993) found them to remove fouling through a combination of reducing the T_w and increasing the shear stress around the tube wall. Ritchie *et al.* (2009) concluded that they can reduce the fouling caused by both salt sedimentation and asphaltene deposition effectively. Petitjean *et al.* (2007) comparatively found that whilst HiTRAN inserts were effective at removing sedimentation fouling in the first few heat exchangers, they were not effective at removing asphaltene fouling in the higher temperature heat exchangers. Petitjean *et al.* also found that in the higher temperature heat exchangers, where fouling is almost entirely from asphaltene deposition, HiTRAN inserts tended to fuse with the foulant on the tube walls. Finally they concluded that their effectiveness is dependent on the Reynolds number of the fluid, and that they are only effective below a Reynolds number of 4000. ESDU (2005) are in agreement that HiTRAN inserts are not useful for removing asphaltene build-ups.

2.12.2.2 SPIRELF

SPIRELF inserts are long helical coils that are fitted within the tubes and secured at either end. The flow of crude causes them to move around, scouring fouling deposits. The use of SPIRELF has been found to increase the lifespan of heat exchangers by 2-3 times before they must be cleaned (Müller-Steinhagen, 2000; ESDU, 2005). They are the most effective at reducing asphaltene fouling (Petitjean *et al*., 2007).

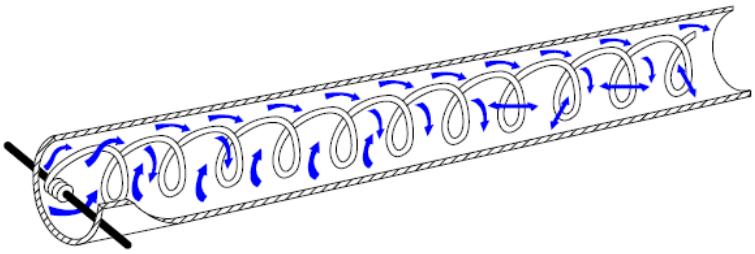

Figure 6: A SPIRELF insert inside a tube (ESDU, 2005)

2.12.2.3 TURBOTAL

TURBOTAL inserts are very similar to the SPIRELF helical coils, except that they have the freedom to rotate within the tubes, enhancing abrasive contact with the tube wall (ESDU 2005). Experimental investigation has found that their use reduces the overall drop in the HTC of an exchanger by around 20% over its lifespan (Bories and Patreaux, 2004).

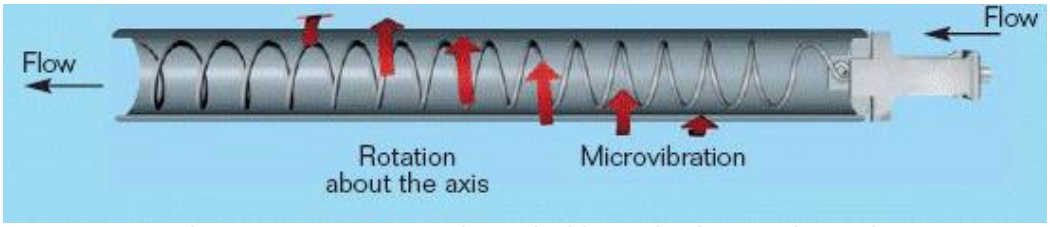

Figure 7: A TURBOTAL insert inside a tube (Petroval, 2013)

There is the possibility with all these technologies that they could break loose and cause an obstruction in the tubes (EDSU, 2005). Inserts also increase the pressure drop across the heat exchanger, meaning more energy must be used in pumping the liquid through to prevent a drop in crude oil flow rate. A reduction in flow rate can be costly because it reduces the quantity of product produced by the refinery per hour (Petitjean *et al.*, 2007). Whilst these inserts all sound beneficial, it is possible that their installation cost will outweigh any savings from reduced energy loss. Therefore, the economics of their installation should always be considered first.

2.12.3 Chemical Mitigation

There are many antifouling chemicals that can be added to crude oil to reduce its fouling potential. These chemicals (called asphaltene dispersants) function by replacing the resinous shell of the asphaltene micelles once they are destabilised. This protective layer prevents the asphaltenes from attracting each other and agglomerating. If the asphaltenes are prevented from agglomerating, they are much less likely to deposit on the tube walls (ESDU, 2005). These asphaltene dispersing chemicals can be expensive to use, and there is always a risk that they will not work for certain process conditions. Thus the potential benefits and costs must be always be weighed up before use.

2.13 Literature Review Summary

This literature review has shown that the fouling of heat exchangers with calcium carbonate and sulfate when using water as a cooling fluid has been a particularly problematic and costly issue in industry for many years. It has, therefore, received a lot of attention worldwide. Whilst in comparison to crude oil fouling, calcium carbonate fouling mechanisms and causes are far better understood, research into its prevention still continues as the problem persists (Zhao and Chen, 2013). The reason for this is that calcium carbonate fouling can be particularly complex in that its deposition mechanism changes with increasing velocity. At low velocities deposition is mass transfer controlled, whilst at higher

velocities reaction control becomes dominant (Pääkönen *et al.*, 2012). Thus increasing velocity can both increase and decrease the fouling rate. Finding the optimal flow conditions for water of varying compositions using a variety of different experimental rigs has hence been vital in attempts to mitigate the effects of calcium carbonate fouling (Albert *et al.,* 2011; Pääkönen *et al.,* 2012).

The focus of this chapter has, however, been on crude oil fouling. This literature review has illustrated that, due to the severity of the financial costs associated with fouling in the crude preheat train, much research has been conducted over the last three decades. Early research focussed on finding the key causes of crude oil fouling. Researchers including Epstein (1983), Crittenden *et al.* (1992) and Asomaning (1997) helped to discover the key role of chemical reaction fouling though the deposition of asphaltenes on heat exchanger tube walls. Subsequent research presented the importance that corrosion fouling, due to the presence of sulfur in crude oil, has on the deposition of iron sulfide particles in heat exchangers. Additionally, corrosion fouling was shown to have a significant impact by roughening tube walls, thereby increasing the chances of other particles sticking (Wiehe, 2006). Lastly, research concluded that inorganic fouling, due to the presence of brine salts in crude oil, was the third major contributor to fouling in the crude oil preheat train exchangers, especially in those upstream of the desalter (Lemke, 1999).

The temperature of heat exchanger tube walls and the velocity of the crude oil flowing through them have been found to have the largest effect on the rate of fouling (Crittenden *et al.*, 1992). Temperature affects the fouling rate through its influence on the chemical reactions that occur in the bulk fluid and near the tube walls; fluid velocity influences it through the effects of the shear forces created by fluid flow reducing, and even preventing the deposition of foulant particles. Research into the effects of temperature and velocity led to the development of the threshold concept by Ebert and Panchal (1995). The threshold concept suggests that all oils have a threshold temperature, above which fouling will start occurring, as well as a threshold velocity, above which fouling will stop occurring. Following this discovery, much research has been conducted into finding the threshold conditions for different crude oils so that refineries can gain a greater understanding of conditions in which crude oils are likely to be problematic in their heat exchangers (Polley *et al.,* 2002; Nasr and Givi, 2006; Yang *et al.*, 2011)**.**

A large proportion of the research into crude oil fouling has been performed using small scale test rigs. These rigs vary widely in design, size and the way they recreate fouling conditions. There are three main designs: (1) tubular rigs, which recirculate crude through a closed loop single pipe (Bennett *et al.*, 2009); (2) modified autoclave, which forces crude over an annular test section held in a small tube inside an autoclave (Kuru and Panchal, 1997); and (3) the stirred batch cell rig, which spins crude at high speeds around a heated

metal finger inside a stirred batch reactor vessel (Young *et al*., 2009). All these rigs have their own limitations, but can be used to investigate a wide variety of fouling research topics which is not possible with the actual exchangers in the preheat train.

Whilst this literature review has demonstrated that much is understood about the problem of crude fouling of the preheat train, there is still a lot that is not understood. Therefore, there are new methodologies and ideas of how the problem can be tackled being created every year. Yang ***et al.'s*** (2011) research which used the stirred batch cell rig at the University of Bath was the first time a negative fouling rate for the removal of fouling had been recorded. This finding generated much interest from the fouling community due to its potential to reduce the effect and costs of fouling if the same could be observed in full scale heat exchangers. It is for these reasons that this discovery will be further tested and investigated in this research. There is still much to be learned from the concept of interpolating between positive and negative rates to find fouling thresholds – a method that has not yet been investigated. Consequently, no comparison between the accuracy of thresholds estimated by extrapolation of fouling data, and those estimated by the interpolation of positive and negative fouling rates, has currently been presented. This is the key aim of this thesis, which builds upon previous work and also adds new understandings to the concept of fouling thresholds, using a stirred batch cell rig to generate fouling data and fouling removal conditions. In the next chapter, further details of the design of the stirred batch cell fouling rig and a summary of methodologies developed are presented. A full explanation is also given of how the rig was operated in this research to obtain fouling data for both calcium carbonate and crude oil fouling.

CHAPTER 3

3 Experimental Methods

Since the stirred batch reactor at the University of Bath was first commissioned in 2007, a number of papers have been published about its use. This chapter summaries these papers so as to give a full explanation of the research capabilities of the rig, key information about it, the different methodologies that have been developed using it, and test rig findings.

3.1 Summary of Previous Work Using the Stirred Batch Reactor Rig

3.1.1 Initial Design

Details of the improvements that were made to the design of the rig compared to Eaton and Lux's original design (1983, 1984) were explained in Chapter 2.11.1.3. An explanation of how the rig functions is now given.

The main body of the rig itself is made from a 304 stainless steel block machined into a 1 litre capacity vessel with an 18mm thick top flange which is held in place by 12 bolts. The test rig is made up of several key parts; these are shown and labelled in a cross sectional diagram of the rig (Figure 8).

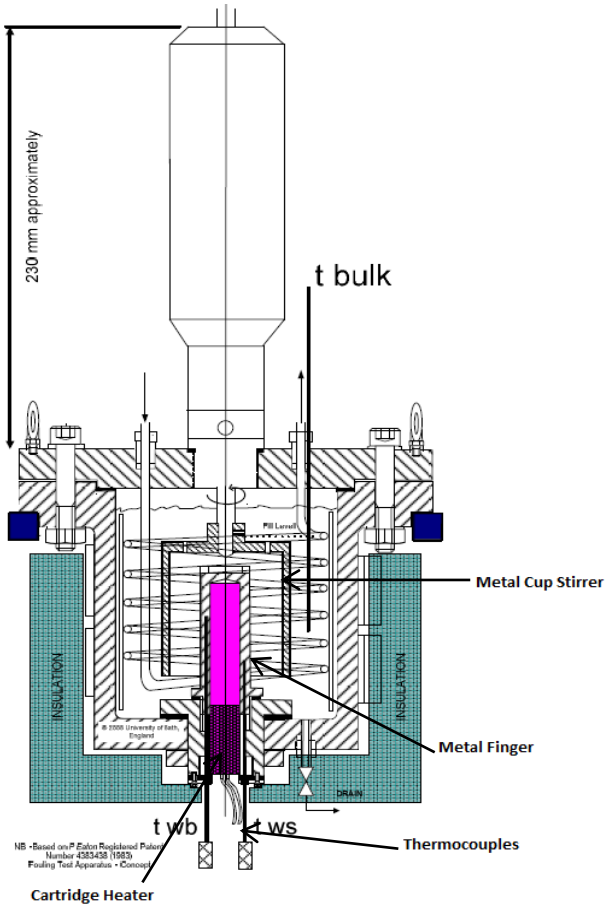

Figure 8: A cross section of the stirred batch reactor fouling rig (Young et al., 2009)

The two main variables in controlling fouling formation are the T_w and the shear stress exerted on the wall by the flow of fluid. This rig is designed to be able to carefully recreate and control these conditions to a high degree of accuracy. The key purpose of this rig is to represent the heat transfer surface of a shell and tube heat exchanger. The deposition

surface is a metal finger that is screwed into the centre of the rig. This finger has a 750W cartridge heater (CH) inserted into it that enables it to be heated to the desired temperature, around 340-400°C in a typical test. This temperature is measured by 2-3 thermocouples embedded into the wall of the finger; the temperature is controlled by varying the power to the CH. The shear stress is created by rotating a cylindrical stirrer, powered by a magnetic stirrer, around the heat transfer surface. The rapid rotation of the fluid around the surface has been found to reach turbulent conditions (as in industrial exchangers) even at relatively low stirrer speeds (Smith and Townsend, 1982; Mullin *et al*., 1983; Churchill, 1988). Computational fluid dynamics (CFD) models were developed by Yang *et al.* (2009) to estimate the shear stress on the surface as it is not possible to accurately estimate the shear stress using hand calculations because it is such a unique system with regards to its fluid dynamics. Typically the rig is operated at stirrer speeds in the range 100-400RPM; by around 400RPM the fouling rate for most oils has typically reached zero.

The other main condition that must be kept very steady during a test run in order to generate reliable data is the T_b: this is typically kept within a margin of +/-2°C of the test T_b. This temperature is measured by 2 thermistors, and controlled by pumping a cooling fluid, Paratherm through a cooling coil held in the vessel at a rate determined by a Eurotherm control system.

Fouling itself is tracked by the change in T_w as a deposit builds up on the surface of the metal finger. The thicker the deposit, the harder it is for the heat provided by the CH to escape due to reduced HTC and therefore the wall of the finger gradually gets hotter. The T_ws, as well as all the other key data parameters, are sent to and recorded by a computer.

3.1.2 CFD Analysis

Much of the analysis of the fluid mechanics, and temperature distribution within the rig has been done using the COMSOL computational fluid mechanics package. The use of CFD has enabled many insights into what is actually going on inside the rig which would otherwise be very difficult to monitor or observe experimentally because it is not physically possible to see inside the rig when it is operating.

As explained in Chapter 3.1.1, previous researchers have found that fluid flow between concentric rotating cylinders becomes turbulent at quite low speeds of rotation. To ensure this was also the case with the stirred batch reactor rig, Yang *et al.* (2009) tested this conclusion using a glass and transparent polycarbonate mock-up of the rig and turbulence was confirmed. Therefore, based on this finding, it was determined that in the CFD simulation of the system, a k-ε turbulent flow model could be used. This particular model functions by using equations similar to those of the Navier-Stokes equations, but modified to include turbulent dynamic viscosity with the viscosity expression in it. The simulation was

made two-dimensional with axial symmetry, as this greatly reduces the time taken to run it on a computer. Checks were made that this system simplification was accurate by also conducting a three-dimensional simulation as well and no difference was observed between the two. The simulation itself represents both the heat transfer aspect and the fluid mechanics elements of the rig. The heat flux provided by the CH is represented by using the power of it, and then the heat transfer through the metal wall simulated using the physical properties of steel. The fluid mechanics are represented by turbulent swirl flow, which simulates the moving fluid itself and the effects of the moving stirrer wall.

The key benefit of building this simulation is to predict what is actually happening inside the rig; this is very useful in terms of properly validating the rig with regards to creating the required conditions. For example, the CFD simulation enables the shear stress exerted on the finger wall by the rotation of the fluid to be precisely calculated. It also provided proof that the shear stress variance across the length of the finger is sufficiently constant to make it a fair test (it was previously a concern that there would be significant variance across the finger length). The T_w readings were additionally validated using CFD: once the rig was up and running, for a given T_b and CH power, the T_w in two of the thermocouples at different heights in the wall was measured. These exact same conditions were then modelled using CFD and a good agreement between the simulation and the real thing was observed Yang *et al.* (2009).

3.1.3 Deposit Thickness Versus Temperature

The surface of the metal finger has a significant variance in temperature along its length: as high as 60°C from top to bottom. This is due to the fact that some of the heat from the CH escapes through the top and bottom of the metal finger, as well as the variance in fluid flow distribution at the top and bottom. Therefore, because the fouling rate will increase with temperature, it would be expected that the fouling deposit would vary in thickness along the length of the finger. This was tested by Yang *et al*. (2009) using a Proscan 2000 – equipment that accurately measures the deposit thickness; the measured thickness was then plotted against length along the finger. The plot when compared to the predicted T_w versus length from the CFD simulation was a very close match. This finding both further validated the CFD, and also proved that the fouling rate is strongly influenced by ST.

3.1.4 Deposit Characterisation

Various analyses were carried out by Young *et al*. (2009) on fouling deposits collected from the metal finger after tests were finished in order to determine the composition of the deposits.

Size exclusion chromatography and UV-Florescence was performed on a fouling deposit, fresh crude before fouling and the crude after fouling. This test showed that firstly there was

a significant amount of heptane insoluble material in the deposit; asphaltenes are the most common heptane insoluble material in crude oil. The analysis of the oil also showed a significant drop in the amount of heptane insoluble material before and after fouling had occurred. This suggested that a large part of the fouling deposit in the rig for the oil tested was most likely asphaltenic.

Elemental analysis was conducted at Imperial College London and it was found that the most prevalent molecules in the deposit were sulfur, iron, carbon, hydrogen and nitrogen. An atomic ratio for hydrogen/carbon of approximately 1.37 was found; this is in line with the typical H/C ratio for asphaltenes, providing further evidence for the high proportion of asphaltenic matter in the deposit. The quantity of iron and sulfur found in the deposit was also quite substantial. This suggested iron sulfide had formed, which is what is usually found when corrosion fouling has taken place.

As a result of analysing the deposit, Young *et al.* (2009) were able to confirm that both asphaltene based chemical reaction fouling and corrosion fouling were the key types taking place in the stirred batch reactor. This is in line with what others have previously found with crude oil fouling (ESDU, 2005).

3.1.5 The Fouling Induction Period

The stirred batch reactor was used to provide fouling data to test a fouling induction period model developed by Yang *et al.* (2009). The aim of the model was to see if it was possible to predict the length of the induction period based upon the T_w and activation energy of the oil. Fouling rates from two different crude oils that had been tested at various T_ws, ranging from 369-411°C were used to test the model. The model defined the induction period time at the time for more than 50% of the surface to become covered in foulant – represented by the term $t_{0.5}$. At this point in time, the rate of increase in fouling rate reaches a maximum and the fouling deposit becomes noticeable

The model equation was defined as: [17]

$$t_{0.5} = \frac{\ln c}{k}$$

Where $t_{0.5}$ is the length of the induction period in hours;

c is a constant that represents the surface characteristics;

k is a lumped rate constant calculated $k = k_a e^{\frac{E_a}{RT}}$ where k_a is a pre-exponential factor.

The model was fitted to a data set for each of the crude oils in order to calculate the *k* and *c* values. The model was then tested by applying it to the other data sets for the two crudes

at different conditions to see if the predicted $t_{0.5}$ was accurate. It was found that for both crudes the model gave an accurate prediction of the induction period in the rig. The model was also found to be successful at predicting the induction period for sets of crystallisation and protein fouling data as well, though these data sets were not collected using the rig and were obtained from literature.

3.1.6 Fouling Threshold Work

In 2011, removal of some of crude oil fouling deposit on the metal finger was found to be possible if the stirrer speed was increased to a significant enough level. This could be seen on a fouling plot as a negative fouling rate; in the tests where this occurred a linear rate of fouling removal was typically observed. Yang *et al.* (2011) utilised this negative fouling rate data in order to predict the typical fouling threshold of a crude oil at varying temperatures.

Fouling thresholds are typically found by plotting the fouling rate versus shear stress at a constant T_w for a crude oil, plotting a line of best fit and then extrapolating the line to $dR_f/dt = 0$ and reading off the shear stress. However, as always when extrapolating a graph, it has to be assumed that the correlation remains the same outside of the measured data points, which may not be the case. Therefore, when points are added to one of these graphs that are below the $dR_f/dt = 0$ point, it means interpolation between the positive and negative fouling rates to obtain the fouling threshold is possible. The theory thus is that because interpolation, instead of extrapolation of the data is done, the fouling threshold will therefore be more accurate. A full data set was obtained for a single oil in this paper, with four different stirrer speeds tested for seven different wall temperatures ranging from 327-387°C.

3.2 Operation of the Stirred Batch Reactor Fouling Rig

3.2.1 Fouling Test Start-Up Procedure

Below are the step by step instructions for operating the stirred batch cell to carry out a crude oil fouling run. These instructions are a modified version of Young *et al.*'s (2009) original instructions. They are updated based upon personal experience over the course of the 12 month project regarding the best ways to achieve stable conditions in the rig, whilst avoiding potential problems. Extra safety steps have been added based upon issues that have occurred such as dealing with excess pressure in the cell and the monitoring and removal of potentially hazardous fumes in the air.

1. Switch on the Dräger H_2S sensor by pressing the 'OK' button for three seconds.
2. Switch on the plug sockets labelled 'Control Panel', 'Aux Power', 'Power to Band Heaters' and 'Heater Power Supply'.
3. Make available the bottled N_2 gas.
4. Purge Vessel if it the rig has just been opened up/refilled:
    a. Pressurise the vessel to 7000kPa with N_2.
    b. Slowly release the vessel pressure to around 2000kPa.

c. Repeat the above steps three times.

5. Pressurise the vessel to around 9000kPa.
6. Set rotation speed on agitator (i.e. 100RPM).
7. Place the two fans to flow air across the agitator to keep it cool.
8. Start heating up by setting the band heater Variac to approximately 140W. Any higher can cause the agitator to overheat.
9. Set the CH Variac to 100W to aid the heating of the bulk fluid.
10. Switch on the ventilation fan using the switch to the right of the window. Note this can affect the CH power reading so switch the 'Control Panel' plug off and on again quickly to reset this. The window should also be opened slightly to help in clearing any smoke that may be in the air. If it is the first time the rig is being used with a new batch of crude oil, the air should be monitored for excess smoke build-up during the heating up procedure and the first few hours of the test.
11. The vessel temperature should increase at 5-10°C/min.
12. The vessel pressure will also gradually increase. Monitor this carefully and if it reaches the vessel limit of 30000kPa, carefully release some of the pressure using the release valve to put it below the limit.
13. When the vessel cell reaches 2°C below the target T_b set the CH to the desired power then start the cooling procedure:
    a. Switch on the two plug sockets labelled 'Rad Fan' and 'Cooler Motor'.
    b. Flick the two switches on the Telemecanique cooling circuit pump control panel to 'On'.
    c. Set the cooling circuit to manual and pulse at 10% manually for 10 seconds to start the flow of cooling fluid (holding both arrow buttons down will enable you to switch between automatic and manual modes).
    d. Then set the cooling circuit to automatic and set the target T_b.
    e. The control system will take around 10-20 minutes to stabilise the T_b.
14. Open the 'LabView' logging software on the computer set a file name and save location, then start logging data.
15. Once the target T_b is reached the band heater Variac can be reduced to 90W.
16. Monitor the vessel pressure, T_b, CH power and stirrer RPM and ensure they are kept stable.

Continuously monitor:

- CH power: +/-5W.
- Agitator speed: +/-10RPM.
- T_b: +/-2.5°C.
- Pressure: must be stable and not leaking.

3.2.2 Rig Normal Shut Down Procedure

1. Stop all heating power inputs:
    a. Set CH power Variac to zero.
    b. Set band heater power Variac to zero.
    c. Switch off the associated plugs at the mains.
2. Stop logging data on the computer.
3. Change cooling controller mode to 'Manual' and increase the cooling rate to approximately 40-60%.
4. Cooling should be rapid -20°C/minute, but monitor this.
5. Agitation can be stopped when the T_b reaches 200°C.
6. Keep cooling until at least 8°C, then switch off all mains plugs.
7. Switch off the H_2S sensor.
8. Shutdown the computer.

3.2.3 Controlling and Monitoring Conditions During a Run

During test runs, it is essential that all the controllable parameters (CH power, agitation speed and T_b) be kept as constant as possible throughout. The effects of fouling over a typical 8 hour test will only likely increase the T_w measured by the wall thermocouples by 5-10°C on average. However, the effect of the variables wandering can easily also change the T_w by this amount. It is therefore imperative that these variables are monitored closely and controlled in order to keep them constant so that the effects of fouling can be distinguished from noise caused by them.

3.2.3.1 Stirrer Speed

Stirrer speed is the most variable and temperamental of all the conditions. It typically fluctuates over a range of +/-5RPM and this is what should be aimed for during a run. However, the agitator is partial to overheating, which has the effect of greatly increasing the variability of the output stirrer speed, causing it to sometimes skip up to +/-60RPM. If during a run it is clear that the agitator is having overheating problems, then a very close eye must be kept on the speed, and the speed changed manually using the controller as often as required. At 100RPM, an increase of just 10RPM will typically decrease the T_w by 1°C which is far larger a variation than typically caused by fouling and can therefore very easily distort the data and results. Hence, the importance of keeping it constant.

3.2.3.2 T_b

The T_b is kept constant by a Eurotherm controller, although this unit can sometimes have problems and not function in its intended way. Therefore, the T_b should always be carefully monitored. If functioning correctly, the T_b should typically fluctuate by approximately +/-2.5°C. There are times when this fluctuation increases to as much as +/-5°C. If this occurs, the pressure should be monitored if it is around the 30 bar limit of the vessel, as fluctuations

can push it over the limit with the risk of opening the pressure relief valve. If there has been large variability in T_b during a run, the effect of this on the data can be reduced by subtracting the T_b from the ST, and using this value in any R_f calculations.

There are also times whereby the cooling circuit and/or control system will suddenly stop functioning. This can be noticed by either a sudden change in the noise made by the pump or the T_b suddenly going up and up without stopping. It is dangerous if the T_b goes too high, due to the amount the pressure will also go up as a result. If this does happen and the T_b shoots up due to control system failure, power to the band heaters should be switched off until the control system is functioning properly again.

3.2.3.3 CH Power

The CH should not fluctuate significantly during a test run. It will often vary over a range of around +/2W, but this is only around 0.4% variance so should not significantly affect the T_w. If the CH power increases greater than +/-5W from the set power for the experiment, then it should be corrected back to its original value. If the heater power keeps on creeping up or down significantly, or is fluctuating over a larger range, then it is often a sign that the CH is near the end of its life and should be replaced with a new one.

3.2.4 Rig Safety Systems

The stirred batch cell fouling rig has a number of safety systems in order to prevent against catastrophic failures.

1. A pressure relief valve connected to the vessel which will open if the bulk pressure reaches around 40 bar. This valve is connected to piping that releases the contents of the vessel to the atmosphere outside the building if the valve opens.
2. An electrical kill switch located outside the room the rig operates in means that all power to the rig can be turned off without going near it if it is not safe to do so.
3. A dump tank located below the rig into which the contents of the vessel can be emptied manually by opening a valve located beneath it. This can be used if the contents of the rig needs to be rapidly purged, but it is not at high enough a pressure to open the pressure relief valve.
4. The walls of the room the rig is stored in are designed to absorb force and disintegrate if an explosion were to occur.

3.3 Differences in the Methodology when Carrying Out Calcium Carbonate Fouling Tests

3.3.1 Conditions

The biggest difference between using the rig to test calcium carbonate fouling compared to crude oil fouling is the severity of the conditions: calcium carbonate requires much less severe conditions, for normal hard water concentrations, to promote fouling.

Runs typically take place with a T_b of around 50°C and a T_w of around 90°C, significantly lower than for crude oil. The rig also does not need to be pressurised, as the solution is not at its boiling point, unlike crude oil. As a result of this, the rig is significantly safer and can therefore safely be left to run unobserved overnight. This means longer tests runs can be carried out in comparison to crude oil which always needs to be continually watched and thus its operation is limited to working hours.

3.3.2 Test Fluid

Calcium carbonate experiments test a solution of varying concentrations of calcium carbonate dissolved in water; this solution needs to be prepared before the experiment. As calcium carbonate powder is not soluble in water, it must be made by mixing a 1:2 molar ratio of $CaCl_2$ and $NaHCO_3(H_2O)_2$, which are both water soluble and react together to form a solubilised form of Calcium carbonate in the following reaction:

$$CaCl_2 + 2\ NaHCO_3(H_2O)_2 \rightarrow CaCO_3 + 2NaCl + 3H_2O + CO_2$$

Three different concentrations of $NaHCO_3$ and $CaCl_2(H_2O)_2$ were dissolved in solution in these experiments:

- 0.84g $NaHCO_3$, 0.735g $CaCl_2(H_2O)_2$.
- 1.26g $NaHCO_3$, 1.1g $CaCl_2(H_2O)_2$
- 1.68g $NaHCO_3$, 1.47g $CaCl_2(H_2O)_2$

These produce solutions with 0.01, 0.02 and 0.03 moles of $CaCO_3$ dissolved respectively. These were chosen as they were the concentrations used in the previous calcium carbonate fouling experiments using the stirred batch reactor.

3.3.3 Test Surface

The purpose of the calcium carbonate experiments was to investigate the effect of increasing the shear stress by wrapping a protruding helical coil around the heat transfer surface. To achieve this, a modified stainless steel sleeve test surface was slipped onto the standard metal test finger for the tests. This is the same as was done in previous experiments carried out by Krishanu Kundu at the University of Bath in summer 2012. He tested the fouling rate of a plain surface stainless steel slip on, and a stainless steel slip on with a negative helical thread. All three sleeves can be seen in Figure 9. Before each test the slip on was thoroughly cleaned, and then put in place over the normal metal finger.

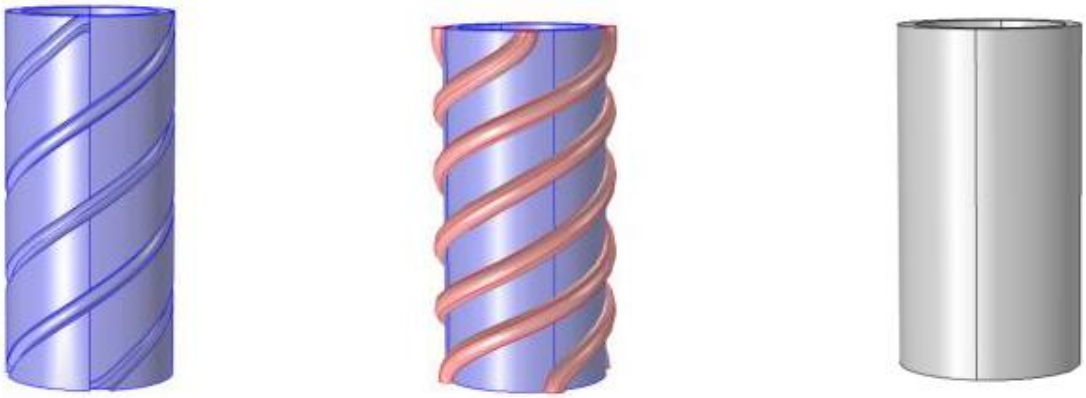

Figure 9: The different sleeves that have been used in the rig, from right to left: negative helical thread, protruding helical thread, plain sleeve (Crittenden et al., 2013)

The aim of testing the different sleeves was both to increase the shear stress forces on the test surface in order to reduce fouling, and to try and better recreate the flow conditions found in a plate and frame heat exchanger in the rig. The differences in shear stress at different stirrer speeds for the three sleeves was simulated by Dr M. Yang of the University of Bath using CFD (Figure 10).

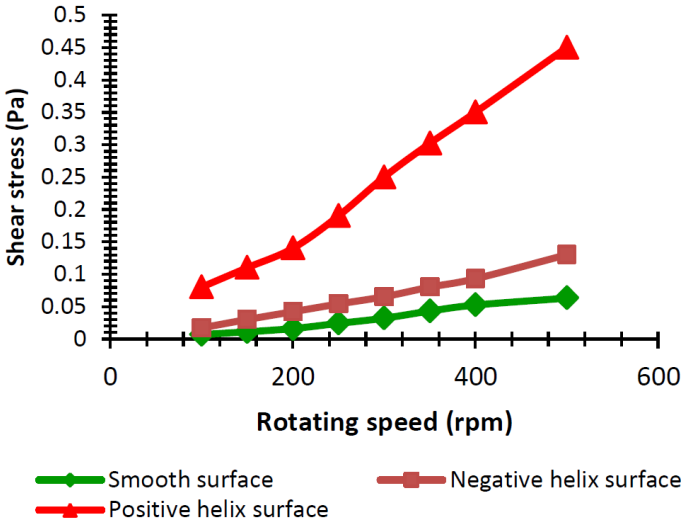

Figure 10: Calculated shear stress versus stirrer speed from CFD (Crittenden et al., 2013)

3.4 Experimental Methods Summary

A review of previously published papers using the stirred batch cell has been presented in this chapter. This has been done to show the methods by which the stirred batch cell can be used to generate fouling data and to investigate the effect of a variety of different variables. The operating procedure for starting up, shutting down and running the rig has also been detailed. In the next chapter, the data analysis methods and the calculation procedures used in this work are described.

CHAPTER 4

4 Calculations and Data Analysis Procedures

When fouling experiments are conducted, a great deal of data is recorded by the computer logging program, and it is important that it is processed and analysed correctly in order to find out exactly what occurred during the experiment. Therefore, the methods for processing the data in order to calculate fouling resistance are detailed in this chapter.

4.1 Fouling Calculation Procedure

As explained in Chapter 2.1.1, the equation for calculating the fouling resistance at any point is:

$$R_f = \frac{T_{st1} - T_{st0}}{Q/A}$$

For the stirred batch reactor, because the measurement of the actual ST of the heat transfer surface is not possible, the T_w measured by the thermocouples embedded inside the metal finger is used instead in the equation. It can be argued that this is not a fair representation of the ST, as the ST will be colder than the wall itself. However, due to the complexity of the system there is no easy way to calculate the exact ST without using CFD for every test run. The actual difference is typically around 5-6°C at the middle section of the metal finger (Yang *et al.*, 2009) and this temperature difference does not change significantly with varying overall temperature. For the purpose of this equation, it is the change in temperature over time (ΔT) that is being looked at; it is a reasonable assumption that every 1°C change in the ST due to fouling will result in a 1°C change in the T_w. Therefore, if the change in T_w is used to track fouling, it is equivalent to if the change in ST was being tracked.

Data from the rig is logged every 60 seconds by the computer programme 'Labview'. This data is then processed using 'Microsoft Excel' in order to calculate the fouling resistance at each of these points in time.

Whilst it is assumed in the fouling resistance calculation equation that the T_b is constant, in reality the control system is only able to keep the T_b to within +/-2.5 of the target T_b. Thus the T_w is constantly varying accordingly to the T_b. Hence when processing the data, it gives a far more representative plot of ΔT_w over time if the T_b is subtracted from the T_w for each plot: [18]

$$\Delta T_{wb} = T_{wb} - T_b$$

This point can be seen in Figure 11 and 12 which show the change in T_w over time for an example fouling data set. The first graph shows the change in T_w over time when the variance in T_b is not taken into account. The second graph shows the change in ST over time when the T_b variance is taken into account.

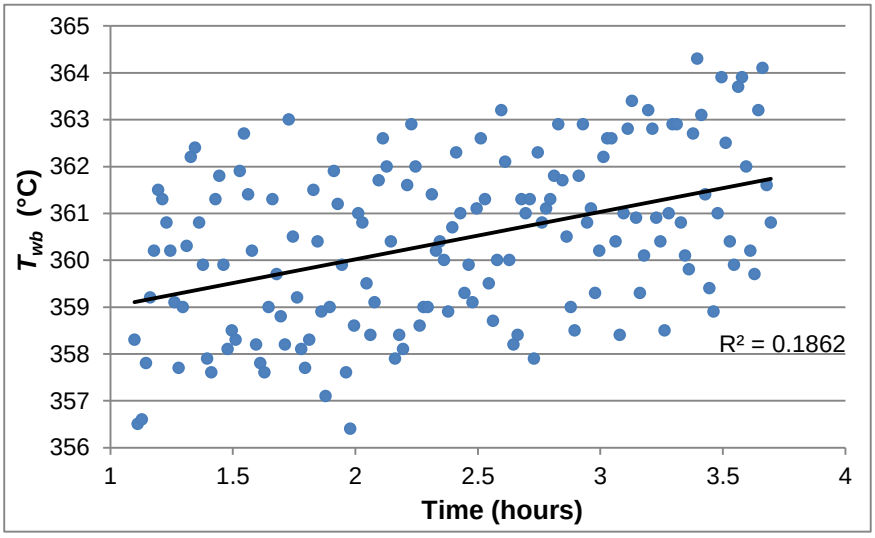

Figure 11: A fouling data set showing the temperature change measured by T_{wb}, not accounting for the variance in T_b

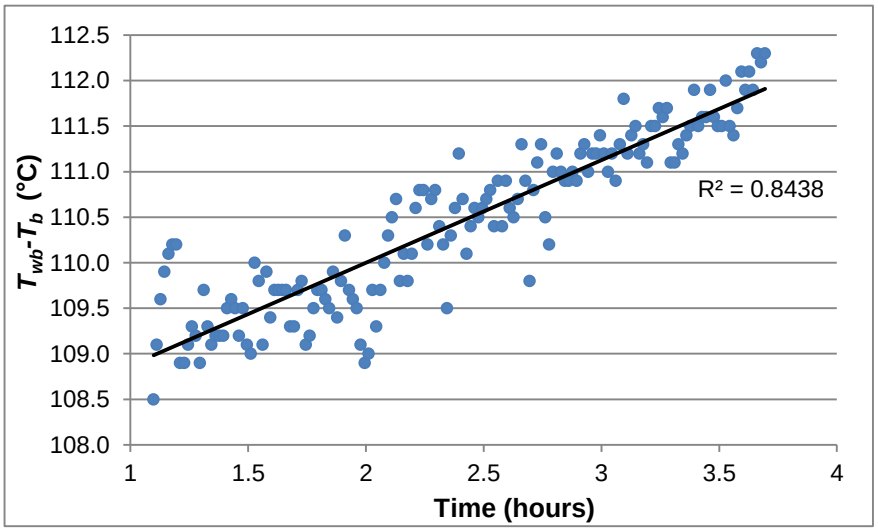

Figure 12: A fouling data set showing the temperature change measured by T_{wb}, accounting for the variance in T_b

Not allowing for the bulk variation gives an R^2 value of only 0.186 for the trend line fit of T_w increase over time (Figure 11). However, simply removing the variation in T_b from the equation improves the fit of the trend line to 0.844 (Figure 12). This demonstrates that the majority of the fluctuation in the T_w is caused directly by the T_b variance. Thus it is the change in the recalculated T_w with T_b subtracted that is used in the fouling calculations of R_f.

In the fouling equation, the heat transfer area is constant and is calculated based on the dimensions of the heat transfer surface, which is essentially a cylinder with the following dimensions: Diameter = 0.026m, Height: 0.062m.

Therefore, as Area = π x Diameter x Height,
Area = π x 0.026 x 0.062 = 0.0051m^2.

4.2 Sorting the Data

Each fouling run collects so many data points that when all of the T_w data is plotted on a graph, there will always naturally be large outlier data points. These points will seemingly be random and affect any correlation or trend line that is being made. However, the cause of these outliers can mostly be determined and thus the points removed from the data. The biggest cause of sudden very large increases or decreases in the T_w (often +/-5-10°C) is sporadic fluctuation in the stirrer speed. Generally this change will be spotted during the run itself and the RPM quickly reset to the desired value, although it is likely that a few points at the different RPM will have been recorded. If an outlier data point is found and it corresponds to a stirrer speed greater than +/-10RPM from the set speed, then it should be omitted from the data.

Sudden change in CH power can also sometimes cause outlier T_w points. However, this is quite a rare occurrence, especially in comparison to the frequency of which sudden RPM changes occur. The only time a significant spike or dip in power is likely to occur is if the extractor fan has been switched on, as this has been known to instantaneously caused a +/-50-100W change in the power output. This is counteracted by switching the power to the CH mains socket off and on again quickly. Therefore, in the same way as with stirrer speed, if sudden change in T_w can be clearly seen to correspond to a sudden change in power, then the data points may be omitted.

4.3 Looking Out for False Fouling Curves

There are times when it can look like fouling is taking place, for example the T_w increases gradually over the time of the experiment. However, the data should always be properly studied before a fouling judgement is made. There are two possible causes of what appears to be fouling, but actually is not: (1) the stirrer speed may have been gradually dropping over the course of the experiment, causing the T_w to rise; (2) CH power may have gradually risen over the course of the experiment which typically only happens when it is close to the end of its lifespan. The quickest way to determine if either of these two variables could be the cause is to plot T_w versus stirrer speed and versus power. If there is a positive correlation there is a distinct possibility that they are the cause of the increase in T_w over time, or if it is fouling, they have caused a significant increase in the T_w increase rate resulting in an inaccurate fouling rate.

4.4 Calculations and Data Analysis Summary

The data analysis and calculation procedures that have been used in this thesis have been presented in this chapter. The modifications that were carried out to the stirred batch cell fouling rig over the duration of the project are detailed in the next chapter.

CHAPTER 5

5 Modifications to the Experimental Apparatus

Over the course of the project, a number of improvements, modifications and fixes were performed on the rig to improve the quality of the data it produced. These are detailed in this chapter.

5.1 Cooling Circuit Holding Frame

When the rig was first made, the stainless steel cooling coil that is connected to the lid of the vessel was supported by a mild steel mesh frame. However, after several years of both crude oil and water fouling testing, a thick layer of both fouling and rust like material had developed on the frame. Given that corrosion fouling of crude oil is known to occur when sulfur present in oil reacts with iron, the rust on the frame would likely add another source of iron and affect the level of corrosion fouling occurring, reducing the quality of the test. It was thus decided to remove the frame from the coil. Once this was done checks were made to ensure the stability of the cooling coil without the frame in place. After removal of the frame, a thin layer of black foulant was discovered along the length of the cooling coil. The coil was completely cleaned using fine grade sand paper and returned to its original state. The cleaned coil can be seen in Figure 13.

Figure 13: A picture of the cooling coil following cleaning

5.2 Pressure Relief Valve

During initial pressure testing of the rig before its first crude oil run in around a year, a large leak was found on the joint where the pressure relief valve is connected to the vessel lid. Due to the size of the relief valve and the location where it was attached to the lid, it was

impossible to tighten it, or remove it by unscrewing because the agitator stopped it from rotating (Figure 14).

Figure 14: The original position of the pressure relief valve

The decision was therefore made to have the relief valve connector piece sawn off in order to remove it. Once it was removed, the rig was modified so as to relocate the pressure relief valve away from the lid itself, connected by a long tube piece so that the valve could easily be attached or removed from the lid.

5.3 Rig Pressure Retention

During the initial pressure testing of the rig, a number of the threaded joints on the vessel were found to be leaking. Teflon tape was thus applied to the threads which significantly reduced the pressure loss.

Additional pressure leakage was observed though the gasket between the metal finger and the vessel. If not tightened sufficiently, gas and crude oil would leak through the joint. The use of two gaskets was preferred in order to reduce the chances of the gaskets being crushed and breaking when the finger was screwed in place. This further reduced the pressure loss in the rig.

Finally, in February 2013 the agitator was found to be leaking pressure through its thread. The agitator was removed and Teflon tape applied to the thread, before replacing and retightening it. Once the agitator was refitted, the pressure leak stopped.

5.4 Band Heater Replacement

In March 2013 during a test run, the band heaters suddenly failed and tripped a fuse. There are two band heaters, each comprising two 250W circuits giving a total power of 1000W, which are wrapped around the main vessel. Replacement band heaters were fitted resulting in a dramatic reduction in the time taken by the band heaters to heat oil from ambient temperature to 250°C from 1.5-2 hours before replacement, to around 30 minutes with the new ones fitted. It is therefore reasonable to conclude from this finding, that parts of the band heaters appear to have failed at some point in the past, and that this had not been noticed.

5.5 Electrical Problems

During January and February 2013, the power input to the CH repeatedly failed due to fuses blowing randomly during a test run. The blown fuses caused significant delays to the research being conducted. The cause was determined to be either the CH overheating, or the CH being faulty. To test these hypotheses, a CH was inserted into a long metal pipe, which functioned as a heat sink. However, a fuse was tripped within several minutes of switching the CH on resulting in the conclusion that overheating was not the problem. To see if the CH was the problem, it was replaced with two other ones. However, both of these also caused the same electrical problems. Finally, a CH of a different design was tried and the electrical problems stopped straight away. It seems that the heaters that were blowing the fuses were from a faulty batch, as all cartridge heaters from that set caused problems.

5.6 CH Design Investigation

Other than the electrical problems described in Chapter 5.5, another significant problem arose from the CHs due to variations in design between them. Different heaters (from different order batches) were capable of producing different maximum T_ws in the rig for the same power input. The different CHs that were used throughout the tests will be referred to by a batch number in this section. They are each described in Table 1 below:

Table 1: A Table Detailing the Different Batches of CHs

Batch #	Manufacturer and Design #	Order Date
1	Watlow Firerod, Design 1	Before September 2012
2	Watlow Firerod, Design 2	Before September 2012
3	Watlow Firerod, Design 2	February 2013
4	Under Control, Design 1	June 2013

The first tests with crude 19 in January 2013 used heaters from batch 2, but because they were found to be faulty and cause electrical problems, batch 3 was ordered as a replacement. Whilst the batch 3 heaters were being manufactured, a CH from batch 1 was used in the fouling experiments from February-June 2013. This CH could create T_ws of 340-

350°C when the bulk fluid was at 240°C and with 500W of power input. In June 2013, the final batch 1 heater broke and the new CHs from batch 3 were put into the rig.

The new heaters from batch 3 were found not to be capable of creating a comparable T_w: at 250°C T_b, with 600W of power input the T_w only reached 298°C. This temperature was too low and meant that fouling T_ws of 340-350°C would not be possible with these CHs. Initially it was unknown as to why this was the case. The Watlow Firerod Design 2 was sold by Watlow as an upgrade of the Watlow Firerod Design 1, but with identical specifications.

The cause of this difference was eventually found when a heater from batch 1 and 3 were cut open. Batch 1 had a heated element 2 inches long at the top section of the unit, whilst batch 3 had a 4 inch heated element along nearly its whole length (Figures 15 and 16).

Figure 15: A cross section of a heater from batch 1 with a 2 inch element at the top of the unit

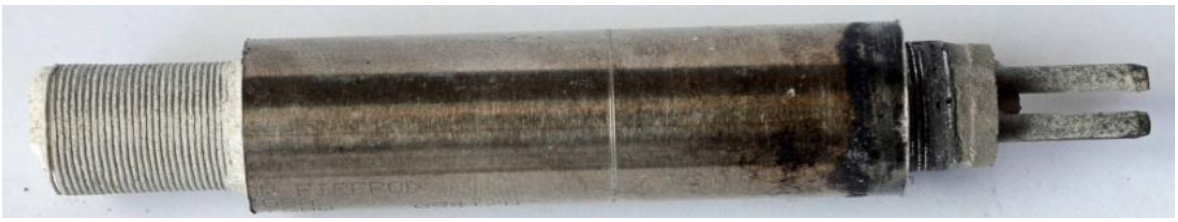

Figure 16: A heater from batch 3 with its metal casing cut away at the top and bottom showing that is has a 4 inch element throughout the entire length

The impact of this difference was that the heat flux was more concentrated through a smaller area in the Watlow Firerod Design 1 than in their Design 2, resulting in a higher temperature where the element is located. When the location of the element in the heaters are lined up against the metal finger it reveals that for The Watlow Firerod Design 1, the 2 inch element lines up perfectly with the location of the thermocouples and where fouling deposits form: the lower middle part of the metal finger.

This can be seen in Figure 17 which is a cross sectional diagram of the CHs inside the metal finger and the location of the element in each. This drawing is to scale.

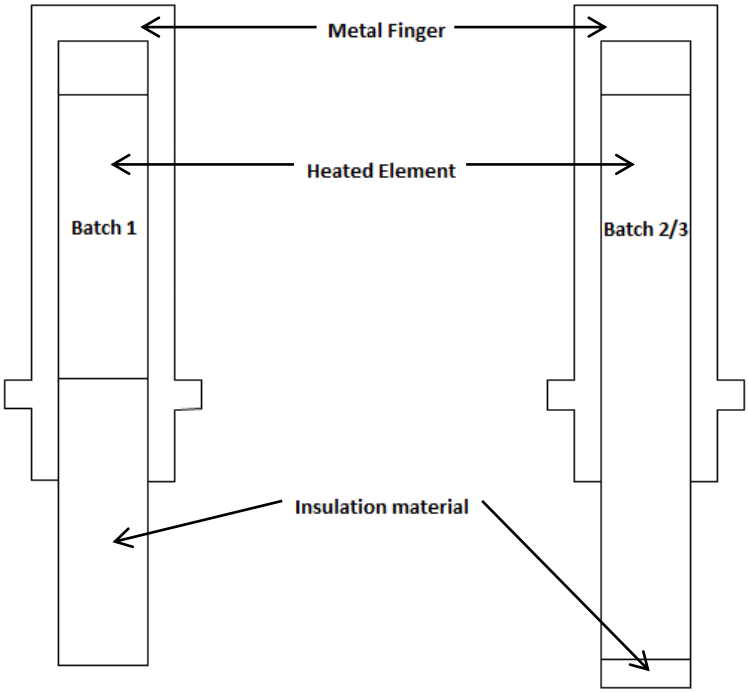

Figure 17: A cross sectional diagram of the location of the CHs and their heated elements in the metal finger

This also explains why the heaters in batch 2 repeatedly failed and caused electrical problems. As can be seen in Figure 17, the element in the Watlow Firerod Design 2 from batch 2 and 3 actually continues past the bottom of the metal finger and is therefore exposed to the air. This meant that because air conducts heat poorly in comparison to metal, heat could not be conducted away easily and thus was likely to build-up at the bottom of the CH. This heat build-up puts a strain on the wire connections to the unit from the bottom, causing them eventually to short out and break. The Watlow Firerod Design 1 from batch 1, by comparison, has an element that is entirely surrounded by the metal finger, but also has a large amount of insulation inside the metal finger below the element to conduct heat through, therefore, reducing the effect of overheating on the connection wires at the bottom.

Watlow no longer manufacture a CH like Design 1 with a 2 inch element, but 'Under Control Instruments LTD' agreed to custom manufacture some new CHs to exactly the same design as the Watlow Firerod Design 1. Initial tests with these showed that they could easily produce a metal finger of T_w of 340-350°C. These were used in all of the fouling tests from July-September 2013.

Observations showed that in order to reach these T_ws, a slightly higher T_b was required in comparison to when the Watlow Firerod Design 1 was used. To reach a T_w of 340°C with a 500W CH input power, a T_b of 260°C (20°C more) was required. This meant that 20°C worth of heat was getting lost somewhere and therefore not reaching the metal finger wall. When a batch 4 CH was inserted in the metal finger it was found to fit slightly less tightly compared to the Watlow Firerod CH from batch 1. A reasonable conclusion is that there was likely a

small air gap between the metal casing of the CH and the metal finger that was causing this heat loss. A gap of air can cause temperature loss because air has a much lower thermal conductivity than metal. Therefore per metre the heat travels through, the temperature will drop more in air compared to in metal as the air resists the heat.

Calculations were therefore made of the gap size of air between the CH and the finger that would be required for a 20°C drop in temperature.

The following equation calculates the heat flux in one direction though a material of known length and temperature difference across it: [19]

$$q = \frac{\Delta T k}{L}$$

(Coulson *et al.*, 2007)

This can be rearranged to the following equation in order to calculate the air gap required for a 20°C drop in temperature when 500W of heat is being transferred over an area of 0.0051m^2. At 350°C, air has a thermal conductivity of 0.0485W/m°K (Stephan and Laesecke, 1985). [20]

$$L = \frac{\Delta T k}{q}$$

The end effect was also accounted for: at a T_b of 260°C 69% of heat goes through the horizontal walls of the metal finger (see Chapter 8.6 for details of the end effect).

$$L = \frac{20 \times 0.0485}{\frac{0.69 \times 500}{0.0051}}$$

$$L = 14.5 \mu m$$

A 14.5micron layer of air between the CH and the metal finger would be required to resist 20°C of heat. As this would be on all sides of the cylindrical CH, the CH would need to be 29microns smaller in diameter for this to be the case. The exact diameter of the batch 4 CHs compared to the batch 1 CHs were therefore measured by a digital calliper.

- Batch 4 CH diameter: 15.65mm.
- Batch 1 CH diameter: 15.68mm.
- Difference in diameters: 30microns.

These two values are incredibly close. Therefore it is highly likely that the reason the batch 4 CHs produce 20°C less heat for the same power input is because they have a slightly smaller diameter which results in an approximately 15micron air gap between the CH and the metal finger.

5.7 Cooling Circuit Faults

In May 2013, issues with the cooling circuit occurred: the cooling circuit would keep the temperature controlled for a few hours, but then would lose control and the temperature would keep rising until the power was switched off. Typically the cooling circuit functions by switching the coolant flow on and off every 30 seconds or so. It allows the temperature to increase until it reaches the target temperature, then engages and brings it back below target temperature and switches off. This process then repeats and can keep the temperature typically within +/-2°C of the target temperature. When the cooling system stops working properly however, the coolant flow suddenly becomes continuous instead of on/off, and the pump speed goes up rapidly. However, this has no effect on the temperature. This seemed to be due to air getting into the pipework, and preventing the flow of Paratherm through the coil. The solution to get the cooling system working again each time was to open up the pipes containing the cooling fluid Paratherm, allow any trapped air to escape, and then top them up with Paratherm. This procedure was repeated many times over a couple of days until all the air in the system was removed completely and the problem stopped occurring. This problem has also been found to occur when the cooling circuit connectors to the immersion cooling coil are not clipped properly in place, so it is essential they are properly attached before any experiment is started.

5.8 Modifications to the Experimental Apparatus Summary

The work that was done to modify and improve the test rig has been detailed in this chapter. This included information on how issues with rig pressure retention, CH designs and the cooling system were overcome. Information on how and why several parts were replaced was also given. As a result of these modifications, the rig was able to operate better and for longer periods of time. It was also able to collect data to a high level of accuracy. The following chapters present and analyse the results of this thesis.

CHAPTER 6

6 Calcium Carbonate Fouling Test Information, Results and Analysis

This chapter will present and discuss the results of the calcium carbonate fouling experiments carried out with the rig. These include the initial rig recommissioning experiments, those investigating the effect of stirrer speed increase on fouling rate, and the tests to see if removal of a deposit by increasing shear stress was possible.

6.1 Calcium Carbonate Fouling Test Information

A total of seven experiments were carried out from October-November 2012. The first three experiments were conducted with the aim of measuring the effect of varying $CaCO_3$ concentrations on the rate of fouling. The primary purpose of these tests was as a training exercise so as to get more familiar with using the rig to create fouling conditions and generate fouling data. The rig had also not been used for several months prior to these tests so the second objective was to get the rig up and running again and collecting good quality data. As the main objective of these experiments was for training and recommissioning the rig, the collected data was not of good quality and had a large amount of variation in T_w, T_b, stirrer speed and CH power. As a result, the data had little discernible trend over time from which fouling rates could be plotted. Therefore, the results of these initial tests will be not be presented in this thesis.

The second set of four tests looked at the effect of stirrer speed on the fouling rate for the raised helical sleeve. The conditions for these tests are displayed in Table 2:

Table 2: A summary of the calcium carbonate fouling tests carried out

Test Date	T_b (°C)	T_w (°C)	Speed (RPM)	Power (W)	$CaHCO_3$ (g)	$CaCl_2$ (g)
25th October 2012	55	94	200	120	1.26	1.1
9th October 2012	55	93	300	120	1.26	1.1
30th October 2012	55	91	400	120	1.26	1.1
31st October 2012	55	83	500	120	1.26	1.1

All tests were run overnight for a total run time of around 20-24 hours. During these experiments, the Eurotherm controller was not functioning properly, and barely did anything to stabilise the temperature during the tests. As a result, when the rig was manned and watched during the day, the T_b had to be continually tweaked in order to keep the temperature stable. Overnight however whilst the temperature would stay stable for a few hours, it would often swing over a range of up to 3-4°C. The precise reason for this is unknown; it could be due to fluctuations in the control system or band heater power, but another possibility is that a change in room temperature overnight was the cause. Due to large variance in T_b, when just the T_w was plotted versus time for all the data it was not possible to draw any correlations from the plots. However, once the T_b was subtracted from the T_w, all of the experiments showed a close to linear rate of fouling.

The fouling rates were calculated for each of the tests, and for both thermocouples T_{wb} and T_{wm} (the top and middle ones respectively), T_{ws} was not measured as a previous thermocouple had snapped off in its hole and could not be removed.

6.2 Calcium Carbonate Test Results and Analysis

The results of these tests are shown in Table 3 and plotted in a graph of fouling rate versus stirrer speed (Figure 18); the fouling rates measured by both of the thermocouples are shown.

Table 3: The effect of stirrer speed on the calcium carbonate fouling rate measured by T_{wm} and T_{wb}

Test Date	Speed (RPM)	Fouling Rate T_{wm} ($m^2°C/kW/h$)	Fouling Rate T_{wb} ($m^2°C/kW/h$)
25th October 2012	200	0.0053	0.0056
9th October 2012	300	0.0019	0.0033
30th October 2012	400	0.0012	0.0010
31st October 2012	500	0.0000	0.0000

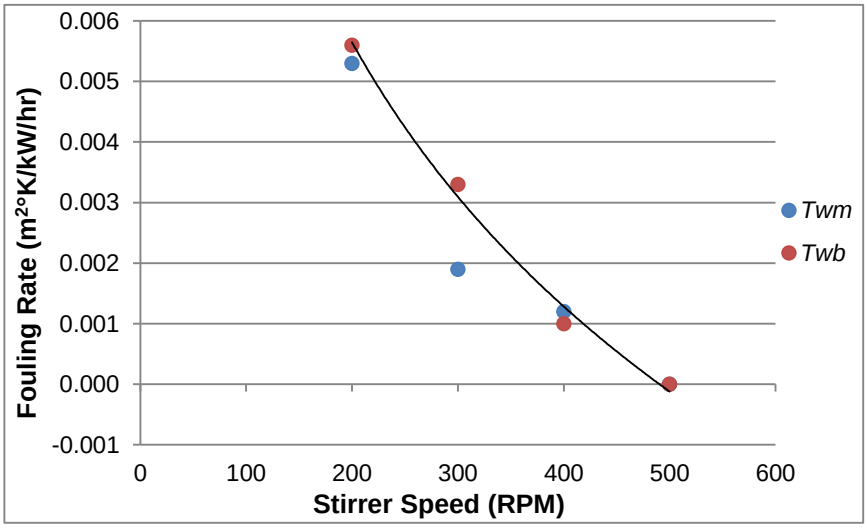

Figure 18: Fouling rate versus stirrer speed for calcium carbonate fouling, recorded by T_{wm} and T_{wb}

Of note is that the fouling rate in these tests measured by both thermocouples was almost identical for all points except for the 300RPM test. This suggests that the fouling rate was not significantly impacted by the difference in T_w. The temperature difference between the thermocouples was typically between 4-7°C. As Figure 18 shows, the fouling rate drops with stirrer speed as the shear stress gradually increases. This correlation is not quite linear however, and when a trend line is fitted to the data it is slightly curved. This is a similar correlation to that found with a negative helical threaded sleeve and a smooth surfaced sleeve in the rig (Crittenden *et al.,* 2013). The fouling shear stress threshold was found to occur at 500RPM for the helical threaded sleeve. According to Figure 10, this was a shear stress of around 0.45Pa. By comparison to previous tests with other sleeves, the fouling threshold at which fouling stopped due to shear stress increase was not found. The reason for this is that the helical threaded sleeve generates the highest shear stresses around the heat transfer surface of the three sleeves resulting in it having the lowest level of fouling.

For the full results and analysis of how fouling rates are affected by the different sleeve surfaces see Appendix 1.

6.3 Calcium Carbonate Fouling Removal Test

In November 2012, a final calcium carbonate fouling test was carried out to see if it was possible to remove a fouling deposit by increasing the stirrer speed and thus shear stress. This test was performed using the raised helical metal sleeve, and at typical fouling conditions of 120W CH power, 55°C T_b with $CaHCO_3$ and $CaCl_2$ concentrations of 1.26g and 1.1g respectively. To ensure there was a significant deposit to try and remove, the test surface was not cleaned following the previous fouling run. It was also allowed to foul for several hours at 100RPM stirrer speed before removal was attempted. During the run the stirrer speed was increased first to 600RPM, and then to 800RPM: even after 10 hours at 800RPM no deposit removal was observed. This is what was expected and confirms what Yang *et al.* (2002) found in their paper.

6.4 Calcium Carbonate Summary

This chapter has discussed and analysed the results of the calcium carbonate fouling experiments that were conducted. A correlation between stirrer speed and fouling rate on a test surface with a positive helical coil was found. Finally a test was performed to see whether fouling removal of a calcium carbonate deposit was possible, and it was not. The results of the fouling tests with crude 19 are detailed in the next chapter.

CHAPTER 7

7 Crude 19 Test Information, Results and Analysis

This chapter presents the results of the tests with a crude oil provided by HTRI referred to as ‘crude 19’. The aim of these tests was to find the conditions under which it would foul.

7.1 Crude 19 Background

Crude 19 was received in December 2012 and tests with it started in mid-January 2013 after some initial problems with the rig holding pressure (see Chapter 5.3). Crude 19 is a very light crude, with a high proportion of it being made up of saturates and has a particularly low level of asphaltenes. The composition of crude 19 is shown in Table 4; this data was provided by HTRI.

Table 4: The composition of crude 19

Component	Weight %
Saturates	54.85
Aromatics	37.52
Resins	16.35
Asphaltenes	0.98

The oil is a deep dark brown colour and is not very viscous; when swirled around in a glass bottle, it runs off the walls of the bottle very quickly. This is in stark comparison to some of the previous oils that have been used in the rig that are kept in the oil storage cupboard in the laboratory, which are more viscous. When these oils are swirled in their bottles they take several minutes for the oil to run down the bottle wall. Crude 19 has a strong smell of sulfur.

7.2 Crude 19 Test Information

In the first week of testing crude 19, there were repeated electrical problems with the rig that resulted in CHs repeatedly breaking. This problem is further explained in Chapter 5.4, but as a result of this it took around 3-4 weeks of down-time to find out what was causing the problems. Following this fouling tests were restarted again.

Overall in January-March 2013, 12 tests were carried out on crude 19 in order to try and find the conditions under which it would foul. The initial conditions were 230ºC T_b, 300º C T_w, 520W CH power, 100RPM stirrer speed and the T_w was gradually increased over the course of the experiments. In order to raise the T_w, the CH power can be increased but there is only so much that it can be raised by. This is because the maximum power of the CH is 750W. However, due to the severity of the conditions in the rig, the closer you get to the maximum, the more likely a CH is to fail. Realistically it is only a good idea to increase the power to around 550-600W, as even at this power the heaters have sometimes failed after only a few days. Therefore any higher would simply be a waste of time and money due

to having to regularly replace them. Consequently, the easiest way to increase the T_w is to raise the T_b of the crude. The band heaters can easily provide enough power to reach T_bs of 280ºC+.

The biggest difficulty with using crude 19 in the stirred batch reactor is due to how high a proportion of the oil is made up of light, low boiling point components. As previously stated, the rig vessel has a pressure limit of 30 bar: crude 19 would typically reach this pressure limit by the time the T_b was at around 220ºC. Consequently in order to keep the rig safe, some of the vapour, and therefore pressure has to be vented when 30 bar was reached. This then allows the rig to be heated higher until it reaches the pressure limit again, and the venting procedure should be repeated again. When venting vapour, the release valve should only be opened slightly and done very gently, otherwise there is a risk of liquid escaping through the valve as well as vapour. As the venting procedure began at around 220ºC, and the T_b in some tests was heated as high as 280ºC, understandably quite a reasonable amount of vapour had to be vented to get to this high a temperature. The conditions in all of the fouling tests that were carried out are listed in Table 5.

Table 5: A summary of the crude 19 fouling tests

Test Date	T_b (°C)	T_w (°C)	Speed (RPM)	Power (W)
17th January 2013	230	300	100	520
22nd January 2013	250	330	100	520
23rd January 2013	250	330	100	540
25th January 2013	250	325	130	520
19th February 2013	250	340	100	420
20th February 2013	250	350	100	500
21st February 2013	260	355	100	510
26th February 2013	237	348	100	520
27th February 2013	250	358	100	550
28th February 2013	250	350	100	550
29th February 2013	260	327	130	470
4th March 2013	280	388	100	600

7.3 Crude 19 Results and Analysis

As can been seen from the above table, the T_w was raised as high as 388ºC in an attempt to get the rig to foul. However, even at this high a temperature, and at as low a shear stress as possible with a stirrer speed of 100RPM, it was not possible to get the rig to foul. Figures 19-21 present graphs of fouling versus time from these tests. These graphs show that there was overall no positive increase in fouling resistance over the tests. Whilst in some of the tests there was a reasonable amount of scatter, the overall trend was a flat line for each. The conclusion that it was not possible to get crude 19 to foul in the stirred batch reactor fouling rig is in keeping with HTRI's finding that they were also not able to get it to foul in their tubular fouling rig either.

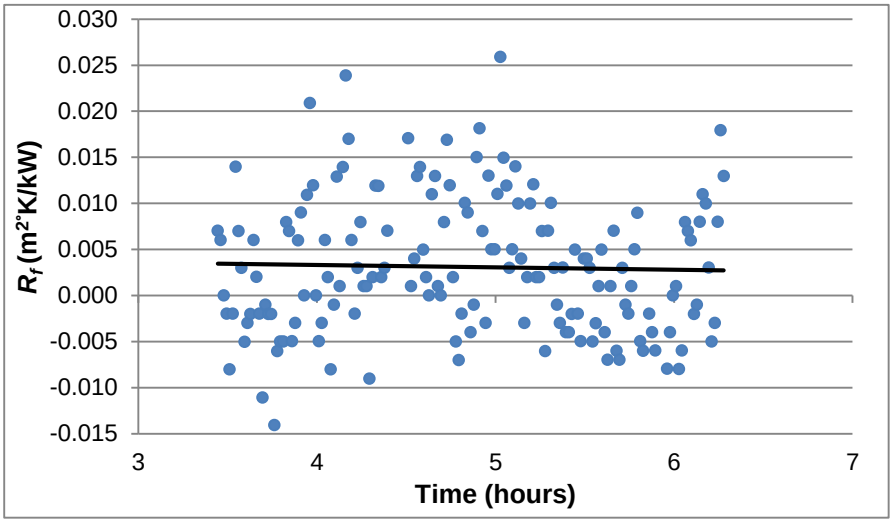

Figure 19: 22nd January 2013, 330ºC T_w, 250ºC T_b, 100RPM, 520W

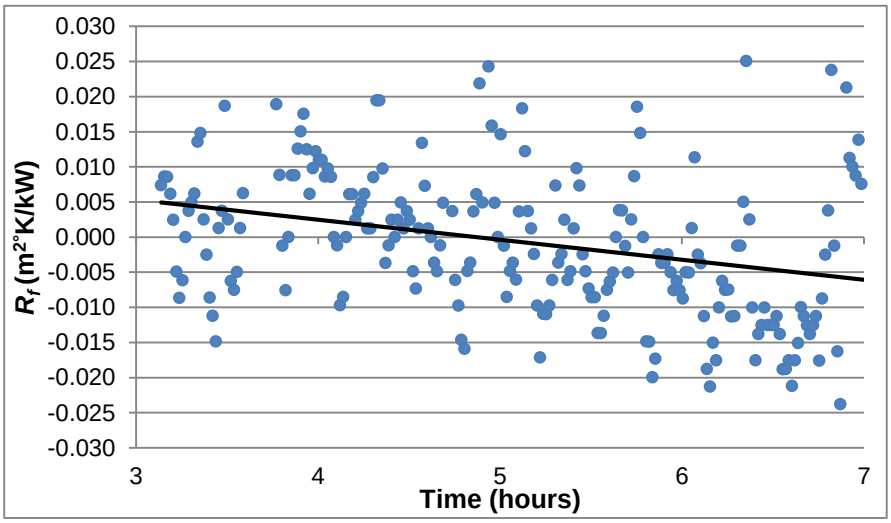

Figure 20: 19th February 2013, 340ºC T_w, 250ºC T_b, 100RPM, 420W

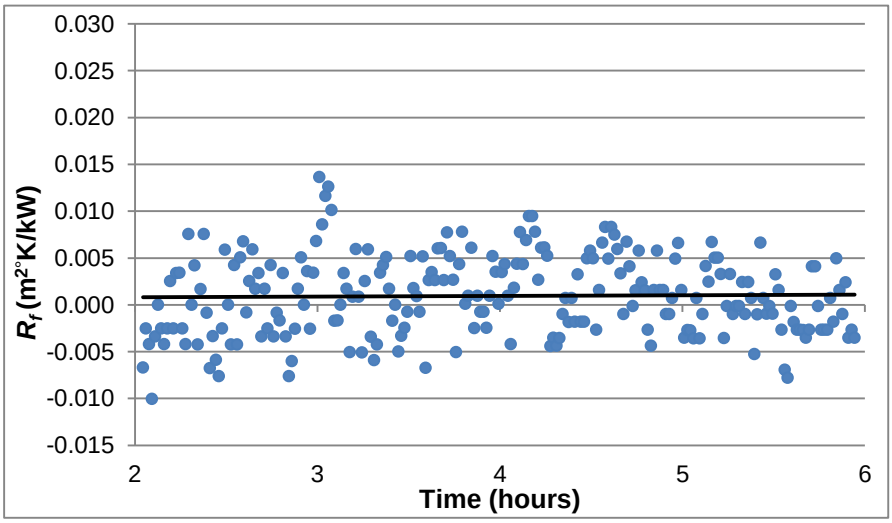

Figure 21: 4th March 2013, 388ºC T_w, 280ºC T_b, 100RPM, 600W

7.4 Crude 19 Summary

This chapter has detailed the results of the fouling tests that were carried out with crude 19, in which it was found not to be possible to get it to foul. Experiments conducted with crude 21 will be presented in the two next chapters.

CHAPTER 8

8 Crude 21 Heat Transfer Test Information, Results and Analysis

This chapter presents the results of the tests with a crude oil provided by HTRI referred to as 'crude 21'. The aim of these tests was to find the conditions under which it would foul. Problems were encountered during this initial work and a series of heat transfer tests were therefore carried out. Details of these tests are presented and their results and implications discussed.

8.1 Crude 21 Initial Observations

Crude 21 was received in April 2013 following the failure to get crude 19 to foul; the oil was also provided by HTRI. The oil is very similar to crude 19 in physical appearance: it is a dark brown colour and it has a low viscosity such that it quickly runs down the wall of a bottle when swirled around. This can be seen in Figure 22, a photograph which was taken shortly after the bottle was shaken so as to briefly cover the bottle walls at the top with oil.

Figure 22: A picture of a bottle containing crude 21

The rig was completely cleaned so that no traces of crude 19 remained, and then it was filled with crude 21 so that tests could begin. Initial tests showed two main issues. Firstly in order to get to even the minimum T_b for a fouling test (240-250°C), a significant amount of vapour had to be released during the heating up process the first time due to the vessel reaching its pressure limit of 30 bar by the time it had reached around 200°C. This was similar to what had happened with crude 19, and highlighted the fact that both are very light crudes compared to crudes previously tested with the rig. Secondly, and also similar to crude 19, in order to reach even a low fouling T_w of 340-350°C, a CH power of 500-600W and T_b of 250°C+ was required. These are far higher conditions than have been required with previous fouling tests using the rig, for example in tests conducted in October 2008 by Young *et al.* (2009) in which T_ws as high as 395°C were achieved at a T_b of 260°C and CH power of only 330W. A decision was therefore made that due to the severe nature of the conditions required to even begin fouling tests for crude 21, that heat transfer tests should be carried out to check the rig was functioning correctly.

8.2 Heat Transfer Test Background Theory

The aim of these experiments was to make sure that the T_w of the metal finger recorded by the thermocouples embedded inside it was being affected by the CH power and stirrer rotation as it should be. T_w is expected to increase linearly with CH power according to the basic heat transfer equation. The relationship between stirrer speed and T_w (and therefore HTC) however is more difficult to predict due to the complex nature of the fluid flow in the stirred batch reactor fouling rig. However, non-dimensional heat transfer equations to represent the heat transfer in a Taylor-Couette system, where fluid flows between two rotating concentric cylinders, developed by Poncet *et al*. (2011) can be used. Their equation is shown below: [21]

$$Nu = 0.0291 Re^{0.82} Pr^{0.3} C_w^{0.09}$$

Where C_w is a dimensionless volume flow rate coefficient calculated:

$$C_w = \frac{V_r}{\nu r_o}$$

Where V_r is the axial volume flow rate (m^3s);

r_o is the radius of the outer cylinder (m).

The biggest difference in the apparatus used to develop this equation by Poncet *et al*. (2011) was that the inner cylinder was rotating, whilst the outer cylinder was stationary. Whereas in the stirred batch reactor fouling rig the inner cylinder (the metal finer) is stationary and the outer cylinder (the agitation cup) is rotating. However, the overall geometry of the system is comparable and therefore the heat transfer correlations between speed of rotation and the heat transfer coefficient should be comparable.

When the stirrer speed of the rig is increased under constant T_b and CH power, the velocity of the fluid around the heat transfer surface goes up, and therefore so should the HTC according to Poncet *et al.'s* (2011) equation. The increase in HTC should then cause a drop in the T_w, as heat is transferred away faster from the wall. The equation expresses the HTC as part of the Nusselt number in the left side of the equation, and the velocity as part of the Reynolds number in the right side of the equation.

In this equation the power that the Reynolds number is raised to can vary dependent on the design of the heat transfer equipment, but around 0.82 was found to give the best fit by Poncet *et al.* for a Taylor-Couette flow situation. For a stirred batch reactor the Reynolds number is calculated differently to tubular flow according to the equation: [22]

$$Re = \frac{\rho d^2 N}{\mu}$$

Where N is the stirrer speed in rotations per second;

d is the diameter of the agitation cup in m.

For the purpose of using the Poncet *et al.'s* (2011) equation to investigate the effect stirrer speed has on HTC, some of the terms in the equation can be adapted, simplified or ignored.

The Prandtl number does not typically vary much, even as temperature is changed because the crude viscosity and thermal conductivity only change a small amount. The Prandtl number will therefore be omitted from the equation in this analysis. The number before the Reynolds number in the equation also varies dependent on the type of heat transfer situation and will not always be 0.00291 as in the original equation. It can therefore be represented by a dimensionless coefficient *a*. Finally, there is no way that the axial volume flow rate V_r can be measured using the rig and therefore it is not possible to include the dimensionless flow rate coefficient C_w in the equation. The only reason that axial flow exists in the rig is due to convection currents caused by difference in fluid density, which is not dependent on the stirrer speed. This term is therefore lumped into the coefficient at the start of the equation for simplicity.

Poncet *et al.'s* (2011) equation can therefore be simplified and expressed as:

[23]

$$Nu = aRe^{b}$$

Where *a* and *b* are dimensionless constants.

In order to test if the stirrer speed is affecting the HTC as expected, it is the constant *b* that must be calculated using data from the rig; this can be done using a log-log plot.

If *Log(Nu)* is plotted versus *Log(Re)* it should give a straight line of equation:

[24]

$$Log(Nu) = bLog(Re) + Log(a)$$

Where the gradient of the line is *b*, the constant in the simplified Poncet *et al* equation. If the HTC is varying with the stirrer speed as expected, the calculated constant should be somewhere around 0.8.

This analysis is still a large simplification of the rig, due to the complexity of it. However it is possible to more accurately predict the effect of stirrer speed on the HTC using CFD. Dr M. Yang at the University of Bath therefore simulated the rig under constant T_b and CH power with a varying stirrer speed and found that the constant *b* should come to around 0.45-0.5 with the rig if it is functioning correctly. This equates to around an 8-12ºC drop in T_w each time the stirrer speed is raised 100RPM.

8.3 Initial Heat Transfer Tests: Experiments, Data Processing and Results

In order to test that CH power increase caused a linear increase in T_w, only a single test was required. At a T_b of 200°C and stirrer speed of 100RPM, the T_w was recorded at different CH powers over the range 100-400W in 100W increments. Each time the CH power was changed, around 10-20 minutes was allowed for the T_w to stabilise before the T_w was recorded from this experiment are plotted in Figure 23.

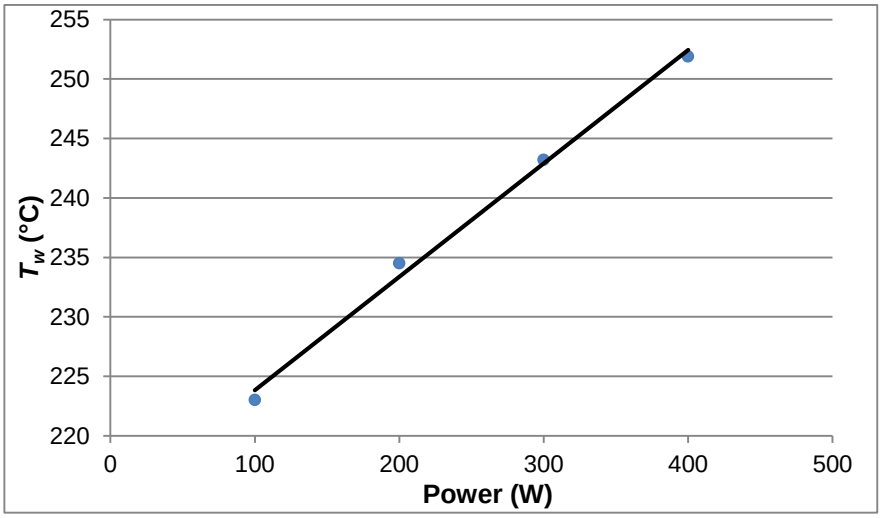

Figure 23: A graph to show the effect of CH power on T_w

As can be seen from Figure 23, the T_w increased linearly with the CH power as expected. This showed that the power output of the CH itself was functioning correctly.

In order to test the effect of stirrer speed on T_w a set of tests had to be carried out under a variety of conditions. In each of these tests the rig T_b and CH power were raised to set values and then kept constant, the stirrer speed was then increased from 100-400RPM in 100RPM increments. At each new stirrer speed the T_w was recorded. Each time the stirrer speed was changed, around 10-20 minutes was allowed for the T_w to reach steady state before its value was taken. This procedure was then repeated for a variety of different starting T_ws by varying the CH power.

In order to carry out the analysis of these results using the simplified Poncet *et al.* (2011) equation, the Reynolds and Nusselt numbers needed to be calculated. However in order to do this, various temperature dependent physical properties for the oil needed to be obtained. There was no physical properties data available for crude 21; however an analysis of the properties of crude 19 had been carried out by HTRI. As the two crudes seemed visually to be of very similar viscosity, it was assumed that they probably had quite similar physical properties. Therefore, a decision was made that it would not be too big an assumption to use the physical properties of crude 19 in the Reynolds and Nusselt number calculations. To make sure the two crudes did indeed have a similar viscosity, their values were measured using a rheometer at the University of Bath.

A rheometer measures the viscosity of a fluid at a gradually increasing rate of shear. Shear rate is a measure of the rate at which the different layers of a fluid move respective to each other. The units of it are 1/s. Measuring the viscosity of the fluid under different shear stresses produces a shear profile. The viscosity profile of each crude over a shear rate range of 0.4-4.44 was measured three times and the average of these measurements taken. The oil was at a constant 25°C in all the tests. Figure 24 displays the average viscosity-shear profile for the two crudes measured using the rheometer.

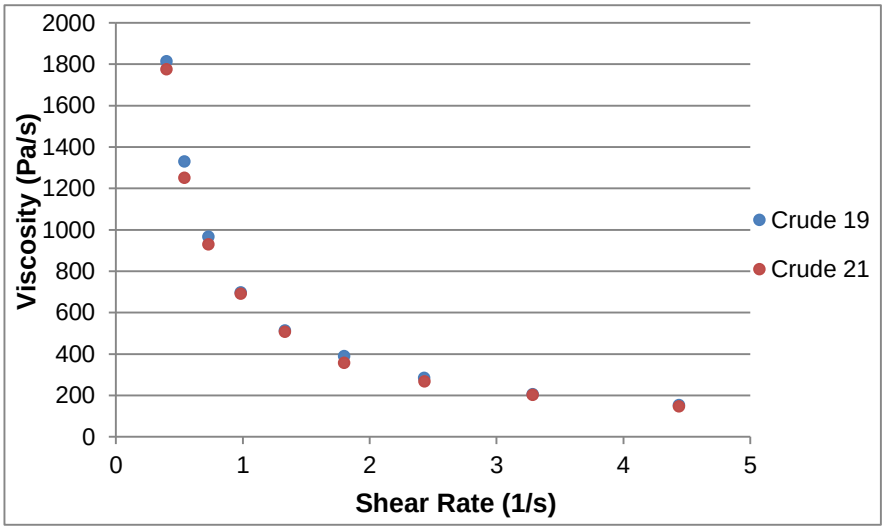

Figure 24: The viscosity-shear profile of crude 19 and crude 21

Two key conclusions can be drawn from the graph. Firstly, that the two crudes have a very similar viscosity at all the measured shear rates with an average difference between the points of only 3.6%. Secondly, that both oils are non-Newtonian shear thinning fluids i.e. the more shear force that is applied, the lower the viscosity gets. This data is only for ambient temperature however, it should be considered that once the crudes are heated (as in a test), that the shear profile would likely change. Crude oil is typically a Newtonian fluid at high temperature, therefore it is possible that the reason these crudes are non-Newtonian is that they have waxes present, as waxes have been previously been found to cause non-Newtonian behaviour in crude (Al-Fariss *et al*., 1992).

Physical property data available for crude 19 was the thermal conductivity, heat capacity, density and dynamic viscosity. This data was provided by Dr A. Smith at HTRI. These properties are all that are required to calculate the Reynolds and Nusselt numbers. The physical properties were presented in the form of equations to predict each relevant property based on the temperature of the oil.

These equations are presented below: [25]

$$\text{Density: } \rho = 5.081E^{-8}T^3 - 7.041E^{-5}T^2 - 1.64E^{-2}T + 5.346$$

Where ρ is density in lb/m^3.

[26]

$$\text{Thermal Conductivity: } k = 4.282E^{-5}T + 7.657E^{-2}$$

Where *k* is thermal conductivity in BTU/hr.ftºF.

[27]

$$\text{Heat Capacity: } C_p = -1.432E^{-7}T^2 + 6.51826E^{-4}T + 4.15585E^{-1}$$

Where C_p is heat capacity in BTU/lbºF.

[28]

$$\text{Dynamic Viscosity: } \ln(\eta) = 8.326E^{8}\frac{1}{T}^{3} - 3.412E^{6}\frac{1}{T}^{2} + 7.876E^{3}\frac{1}{T} - 6.918$$

Where η is Dynamic Viscosity in centipoise.

In these equations, *T* is temperature in ºF, except for dynamic viscosity where it is in ºR.

Because the crudes were non-Newtonian at atmospheric temperature, the viscosity calculated from the equation is not comparable to that measured by the rheometer. The data provided by HTRI was measured according to the standards of the 'American Society for Testing and Materials' and the values will have been for temperatures where the crude behaved as a Newtonian fluid.

For each heat transfer test performed, the T_b of the experiment was used to calculate physical properties using the above equations so that the Reynolds and Nusselt numbers could be calculated.

The other key values required for the Reynolds and Nusselt number calculations were the stirrer diameter *D,* and the HTC *h*. *D* was measured as 0.07m, and *h* was calculated for each stirrer speed using the rearranged basic heat transfer equation based upon the difference between the wall and T_b: [29]

$$h = \frac{Q}{A(T_w - T_b)}$$

The first few of these experiments were carried out at a T_b of 200°C with a power of 400-500W and stirrer speed was observed to have little effect on the T_w and therefore the HTC. A graph showing the T_w change with stirrer speed of a test at 200ºC T_b and 450W is shown in Figure 25.

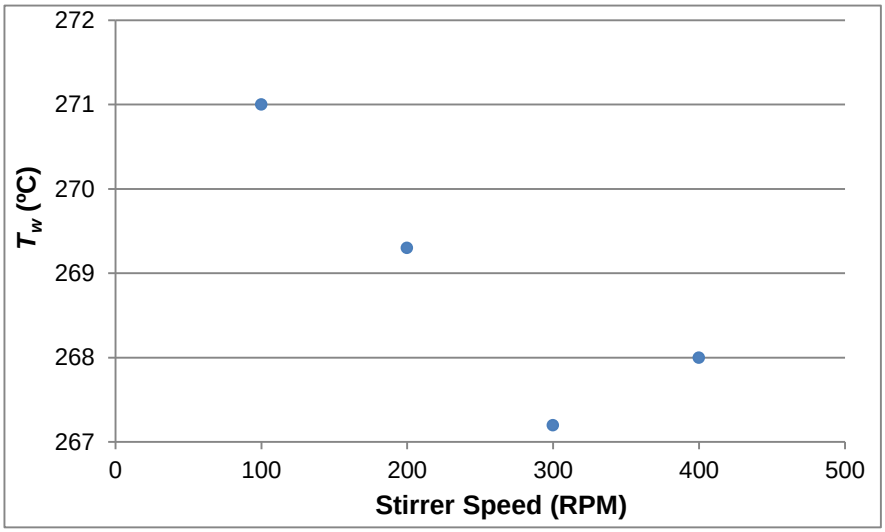

Figure 25: The effect of stirrer speed on T_w, 200ºC T_b, 450W

As can be seen in the graph, over an increase of 100-300RPM, the T_w only drops a total of around 3.8ºC. This is far less than the predicted 18-20ºC change by CFD. In addition, when the stirrer speed gets to 400RPM, the T_w goes up compared to at 300RPM. This is completely unexpected and at the time of the initial experiments was unexplainable. The experiment was repeated several times at different T_ws above 200ºC, and similar results were obtained each time. When the *Ln(Nu)* and *Ln(Re)* values were calculated and plotted for this data set, the constant *b* in the simplified Poncet *et al* equation was found to be around 0.04-0.05, again well below the 0.6-0.8 expected for normal single phase tubular heat transfer and the 0.45 predicted by CFD.

It was therefore decided to repeat the experiment at a much lower T_b, T_w and CH power to see if it made a difference. This was done at a T_b of 39.5ºC and CH power of 27W which gave a starting T_w of 56.5ºC at 100RPM. The resultant T_w versus stirrer speed graph and *Ln(Nu)* number versus *Ln(Re)* number graph are shown in Figure 26 and 27 respectfully.

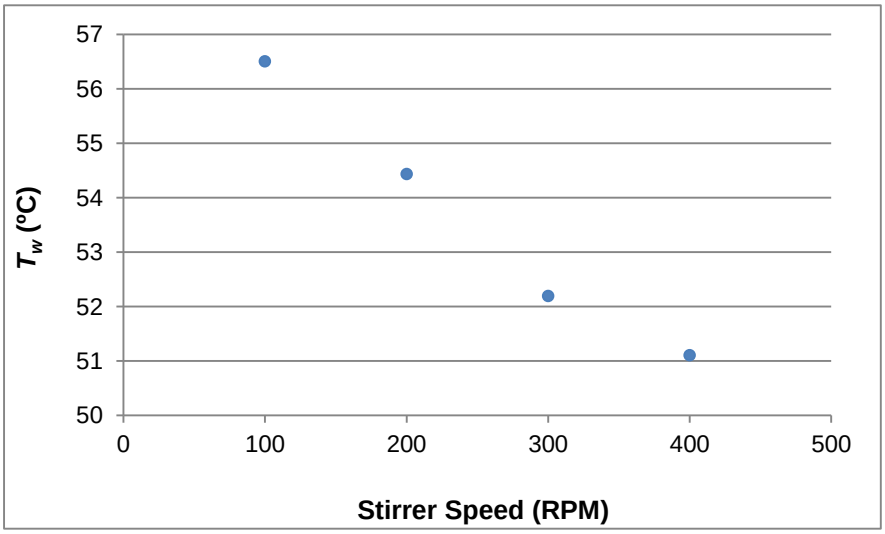

Figure 26: The effect of stirrer speed on T_w, 39.5ºC T_b, 27W

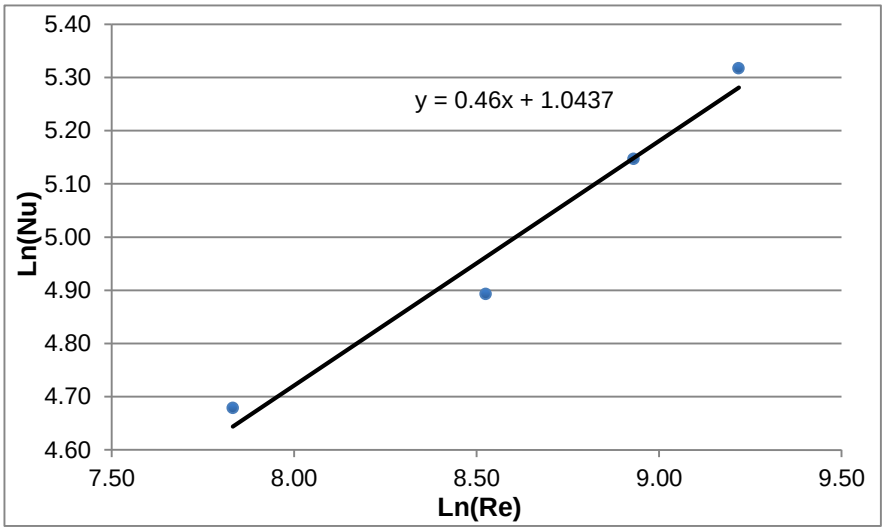

Figure 27: A dimensionless heat transfer plot for conditions 39.5ºC T_b, 27W

Figure 26 shows that even though there was such a low power and therefore ΔT between the T_ws and T_bs, the stirrer speed has a significant effect on the T_w. There was an overall change of 5.4ºC over the range 100-400RPM. This equates to a *b* value of 0.46 (Figure 27); very close to what CFD predicted.

8.4 Evidence for Nucleate Boiling in the Rig

From these initial high and low temperature heat transfer tests the conclusion was that whilst at low temperatures the rig seemed to be behaving as it would be expected to when stirrer speed is changed, at higher temperatures something was happening that was stopping it behaving normally. It was at this point that the hypothesis was made that the reason for this could be due to nucleate boiling on the surface of the metal finger. If this was occurring, then there would be a layer of bubbles in between the heat transfer surface and the bulk fluid that would reduce the contact between the two, and therefore the impact on heat transfer of increasing the fluid rotation speed. As well as the reduction in the effect of stirrer speed on T_w, several other observations and data sets suggested nucleate boiling was occurring. These will be presented below.

8.4.1 The Impact of Sudden Pressure Change on T_w

During a heat transfer test, it was discovered that if a sudden increase in pressure was applied to the vessel, a sudden spike in temperature was created that very rapidly then dropped back to its original level. An example of this occurring can be seen in the graph shown in Figure 28; in this case a sudden increase in pressure of around 2 bar was applied. As can be seen, this caused an instantaneous temperature spike of around +11ºC bar which then fell away within around 3-4 minutes (each point on the graph represents 1 minute).

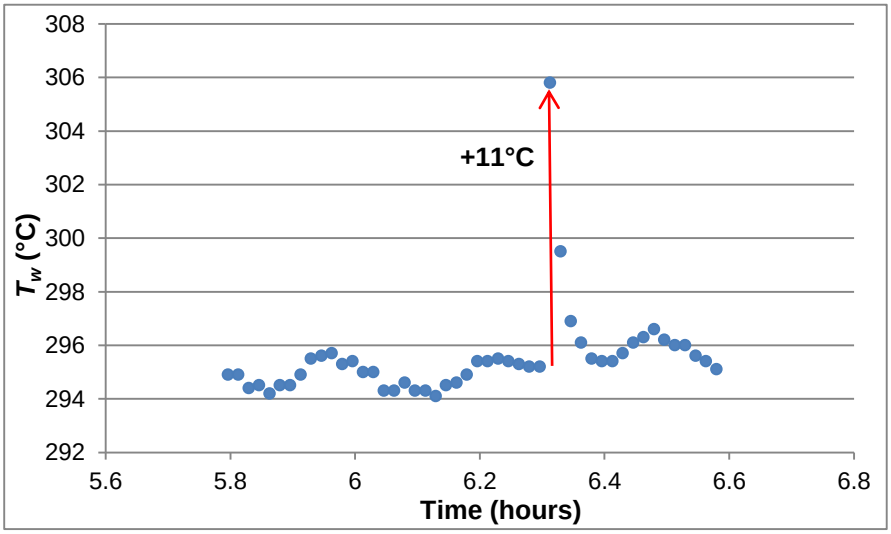

Figure 28: The effect of a sudden increase in pressure on the T_w for conditions 200ºC T_b, 100RPM, 500W

If there were just simple single phase liquid heat transfer occurring in the rig then pressure should not have any significant effect on the T_w. However, what seems to be happening here can only be explained by the occurrence of boiling heat transfer. Nucleate boiling heat transfer on a surface has a higher HTC than for just liquid heat transfer alone (Coulson *et al.,* 2007). It appears that the sudden pressure increase disrupts the layer of bubbles surrounding the surface of the metal finger, and for a very short time period the heat transfer mechanism becomes liquid phase heat transfer which causes the HTC to drop, raising the T_w. The nucleate boiling bubble layer then quickly reforms, the HTC increases and the T_w drops back to where it was initially. Increase in pressure should in theory supress boiling. However, as the temperature returned back to its initial level after the pressure was added it suggests the pressure increase was not sufficient to reduce the boiling.

8.4.2 Boiling Point Data

Some boiling point versus pressure data for crude 19 had been collected by HTRI. This data was input into the HTRI's physical properties package in their software Xist by Dr A. Smith at HTRI and a full boiling point versus pressure curve simulated; this is shown in Figure 29. Again whilst this boiling plot is not that of crude 21 but crude 19, due to their similarity in viscosity, as well as how they behave in the rig with regards to vapour release it is still a good gauge of crude 21's likely potential boiling temperature in the rig. It is also likely to have some error as it is a simulated curve based upon a data set.

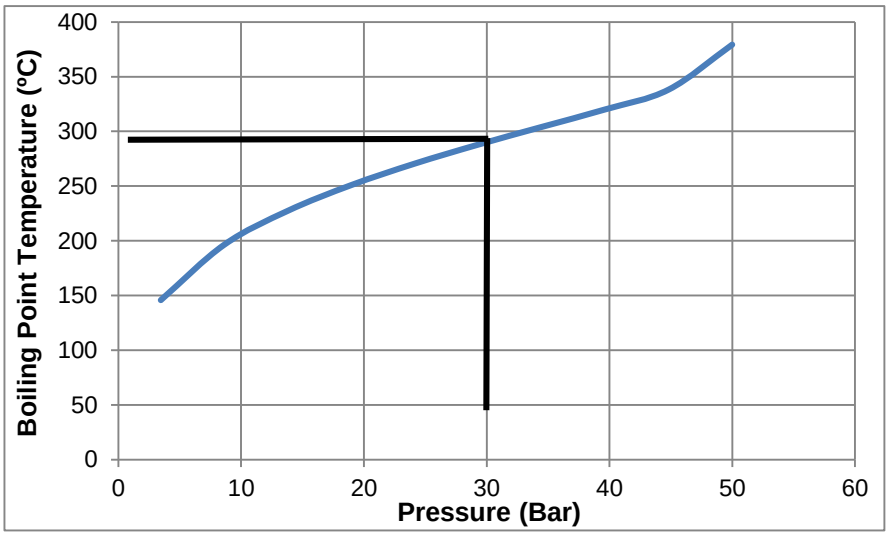

Figure 29: A boiling point temperature versus pressure plot for crude 19 simulated using HTRI software

The absolute maximum pressure the rig operates at is 30 bar. This point is represented on the graph by the black line and shows that at this pressure the oil would be boiling by around 280ºC. It is worth pointing out that the rig does not always operate at its maximum pressure of 30 bar, generally it is typically at between 25-30 bar, lowering the required temperature for boiling to occur further. Based on this plot, a logical conclusion is that the oil is likely to boil somewhere in the region of the temperature range 250ºC-325ºC. Thus in fouling tests which start from a T_w of 340ºC, there would definitely therefore be some boiling of the oil at this temperature based upon Figure 29. The heat transfer test shown in Figure 25 which first suggested that boiling was occurring started at 271ºC; again well within the region that Figure 29 suggests boiling would be occurring.

8.4.3 The Composition of Crude 21

An analysis of the chemistry of crude 21 was carried out by Intertek, Middlesex, UK. They were contacted initially to perform a SARA analysis of the oil. SARA analysis tests for the relative amounts of saturates, aromatics, resins and asphaltenes in the oil. However, Intertek advised that a typical SARA analysis vaporises and loses a large proportion of any lights in the oil and does not include this in the results. Therefore, if the oil is light it is better to first separate the C1-C9 fraction and measure the SARA of it, then measure the SARA of the rest of the oil and combine the results; this is what they did with crude 21. The C1-C9 fraction was analysed by gas chromatography, and the C10+ fraction analysed by high performance liquid chromatography and an IP143 asphaltene test.

This analysis showed that the oil C1-C9 fraction comprised 27.53% of the total volume, whilst the C10+ fraction made up the remaining 72.47%. This is quite a high proportion of C1-C9's, especially as this fraction will have a low boiling point in comparison to the rest of the crude oil. The composition of the oil is shown in Table 6.

Table 6: The composition of crude 21

Component	Weight of Oil %
Saturates	68.02
Aromatics	25.59
Resins/Polars	6.04
Asphaltenes	0.35

The oil also has a particularly low level of asphaltenes, especially in comparison to other oils tested in the rig previously which had asphaltene levels in the range of 2.87-8% (Young *et al*., 2009). Asphaltenes are some of the heaviest molecules in crude oil and therefore having a low level is another indicator of the crude being quite light.

8.5 Follow-Up Heat Transfer Tests: Results and Analysis

Based upon the above evidence, at least some nucleate boiling was occurring on the surface of the metal finger. This was causing the rig to behave differently compared with what would be expected with just single phase heat transfer. In order to better understand exactly when the boiling starts, and its impact on heat transfer in the rig, the stirrer speed heat transfer test was repeated with a wider range of T_ws. To ensure that there was no risk of boiling in the bulk fluid, the tests were performed at low, constant T_bs where possible. Figure 30 displays the results of a heat transfer test carried out over a single day. In this test the T_b was kept at 100ºC and the effect of stirrer speed on the T_w measured at a variety of different starting T_ws controlled by increasing the CH power each time. This was done with a fresh batch of oil.

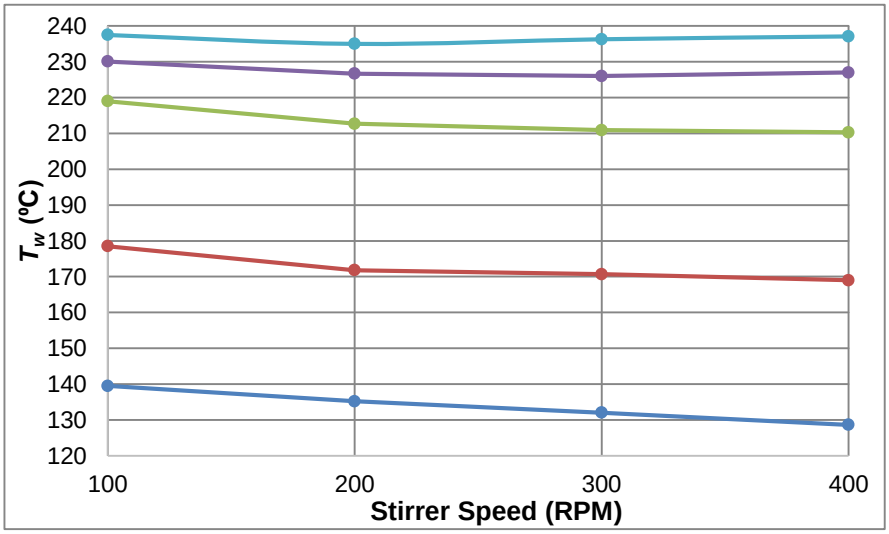

Figure 30: The effect of stirrer speed on T_w at a number of different starting T_ws, 100ºC T_b

This graph very clearly shows the effect of increasing stirrer speed on reducing the T_w. The effect gradually drops as the T_w reaches the temperature region where nucleate boiling starts to occur, above around 200ºC. This graph shows that for the first three lower starting T_w data plots, the T_w always goes down when the stirrer speed goes up. However once a starting T_w of 230°C was reached, after 300RPM the T_w went up instead. At a slightly higher starting T_w of 238°C after only 200RPM the T_w then started to increase.

It is difficult to explain what could cause the T_w to suddenly start increasing with stirrer speed. One possible explanation is that that the stirrer speed increases the HTC sufficiently so that the boiling type goes past the critical heat flux, from nucleate boiling and into transition boiling. The result of this would be that the HTC would then drop, causing a drop in temperature. This is shown below in Figure 31, transition boiling is region IV on the graph.

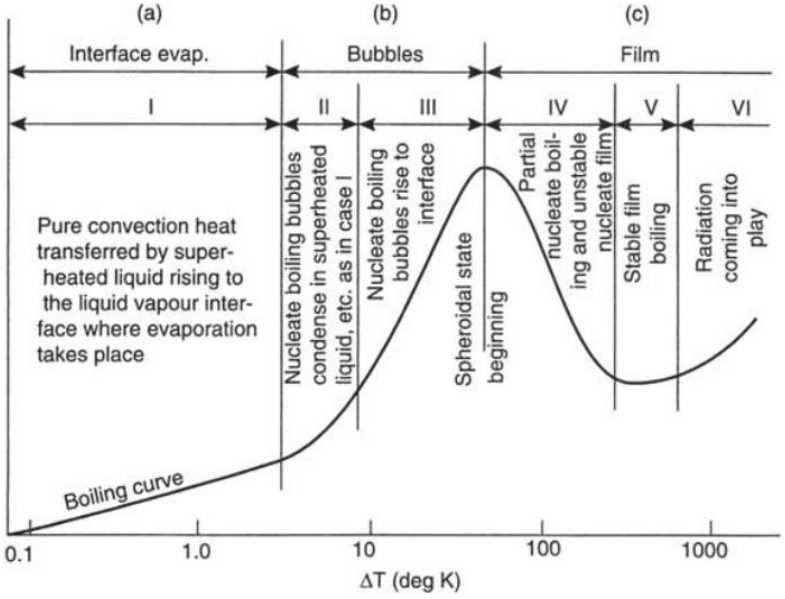

Figure 31: How boiling regime changes as HTC and ΔT increase (Coulson et al., 2007)

This explanation is further supported by the finding that whilst for fresh crude at 237°C, the T_w started going up after 200RPM, when a heat transfer test was done with a flashed crude at 350°C the T_w did not increase until after 300RPM. This can be explained by the fact that the flashed crude would have had a lower boiling point, and hence have a greater rate of heat transfer to it before reaching the critical heat flux. The critical heat flux is the crest in between regions III and IV on the graph.

Figure 31 shows that when ΔT increases under nucleate boiling, the rate of change in HTC with it increases. Thus if there was nucleate boiling occurring on the surface of the metal finger in the heat transfer tests, if ΔT is plotted versus HTC for a single stirrer speed a similar trend would be expected. A graph of the temperature change versus HTC is plotted (Figure 32) for the data points measured at 100RPM. The first 2-3 points of Figure 32 are roughly in a straight line; this is what would be expected for single phase heat transfer. After this, however, it starts to curve upwards and the graph clearly shows that the change in the HTC is increasing as ΔT goes up. This only starts occurring past around 120°C. The shape of the graph agrees with the nucleate boiling section of the boiling regime graph shown in Figure 31. The third data point was when the T_w was at 220°C and therefore nucleate boiling has begun by at least this temperature. As the graph starts to curve up somewhere before the third point, it suggests that nucleate boiling begins earlier than this, probably around 200-210°C.

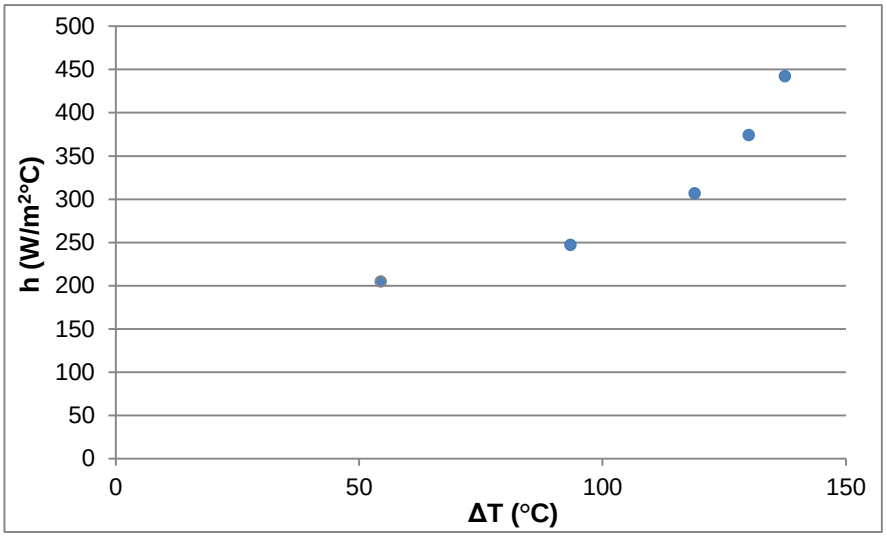

Figure 32: ΔT versus HTC at 100RPM

The heat transfer tests shown in Figure 30 were not the only stirrer speed tests done. There were many others conducted, but they were done at a variety of different T_bs and T_ws. A summary of all the tests conducted is presented in Table 7. The results of each of these tests were used to calculate the Reynolds and Nusselt numbers and these were then plotted so that the constant *b* could be calculated. The calculated constant *b* for all of the different starting T_ws is shown in Figure 33.

Table 7: A list of the heat transfer tests

Test Date	***T_b* (°C)**	***T_w* (°C)**	**Speed (RPM)**	**Power (W)**
12th April 2013	150	226	100-400	500
16th April 2013	120	209	100-300	500
18th April 2013	200	254	100-400	450
19th April 2013	50	68	100-400	50
13th May 2013	237	353	100-400	500
15th August 2013	39.5	56.5	100-400	27
19th August 2013	200	289	100-400	400
29th August 2013	100	140-237	100-400	100-500

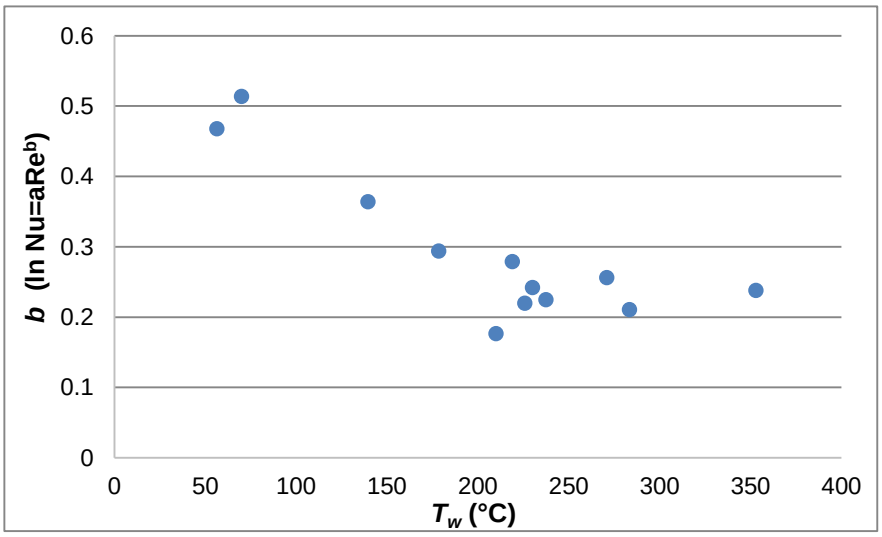

Figure 33: The calculated Reynolds power versus starting T_w for all heat transfer tests

Figure 33 shows the declining effect of increasing stirrer speed on the T_w; between 56°C and 187°C *b* gradually drops. After 178-200°C equilibrium appears to be reached and any further increase in T_w does not seem to impact the constant, and therefore stirrer speed does not have any further effect on temperature change. This graph confirms the findings of Figure 32; that nucleate boiling is having an impact on the heat transfer results by at least 200°C. The constant seems to start dropping significantly between 150-180°C, so it is likely that nucleate boiling actually begins to occur at some point in this range.

8.6 The End Effect: Evidence for its Occurrence and its Implications

Whilst nucleate boiling on the heat transfer surface seems a key contributor to the T_w not responding to an increase in stirrer speed, there are other possible causes. The first one is due to what is referred to as the end effect. The end effect refers to the fact that in the rig, not all of the heat being produced by the CH goes through the vertical walls of the metal finger. Some heat conducts through the bottom of the finger and through the cell base, whilst some also conducts through the top of the finger. The proportion of the heat flux transferred through the metal finger wall compared to the total heat flux of the CH can be represented as a factor. However, the only way this factor (which will be referred to as the end effect factor) can be estimated is by using CFD. The end effect factor also changes with stirrer speed, as the higher the stirrer speed then the higher the rate of heat transfer through the metal finger's wall is increased compared to than through the top or bottom. The end factor at different stirrer speeds is shown in Figure 34. This was simulated by Dr M. Yang at the University of Bath; full results summaries of the CFD simulations he carried out can be found in Appendix 2.

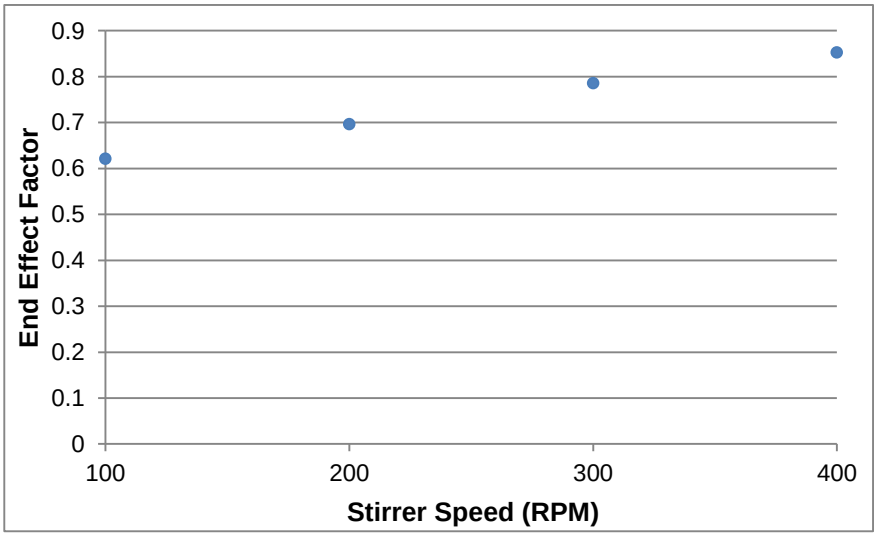

Figure 34: End effect factor versus stirrer speed for crude oil at 100°C T_b

This factor also changes based with the T_b, as this will impact on the ΔT and therefore the temperature driving force. The end effect factor at three different T_bs, 39°C, 100°C and 200°C and at all 100-400RPM was simulated by Dr M. Yang at the University of Bath with

the results plotted in Figure 35. The equation of each of the lines can be used to predict the factor at a given T_b for each stirrer speed.

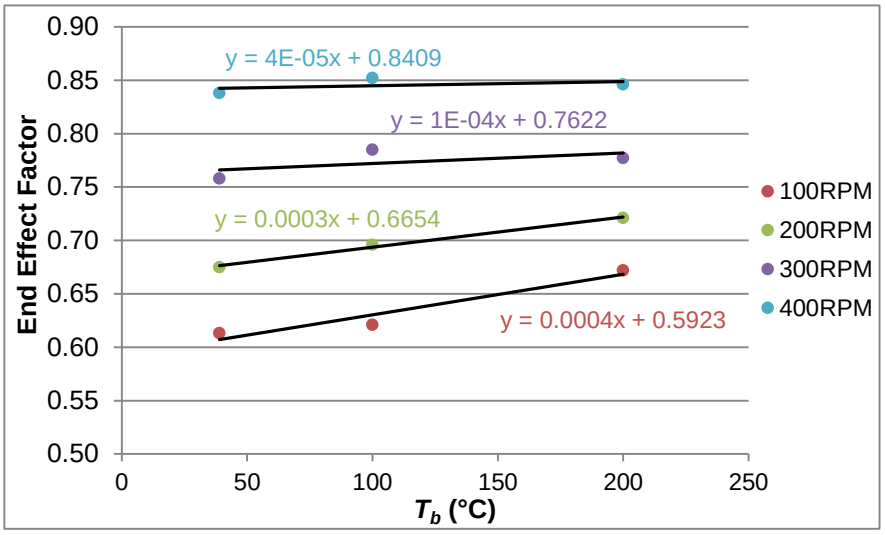

Figure 35: End factor versus T_b at increasing stirrer speed

When the end effect factors are applied to the different initial heat fluxes for the data set shown in Figure 30, the following graph (Figure 36) is produced.

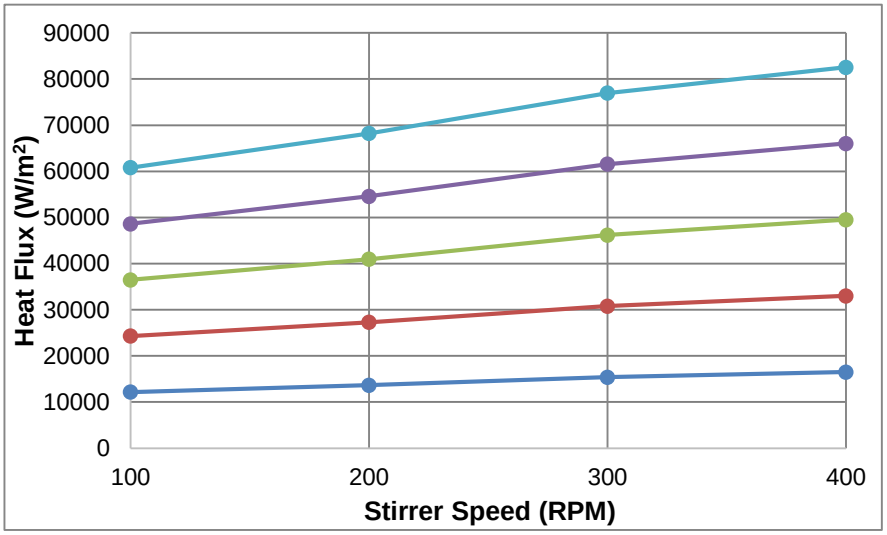

Figure 36: The calculated heat flux for each of the data points depicted in Figure 30

Figure 36 shows that there is a far higher change in the overall heat flux over the 100-400RPM stirrer speed range at higher initial heat flux, and therefore T_w. This is due to the way the factor causes the heat flux to scale, for example a change in end effect factor of 0.62-0.85 at a CH power of 100W changes the heat flux by 4800W/m^2, whereas the same factor change for an input power of 500W changes it by 22100W/m^2. The impact of this effect is that at a higher starting CH power and T_w, the amount of heat passing through the walls is increasing a greater amount as a function of stirrer speed compared to at a lower CH power and T_w. This causes the T_w to increase slightly with stirrer speed, counteracting the decrease in T_w caused by increase in the HTC.

This change in heat flux at increasing stirrer speed and initial T_ws has an influence on the calculated HTCs for each data point. In Figure 30, temperature was seen not to change very much with stirrer speed; this would generally suggest that the HTC is not changing much. However, when the HTCs are calculated from this data and plotted they are seen to be still increasing with stirrer speed (Figure 37).

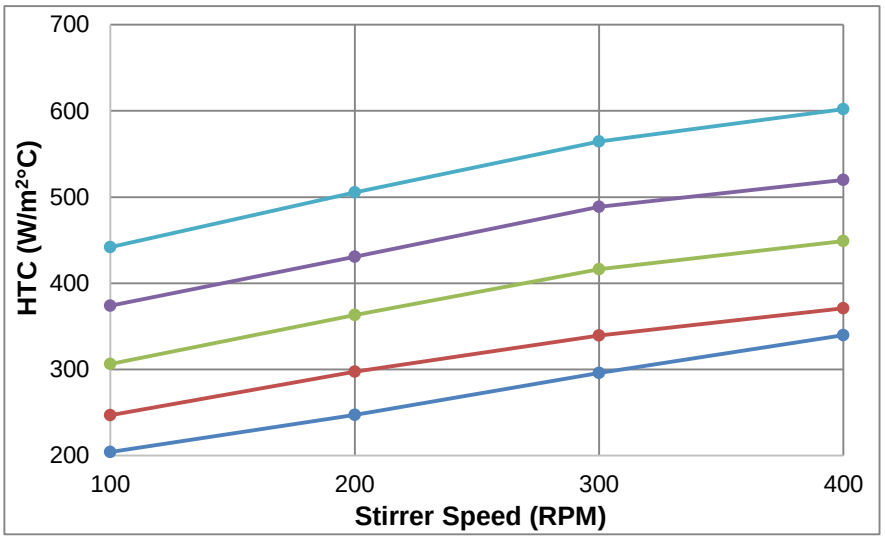

Figure 37: The change in HTC for the data from the heat transfer test described in Figure 30

Therefore, what appears to be happening is that in the calculation of the HTC whilst typically the change in T_w is the controlling factor in increasing the HTC, in this case it is the heat flux that is instead the dominant change. This is best expressed by restating the rearranged basic heat transfer equation:

$$h = \frac{Q/A}{T_w - T_b}$$

There are two ways that *h* in the left hand side of the equation can be increased, either *Q* can increase, or T_w can decrease. Typically both will change, but it is the amount that each changes that is important here. For the lower temperature test, the T_w significantly decreased with stirrer speed (Figure 30), whilst the heat flux only increased by a small amount (Figure 36). It is the change in temperature that controls the change in *h* as stirrer speed increases in this case. Comparably for the higher temperature test, the T_w barely changed (Figure 30), but the heat flux increased significantly (Figure 36); it is the change in *q* that controlled the change in *h* this time.

The overall effect of the end effect can therefore be used to some extent to explain how it is possible that the T_w did not drop as much at higher temperatures with stirrer speed. It also explains how it is possible for the T_w to go up after 200RPM for the highest temperature test. Here the increase in heat flux due to end effect factor increase was higher than the increase in HTC due to stirrer speed. Therefore, whilst there would have been a drop in temperature due to HTC increase, a greater increase in temperature was caused by the heat flux increase, resulting in an overall positive temperature change.

Of note is that whilst the calculated HTC did increase with stirrer speed at higher T_ws, it did not increase anywhere near as much as CFD predicted. The CFD simulations estimated that the HTC would increase by 470W/m^2°C across the 100-400RPM range, whereas in reality it only increased by 160W/m^2°C. This restates the issue that something was definitely still preventing the HTC from being influenced as much as it should be by stirrer speed, even if the reduced T_w change can be partly explained by the end effect. It is therefore likely that nucleate boiling accentuates the problem alongside the end effect.

8.7 Natural Convection in the Rig

Another possible cause of the T_w not responding to an increase in stirrer speed at high temperatures is that natural convection is occurring. Natural convection is where a fluid moves based on differences in density caused by temperature difference. When this occurs, convection currents are created. Natural convection typically occurs more at higher ΔTs (Coulson *et al.*, 2007). In the stirred batch cell rig, most heat transfer will be by forced convection, as the movement of the fluid by the stirrer is what drives heat transfer. Natural convection will still be occurring, but to a much less extent than forced convection, this is called mixed convection. Although it is possible that at higher ΔTs the amount of natural convection becomes more prevalent, if this did occur then a convection current layer could surround the heat transfer surface, reducing the effect of increase of stirrer speed on the HTC and T_w. It is, however, quite difficult to prove whether a significant amount of natural convection is occurring. Never the less, if natural convection was occurring, the following relationship would be expected to apply: [30]

$$\frac{hL}{k} = C'\left(\frac{C_p\mu}{k}\frac{g\beta\rho^2(\Delta T)D^3}{\upsilon^2}\right)^{0.25}$$

(Coulson *et al.*, 2007)

Where β is the volumetric expansion coefficient;

C' is a dimensionless constant;

υ is the kinematic viscosity (m^2/s).

All of the physical properties in the equation would stay the same at constant T_b with the consequence that when T_w is increased, the only values that would change are h and T_w. The relationship between these two would therefore be: $h = \Delta T^{0.25}$. It is therefore possible to check if natural convection is occurring by seeing if the data does have this relationship by plotting *log h* versus *log* T_w. If natural convection occurs then the line of the graph would have a gradient of 0.25. However, as Figure 32 shows, there is a nonlinear relationship between ΔT and h, and therefore this relationship was not seen. Whilst this suggests that natural convection is not occurring significantly, it is likely that it is still occurring to a small amount; however, how much cannot be judged. There may well be some convection

currents that are reducing the effect on stirrer speed slightly, but it is likely that nucleate boiling and the end effect are influencing it more.

8.8 Crude 21 Heat Transfer Tests Summary

In conclusion it is unlikely to be a single problem that is causing stirrer speed to affect the T_w and HTC as much as expected. Nucleate boiling seems to be the key cause as there is so much evidence in favour of its occurrence. From the various graphs, nucleate boiling seems to begin occurring somewhere in the range 150-200°C. The end effect also seems to have a quite significant effect on the T_w, and it definitely has a large effect on the heat flux variation with stirrer speed. This is something which has not been considered with the rig before, or in calculations, and it would be of value to find out how much it impacts the T_w for a crude oil where nucleate boiling is not occurring. Lastly it is possible that natural convection currents surrounding the metal finger are occurring and impacting the heat transfer test results, but there is no easy way of finding out the extent of the impact if any. The fouling investigations with crude 21 conducted following this heat transfer work are now presented.

CHAPTER 9

9 Crude 21 Fouling Tests Information, Results and Analysis

This chapter details the results of the fouling experiments with crude 21 investigating the effect of stirrer speed and T_w on the fouling rate. The results of the tests to see if a crude oil fouling deposit could be removed by increasing the shear stress are also presented.

9.1 Getting the Oil to Foul

The initial aim of the first crude 21 tests was to find the T_w at which it would start to foul. As with crude 19, tests started at a low T_w of around 300°C, and the T_w was then increased over the following tests. Tests went up to a T_w of 355°C and no fouling was observed. Following this testing during the start-up heating procedure of the oil, the band heaters were accidentally set higher than normal. During start-up the band heater Variac is typically set at 160W; this time they were set at 200W. It was also shortly after the band heaters had been replaced after breaking, and their change in heating potential had not been properly gauged in terms of the rate at which they heated the crude bulk. The effect of this with crude 21 (which is very light), is that it started to vaporise and the pressure increased at a far higher rate than a typical test. This was probably because the oil started boiling on the walls of the vessel. Hence, a substantial amount of vapour had to be released from the vessel using the gas release valve. As previously outlined, with crude 21 some gas always had to be vented during start-up when getting it to a T_b of around 240°C. However, on this occasion the pressure rise and resultant required gas release was far greater. Following this the band heater power was reduced and the start-up heating procedure carried on as normal until the test T_b of 249°C was reached. The fouling test then began at a T_w of 347°C and it started fouling within an hour. This took place after a number of the heat transfer tests, and conclusions already drawn that nucleate boiling was likely to be occurring on the surface of the metal finger where fouling should take place. It was, therefore, hypothesised that a possibility was that the over venting of the crude oil had flashed it, reducing its boiling point and consequently either stopping or reducing the nucleate boiling on the fouling surface. Once this had stopped, fouling was then able to occur.

Following this event, several weeks of successful fouling tests took place before the rig was emptied and refilled with a fresh batch of oil. Tests began at the temperatures that fouling had been occurring at before with the previous batch oil crude oil: around 345-350°C, but no fouling was observed. The T_w was then gradually increased in tests over the following week until eventually it had reached 370°C and still no fouling was observed. To reach this high a T_w, the T_b had also been gradually increased each day until it was at 260°C. As the T_b was increased, gradually more and more vapour had to be released as the pressure rose with the temperature each time. By the time 260°C T_b was reached, quite a significant amount had been vented. As the high T_w test had still not produced any fouling, a decision was taken to do one more test at the previous conditions under which fouling had taken place. A run was done therefore at 350°C T_w and it started to foul again. It seems that for

the second time that crude 21 would only start fouling once a certain amount of its light end fraction had been released. Later, after all the fouling tests were completed, the oil was removed from the rig and it was observed that around 14-18% of the initial 1 litre put in the rig had been lost through the venting. Given the C1-C9 fraction of the oil was measured to comprise 27.53% of the oil (see Chapter 8.4.3); at least half of this fraction seems to have been lost.

Based upon these tests on two batches of crude 21, as well as the findings from the heat transfer tests, nucleate boiling seems to be inhibiting fouling from occurring. This is most likely because of the increased turbulence that is created by the rapid production of bubbles on the fouling surface. This turbulence would increase the shear stress around the surface itself, reducing the chances of foulant particles sticking to the wall, and removing any foulant particles that do manage to stick to it. It is also possible that nucleate boiling inhibits fouling because the heat transfer surface is surrounded by a two-phase mixture; there is therefore less liquid phase oil in contact with it, reducing the chance of foulant particle deposition. It is also a possibility that nucleate boiling inhibits fouling by increasing the HTC of the heat transfer surface, thereby reducing the actual ST to below the fouling temperature threshold. As the stirred batch cell measures the temperature in the wall, around 1mm away from the actual heat transfer surface, it is not possible to measure if the actual ST has changed significantly with or without nucleate boiling. Whilst the T_w is a very good reference for what the ST is, CFD predicts it to be approximately 6-8°C less than the T_w for single phase heat transfer. It is not possible to tell how much the actual metal-oil interface temperature changes with boiling to know if this would drop it significantly to below the threshold temperature. The effects of turbulence and bubbling on the heat transfer seem therefore to be the most likely way that nucleate boiling inhibits fouling.

9.2 Fouling Results from the Different Thermocouples

There are two thermocouples in the wall of the metal test finger (T_{wb} and T_{wm}). These are designed to sit at different heights within the wall in order to measure if there is any difference in the fouling rate at different parts of the metal finger. The T_w changes across the height of the metal finger due to the way heat flux distribution varies across it (Yang *et al.*, 2009). Therefore, there is typically a difference in the fouling rate at the different thermocouples. The thermocouples are normally 10mm apart from each other in terms of their height up the metal finger, and they typically have a difference of 10°C in temperature. In all of the crude oil fouling tests undertaken, however, there was a negligible T_w difference recorded by the two thermocouples; typically between 0.5 and 1.5°C. This must have been because they both sat at a similar height up the metal finger. This is likely because when the thermocouples were put in place in January 2013, it was very difficult to fit them inside the holes in which they should sit without bending them and they were therefore inserted as far as they would go. One thermocouple was clearly, therefore, not pushed in enough.

Due to the similarity in T_ws and thus fouling rates, it was not worth plotting the fouling trends for both thermocouples in the fouling graphs for crude 21 in this report. Two data sets are now displayed to illustrate this point (Figures 38 and 39; Figures 40 and 41).

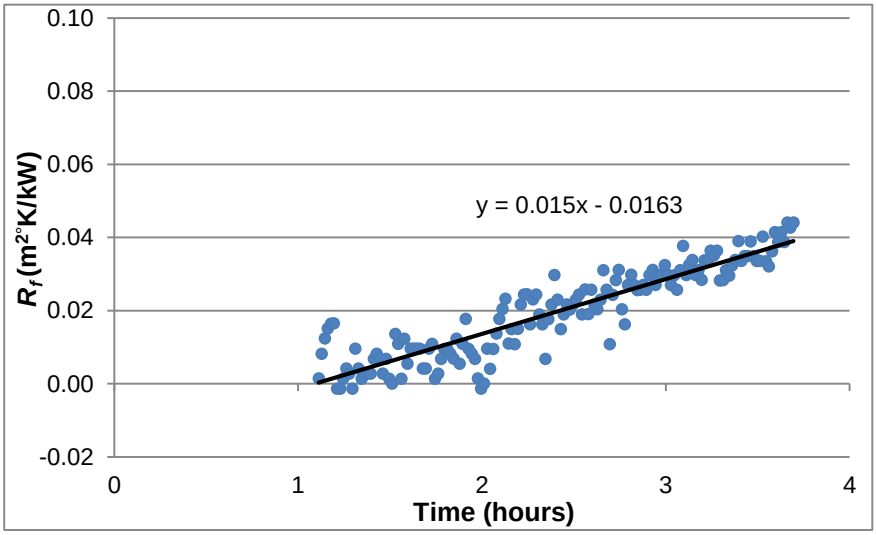

Figure 38: 28th August 2013 fouling plot recorded by T_{wb} with a starting T_w of 359.8°C

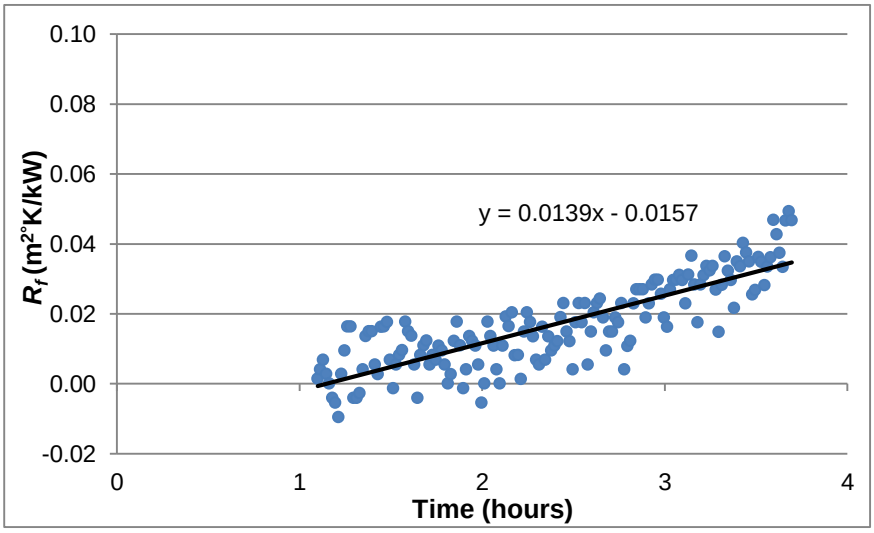

Figure 39: 28th August 2013 fouling plot recorded by T_{wm} with a starting T_w of 361°C

For Figures 38 and 39, the average difference in temperature measured by the two thermocouples was 1.2°C, and this difference resulted in a fouling rate difference of 0.0011m²°K/kW/hr.

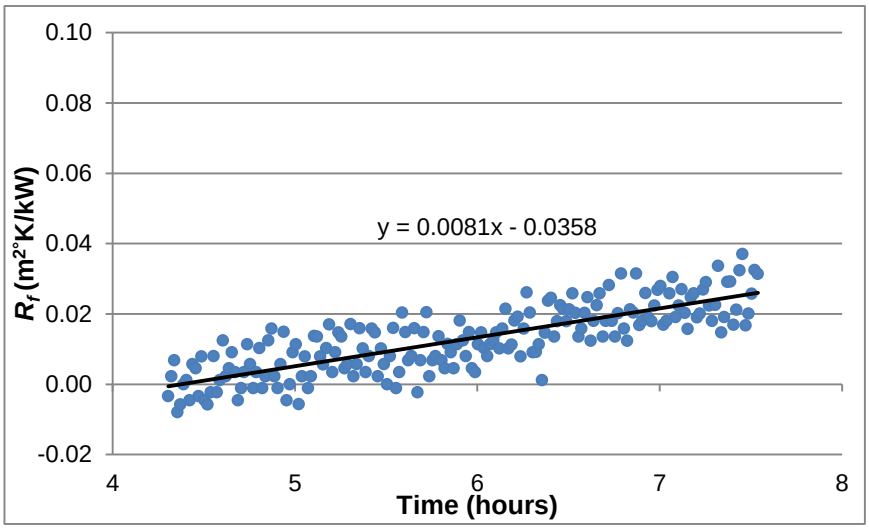

Figure 40: 26th July 2013 fouling plot recorded by T_{wb} with a starting T_w of 346°C

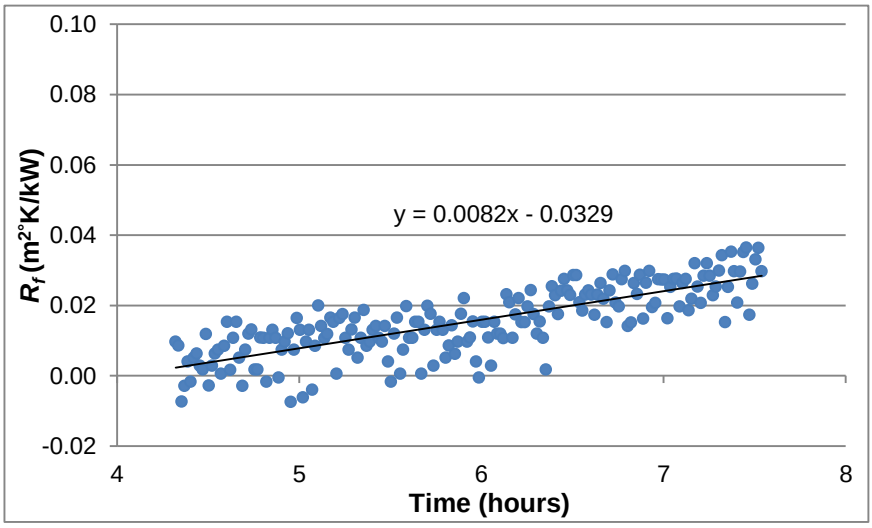

Figure 41: 26th July 2013 fouling plot recorded by T_{wm} with a starting T_w of 347.3°C

For Figures 40 and 41, the average difference in temperature measured by the two thermocouples was 1.3°C and this difference resulted in a fouling rate difference of 0.0001m²°K/kW/hr.

As can be seen in both sets, the difference in recorded temperatures and fouling rates between the thermocouples was negligible. Similar differences between measured T_ws and resultant fouling rates at the two thermocouples were recorded in the majority of the fouling tests.

9.3 Modification of the Method to Calculate R_f

In Chapter 8.6, the end effect was found by CFD simulation to strongly affect the heat flux as the stirrer speed increases. In the past, when fouling resistance calculations have been carried out using the data from the stirred batch cell, the end effect factor has not been accounted for, and the power input to the CH has been used. This is clearly not accurate

and hence the end effect factors at varying stirrer speeds and T_bs predicted in Chapter 8.6 have been applied to the heat fluxes in all R_f calculations in this thesis.

9.4 The Different Fouling Tests with Crude 21

Once fouling was achieved with the oil, a variety of fouling rate tests took place between May-August 2013. These tests can be split into three categories:

1. Measuring the effect of stirrer speed on the fouling rate.
2. Measuring the effect of T_w on the fouling rate.
3. Attempting to get negative fouling rates by deposit removal at high stirrer speeds.

The results of these different sets of experiments are now discussed.

9.5 The Effect of Stirrer Speed on Fouling Rate: Results and Analysis

The first three fouling rate tests were all performed at a stirrer speed of 100RPM. This was primarily to ensure that fouling definitely was occurring, and that the seeming increase in T_w over time was not being caused by anything else. Secondly they were undertaken to see if the fouling rate was consistent on consecutive days at similar conditions. Following this, experiments were run at increasing stirrer speed, with tests performed at 200, 300 and 400RPM to measure the impact stirrer speed had on the fouling rate. The details of these tests are shown in Table 8.

Table 8: A list of the fouling tests at varying stirrer speeds

Test Date	T_b (°C)	T_w (°C)	Speed (RPM)	Speed STDEV	Power (W)	Power STDEV	Fouling Rate (m^2°K/kW/hr)
7th May 2013	249	347-356	104	12.1	497.2	1.6	0.0333
8th May 2013	239	344-350	101	7.4	496.8	1.4	0.039
9th May 2013	239	350-358	101	9.7	501	2.4	0.0233
13th May 2013	239	344-348	202	11.6	504.7	2.9	0.0113
15th May 2013	239	342-344	301	18.1	504.5	2.2	0.0202
15th May 2013	239	343-343	405	14.3	509.5	1.2	0

Figures 42-44 are the fouling graphs of the first three tests at 100RPM; they were all conducted at approximately the same starting T_w, with a range of 345-350°C. The fouling plot of the test on the 7th May 2013 had the largest amount of spread, shown by its R^2 value of 0.37. This variance seems to have been caused by fluctuations in the stirrer speed, as of the three tests, it is the one with the biggest standard deviation in stirrer speed. This was most likely due to problems with the agitator that day, with it overheating slightly, making it far more difficult to control.

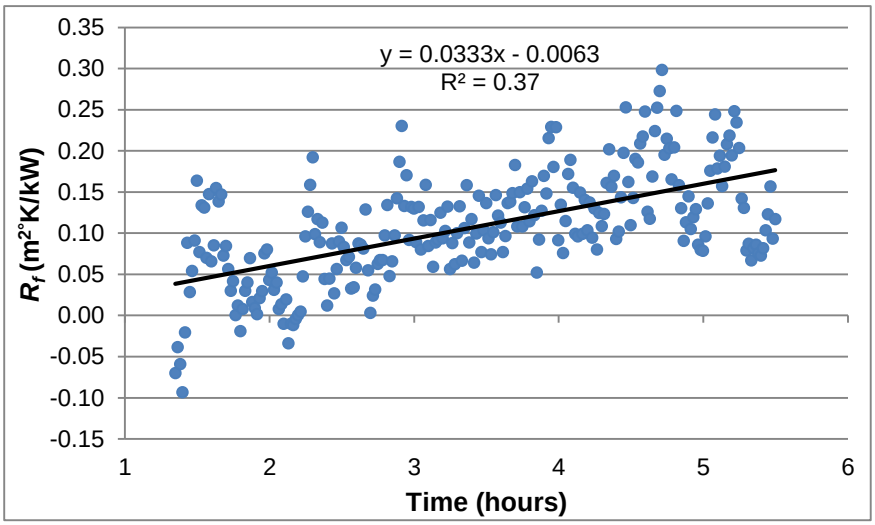

Figure 42: 7th May 2013, 347°C T_w, 240°C T_b, 100RPM, 500W

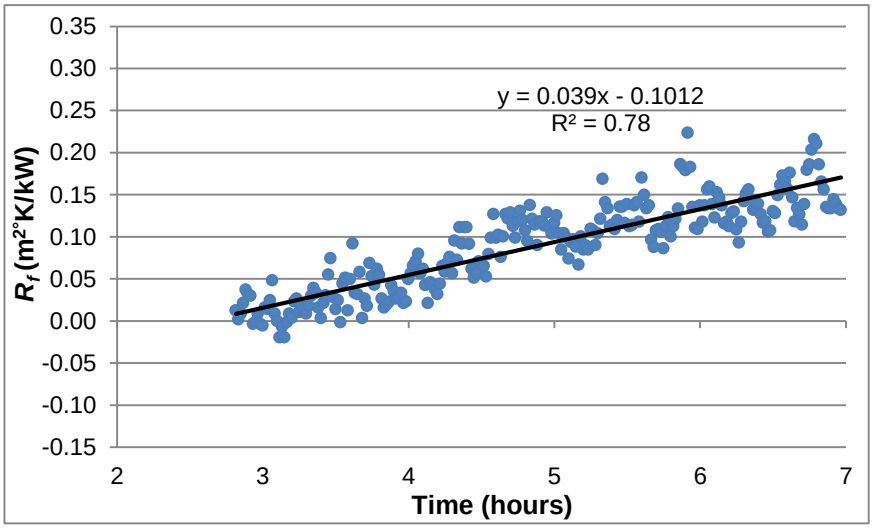

Figure 43: 8th May 2013, 345°C T_w, 240°C T_b, 100RPM, 500W

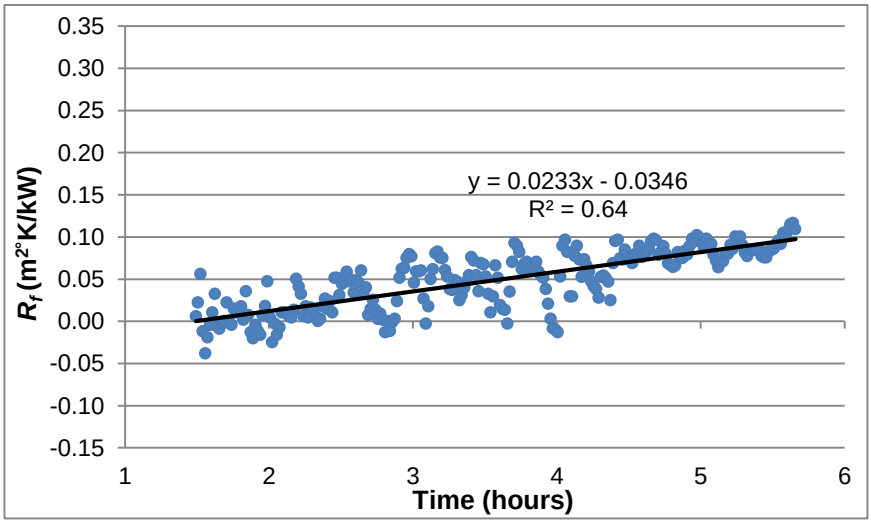

Figure 44: 9th May 2013, 350°C T_w, 240°C T_b, 100RPM, 500W

The change in standard deviation of the CH power was negligible for all of the tests, so it is unlikely that this variation caused much fluctuation in the T_w and therefore the fouling data. Variation in T_b does not have any effect on the calculated R_f or calculated fouling rate,

because as explained earlier (Chapter 4.1), the T_b is subtracted from the T_w and the variation in the resultant ΔT used in the R_f calculations. The overall level of data scatter in the tests on the 8th and 9th May 2013 was low, shown by the quite high R^2 values in Figure 43 and Figure 44 of 0.78 and 0.64 respectively. Variance in T_w and therefore R_f in these tests was again most likely to predominantly have been caused by stirrer speed fluctuation. The fluctuations seen in all three of the plots do not appear to have affected the overall correlation in them and therefore the fouling rates calculated from the trend lines fitted to the data can be taken to be accurate.

There was quite a large range in the measured fouling rates between the three tests of 0.0157m^2°K/kW/hr. However, there is no obvious reason for this finding; there was barely any difference in the average stirrer speed for each test and whilst the starting T_ws were slightly different, the temperatures do not correspond with the higher fouling rates. For example, the highest starting T_w of the three was the 9th May 2013 test at 350°C and this had the lowest fouling rate.

The fouling plots for the tests at 200, 300 and 400RPM are shown in Figures 45-47. Of note is that the 300 and 400RPM tests were done on the same day back to back, without switching the rig off. This is because on this day, when only 2 hours into the fouling run, the positive trend was so clearly linear that a decision was made that it was unnecessary to keep going any longer, as the rate could already be clearly calculated.

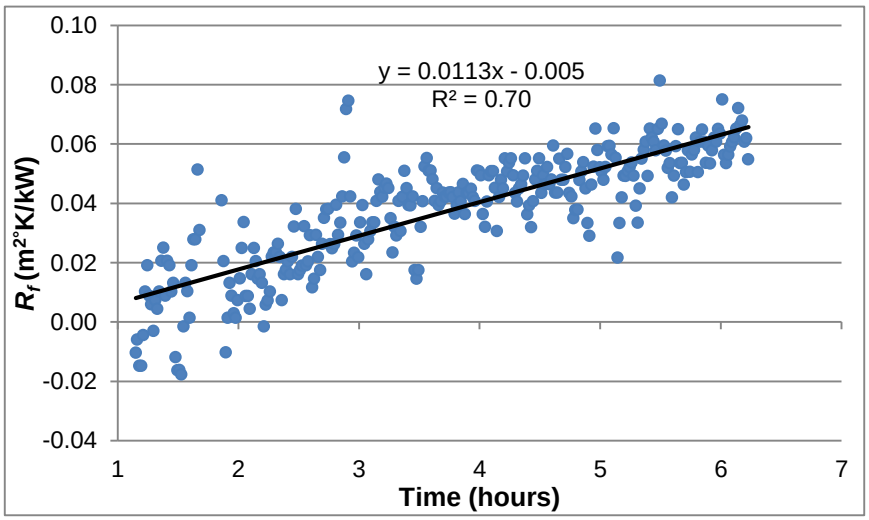

Figure 45: 13th May 2013, 344°C T_w, 240°C T_b, 200RPM, 500W

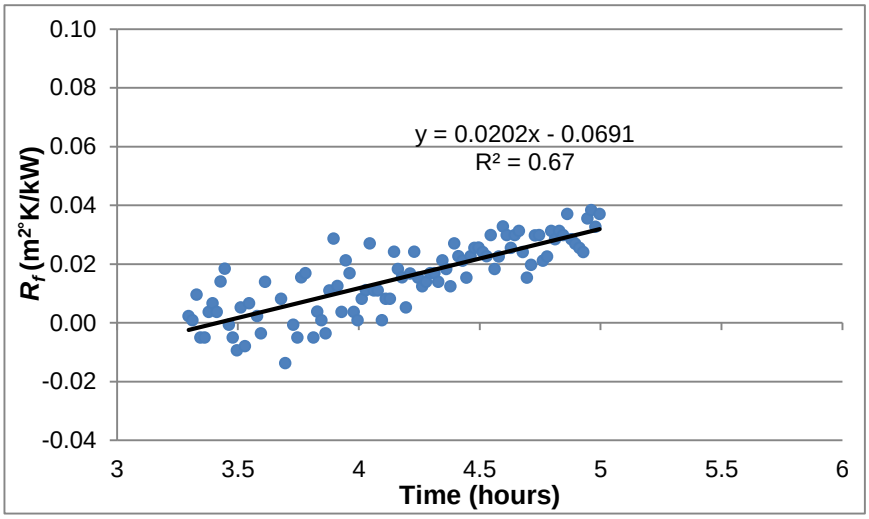

Figure 46: 15th May 2013, 343°C T_w, 240°C T_b, 300RPM, 500W

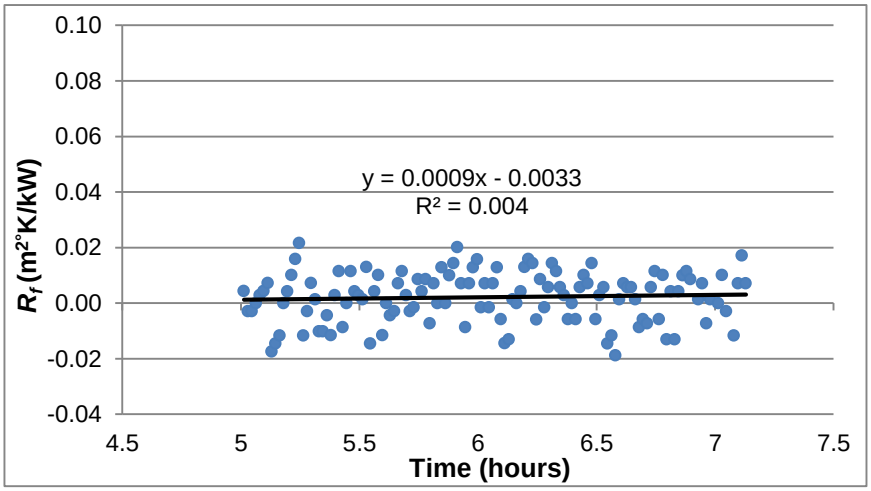

Figure 47: 15th May, 343°C T_w, 240°C T_b, 400RPM, 500W

There was a small amount of fluctuation in all three tests, but clear linear trends were observed in all of them. The 200 and 300RPM tests had comparable R^2 values to the 100RPM tests – around 0.65-0.7. Again, the fluctuation seen in the graphs was most likely caused by variance in the stirrer speed, especially as the RPM is harder to control and fluctuates more at higher speeds. No fouling occurred during the 400RPM test and this can be seen by the flat line plot in Figure 47. The R^2 value is so low for this graph as R^2 statistical analysis are not suitable for application to flat line graphs as there is no relationship between the x and y axis. Whilst the fluctuation in power for all the tests had a slightly higher standard deviation than for the 100RPM tests (a maximum of 2.9W at 300RPM), this was still only a 0.6% deviation and therefore unlikely to have much significant effect on T_w or R_f.

Of particular interest from these three results is firstly that the 200RPM test had a lower fouling rate than the 300RPM test, which is not what is to be expected as the shear stress should reduce the fouling rate. There is no obvious explanation for these findings and unfortunately there was no time to conduct either of these tests again. The second key result from these tests is that as no fouling occurred at 400RPM, this suggests that the shear stress threshold for crude 21 lies at around 400RPM.

9.5.1 The Effect of Stirrer Speed on Fouling Rate: Summary

All of the measured fouling rates from these tests are plotted versus the stirrer speed (Figure 48). Whilst there are the obvious issues that have already been discussed: the variation in fouling rates at 100RPM, and the 200RPM rate being lower than the 300RPM rate, a line of best fit can still be plotted. This plot confirms that the threshold seems to fall at around 400RPM, though more tests would be needed to gain a more precise threshold. The reason more tests were not performed at the time was because these were the first fouling tests performed with the rig. The main aim of the tests was therefore to test the rig and the methodology, by checking that the fouling rate was indeed reduced by stirrer speed/shear stress for crude 21 and not specifically to determine a precise correlation.

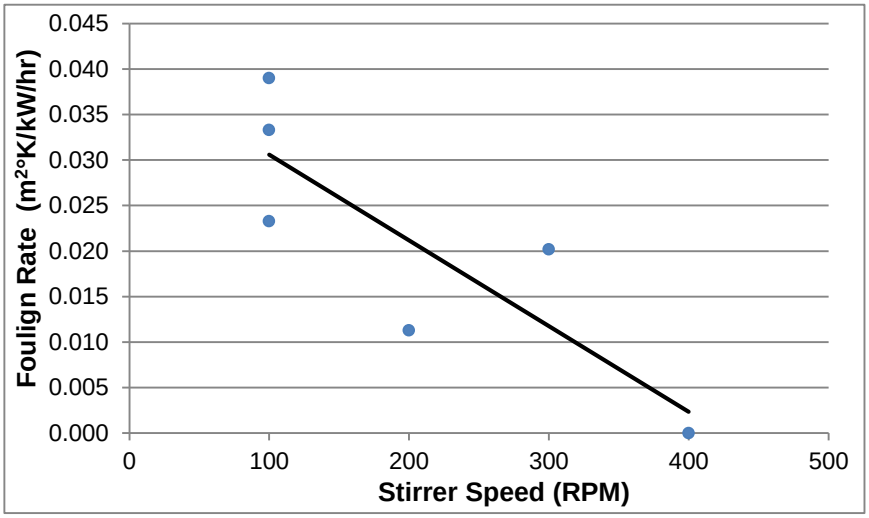

Figure 48: A graph of fouling rate versus stirrer speed at constant T_w

9.6 The Effect of T_w on Fouling Rate: Results and Analysis

In order to carry out the fouling removal experiments, a significant deposit first had to be formed on the metal finger's surface. This was done over a number of fouling runs July-August 2013. During these runs, the tests were done at a number of different T_ws over the range 340-360°C to gather data on the effect of temperature on the fouling rate (Table 9).

Table 9: A list of the fouling tests at varying T_ws

Test Date	T_b (°C)	T_w (°C)	Speed (RPM)	Speed STDEV	Power (W)	Power STDEV	Fouling Rate (m²°C/kW/hr)
19th July 2013	250	350	106	9.4	543.7	1.6	0.0057
22nd July 2013	260	360	108	5.3	540	1.9	0.0133
23rd July 2013	260	360	107	4.2	540	2.1	0.0191
24th July 2013	260	360	110	6.7	543	1.3	0.0202
25th July 2013	260	360	108	1.9	541.5	1.3	0.0135
26th July 2013	260	360	110	2.5	541.8	2.5	0.015
30th July 2013	260	355	109	2.2	542.9	2.3	0.0112
31st July 2013	260	355	109	5.2	539	3.7	0.0157
9th August 2013	260	360	103	7.0	542	1.8	0.0111
20th August 2013	260	350	110	8.7	487.5	4.4	0.0116
21st August 2013	260	350	105	5.1	495.1	3.7	0.0132
28th August 2013	250	340	109	3.1	404	4.7	0
28th August 2013	250	345	108	1.6	447	3.1	0.0082

The fouling plots for each of these data sets are now shown and discussed. They are put in order of increasing T_w and not by date as in Table 9.

9.6.1 340°C T_w

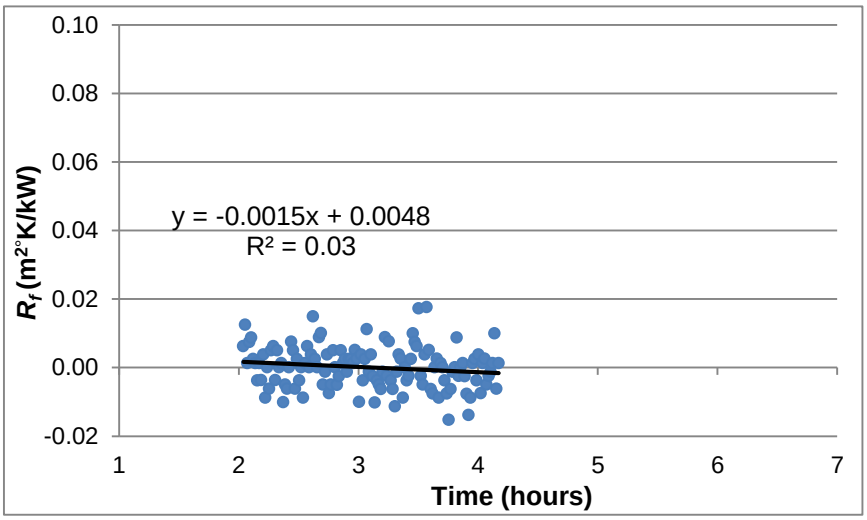

Figure 49: 28th August 2013, 250°C T_b, 340°C T_w, 100RPM, 404W

340°C was found to be the fouling threshold for crude 21 in this test and after 2 hours at constant conditions the T_w did not rise at all. Figure 49 shows how R_f remained at zero. There was a small amount of variance in this test as usual, but this does not alter the overall flat trend. The stirrer speed and power standard deviations were 3.1RPM and 4.1W respectively. Whilst in most of the runs it was the fluctuation in the stirrer speed that is the predominant cause of T_w variance, in this case it seems that power may have had more of an impact. The deviation in the power in this run was higher than in any other test, whilst the stirrer speed varied less than in most other runs.

9.6.2 345°C T_w

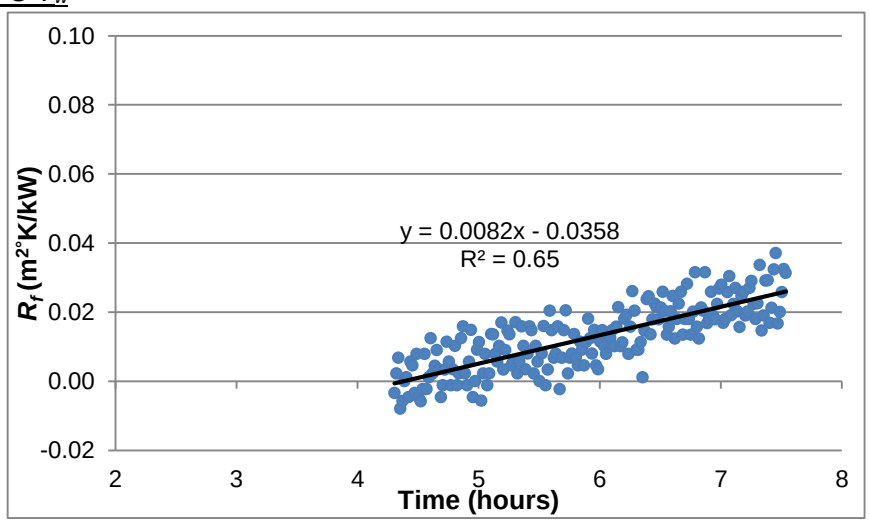

Figure 50: 28th August 2013, 250°C T_b, 345°C T_w, 100RPM, 447W

This run was done directly after the 340°C test shown in Figure 49 and as shown in Table 9, the deviations in stirrer speed and CH power were very similar with the power fluctuation appearing to be the dominant of the two. The R^2 value of 0.65 is approximately the same

as in stirrer speed fouling tests (Chapter 9.5) and thus the condition variations do not seem to have affected the overall positive trend showing that fouling was occurring at a slow rate.

9.6.3 350°C T_w

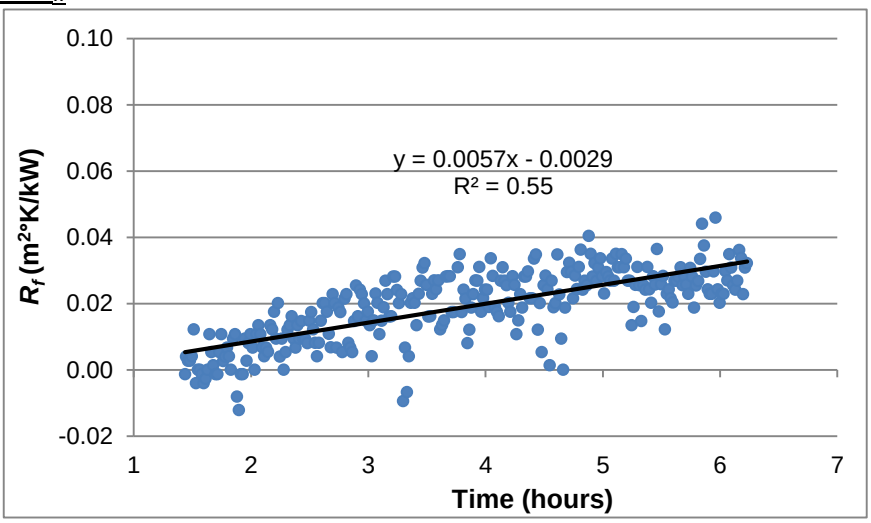

Figure 51: 19th July 2013, 250°C T_b, 350°C T_w, 100RPM, 550W

The fouling data shown in Figure 51 was the first time fouling was observed with the second batch of crude oil. This was therefore the first layer of deposit on the clean metal surface. The graph has a relatively low R^2 value compared to most of the other fouling graphs; it is probable that this was partly caused by variation in the stirrer speed. It had a standard deviation of 9.4RPM, which was one of the largest recorded. However, the other reason it has a low R^2 value is because of the overall trend: the fouling deposit seems to increase at two different rates, one rate from 1.5-3.5 hours and a second slower rate from 3.5-6.5 hours. The reasons for this difference are unknown, as whilst the CH power and stirrer speed fluctuated, their average values did not increase or decrease over the length of the run. It is possible that these findings are because this was the initial layer of foulant; the deposit may have consequently been quite weak and removal due to foulant particles shearing away consequentially more prevalent than for a deposit built up over several days, resulting in an overall more variable fouling rate.

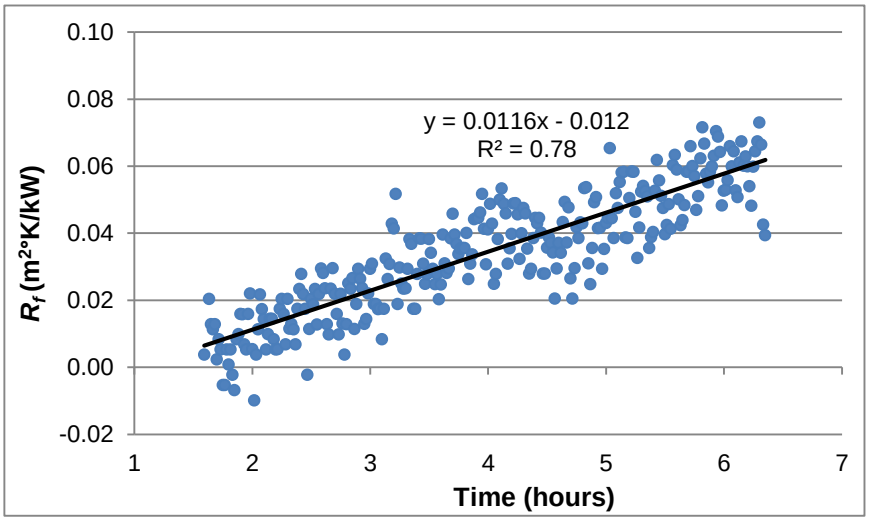

Figure 52: 20th August 2013, 260°C T_b, 350°C T_w, 100RPM, 500W

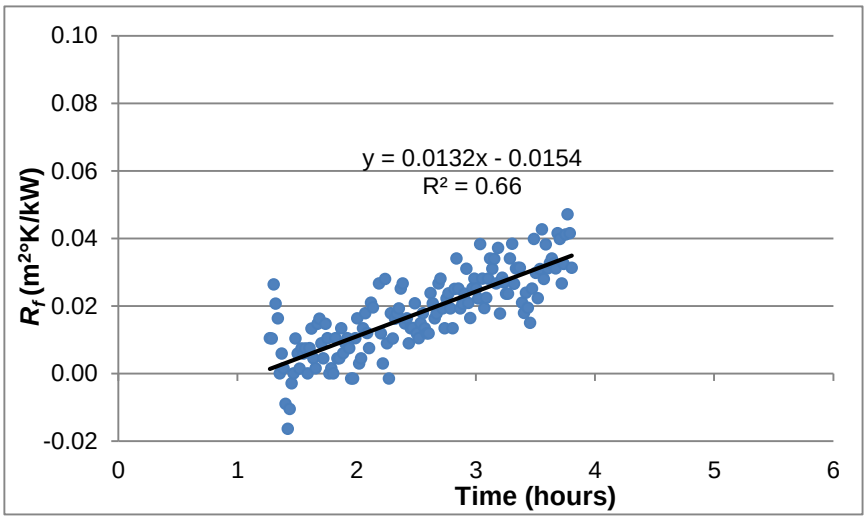

Figure 53: 21st August 2013, 260°C T_b, 350°C T_w, 100RPM, 500W

The two fouling data sets shown in Figure 52 and Figure 53 by comparison have a higher R^2, and thus the level of fluctuation was not significant. The runs had a standard deviation in the CH power of 4.4 and 3.7 and in stirrer speed of 8.7 and 5.1 respectively. The CH variation is at the higher end of all those measured in the tests and therefore likely to have a slightly higher impact on the T_w and R_f variability, especially as the deviations in stirrer speeds were low. Regardless of these factors, both of these plots have a very clear positive linear trend over time, validating the calculated fouling rates for the tests.

Of these three runs at 350°C the second and third tests (Figure 52 and Figure 53) have a comparable fouling rate. The test on the 19th July 2013 in Figure 51 by comparison had a much lower fouling rate. The reason for this is probably the same as was explained for its R^2 value being much lower: the fact that this was the first day of fouling of the second crude batch, and therefore first layer of foulant, which would have thus been quite weakly attached, resulting in a higher removal rate.

9.6.4 355°C T_w

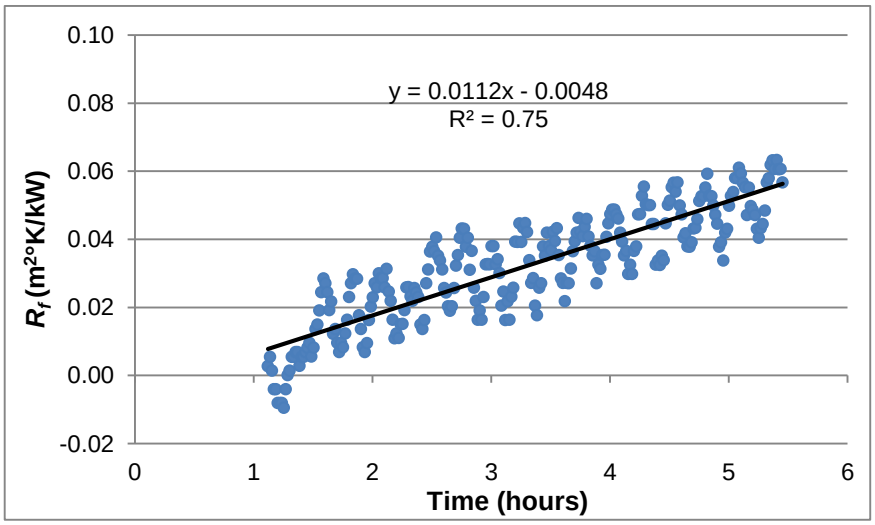

Figure 54: 30th July 2013, 260°C T_b, 355°C T_w, 100RPM, 550W

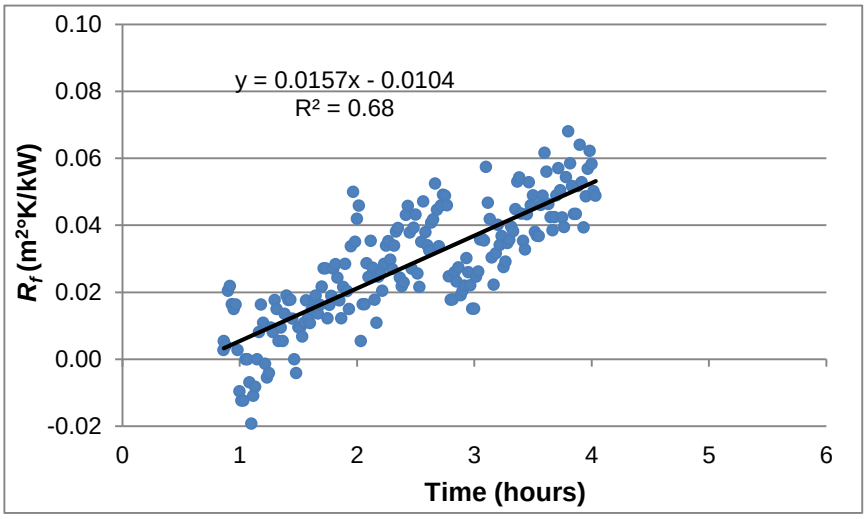

Figure 55: 31st July 2013, 260°C T_b, 355°C T_w, 100RPM, 550W

Both of the fouling tests at 355°C T_w shown above had some of the lowest levels of variation in CH power and stirrer speed in all of the tests with power standard deviations of less than 3W, and less than 6RPM for the stirrer speed. The R^2 values for the tests of 0.75 and 0.68 are some of the highest in all of the fouling plots. The run on the 31st July 2013, however, did have a small dip in fouling level around half way through the test. Following this dip over a 5-10 minute period fouling starts to increase straight away. This was most probably caused by some foulant deposit shearing away on the metal surface, reducing the T_w. This occurrence does not however seem to have significantly impacted upon the calculated fouling rate.

9.6.5 360°C T_w

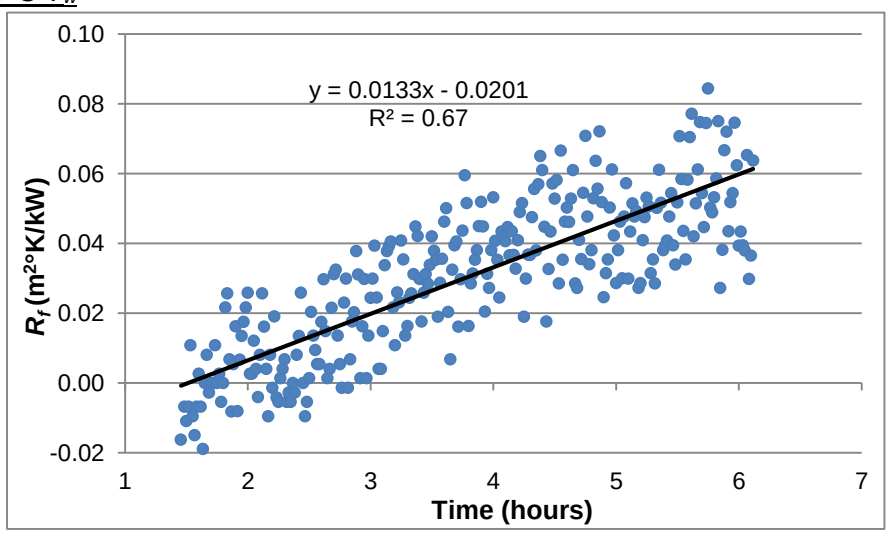

Figure 56: 22nd July 2013, 260°C T_b, 360°C T_w, 100RPM, 550W

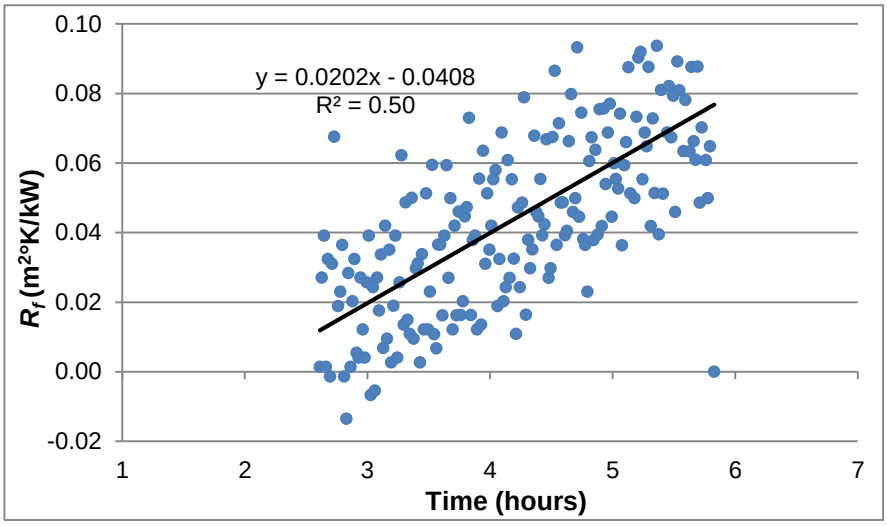

Figure 57: 24th July 2013, 260°C T_b, 360°C T_w, 100RPM, 550W

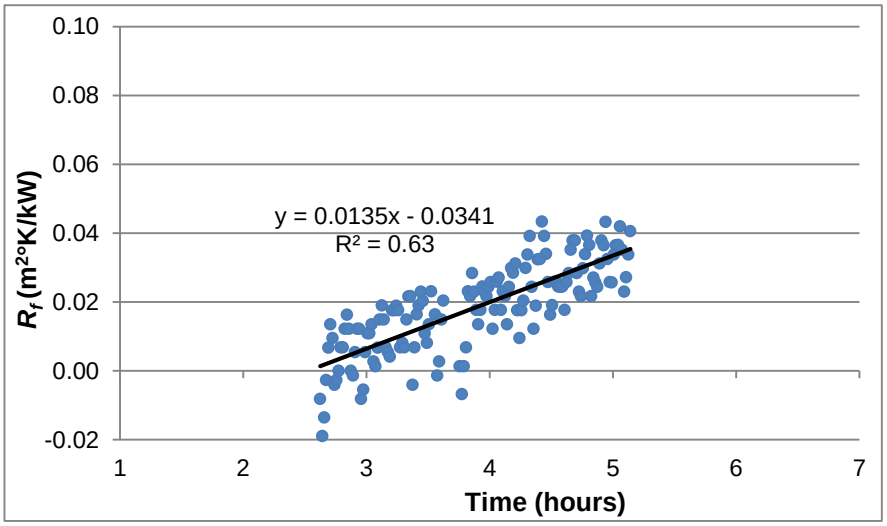

Figure 58: 25th July 2013, 260°C T_b, 360°C T_w, 100RPM, 550W

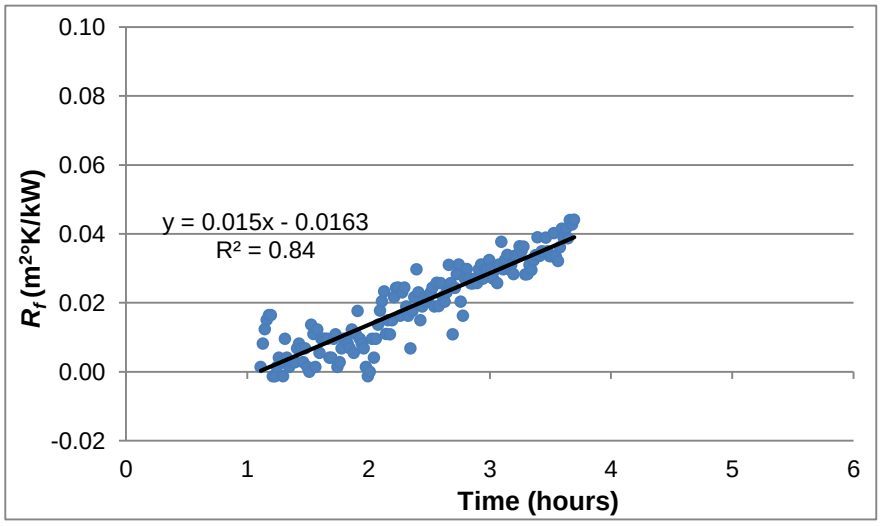

Figure 59: 26th July 2013, 250°C T_b, 360°C T_w, 100RPM, 550W

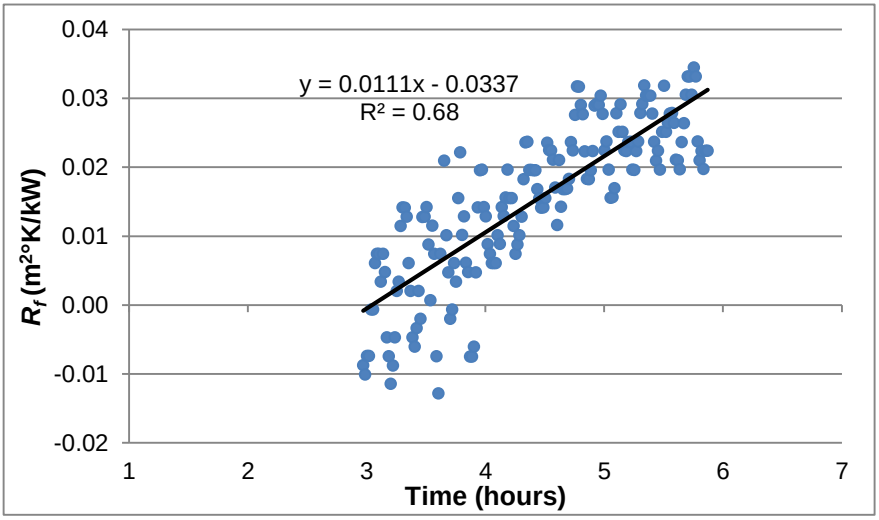

Figure 60: 9th August 2013, 260°C T_b, 360°C T_w, 100RPM, 550W

All of the fouling tests at 360°C T_w showed a strong positive increase in T_w, and therefore fouling level as the experiment proceeded. As shown in the above five graphs, there is a slight variance in fluctuation due to the operating parameters and therefore the calculated R^2 values, but these fluctuations do not affect the overall trend in each test. The standard deviation in CH power for all of the 360°C tests was under 2.5, and therefore the lowest of all the experiments. Therefore, it can be assumed that variance in the CH power probably did not significantly affect T_w in these data sets. The standard deviations of the stirrer speeds were also amongst the lowest in the 360°C T_w tests compared to the other T_ws, with a maximum of 6.7RPM. There was, however, little correlation between the standard deviation in stirrer speed and R^2 values of the plots. A definite conclusion cannot be made about what was the key cause of variance in the 360°C tests, although it was most likely to be the stirrer speed as it fluctuated more than the CH power.

There was one other test at 360°C that had a larger amount of data spread and also an overall interesting trend, shown in Figure 61. The spread in the data is difficult to explain as there was such low standard deviation in the stirrer speed and CH power: 4.2RPM and 2.1W respectively. Whilst variation in T_b is already accounted for in the calculation of R_f, this was checked to see if anything unusual had happened and found not to vary more than in a typical test: around +/-2.5°C. What is interesting about the graph is that fouling seemed to occur at a constant rate between 2-3.5 hours, then plummeted between 3.5-4.2 hours, and then continued fouling at the same rate as before from 4.2 hours onwards. The only way this sudden drop can be explained is by fouling removal during this time and it is probable that some of the freshly deposited foulant broke away. There were no sudden changes observed in any of the other conditions during this time when the data was inspected.

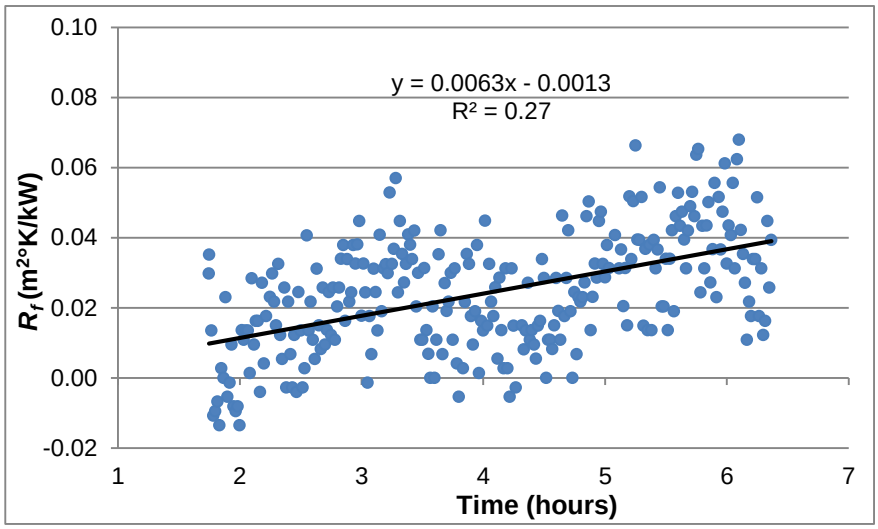

Figure 61: 23rd July 2013, 260°C T_b, 360°C T_w, 100RPM, 550W

Due to the drop in R_f half way through the experiment, the overall fouling rate is much lower than the other fouling tests at 360°C when a trend line is plotted straight through the data. A better representation of the fouling rate would be achieved by calculations based upon one of the two sections where R_f was increasing. A graph of the first section of the data where fouling was occurring is shown in Figure 62 and it gives a fouling rate of 0.0184 m²°C/kW/hr.

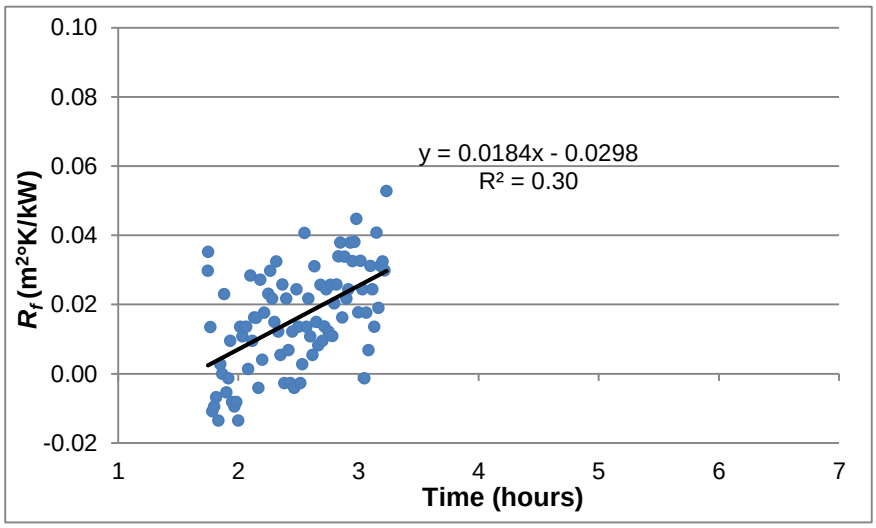

Figure 62: The fouling rate of the first section of the data shown in Figure 61

For comparison, the second section of the data had a fouling rate of 0.0191 m²°C/kW/hr; this is very close to the rate measured for the first part of the test. Due to how close it was to the rate measured in the first part of the test shown in the above graph, the graph of the isolated second part of the data is not given.

The fouling rates measured for the above tests at 360°C T_w had a reasonable range of 0.011-0.0202m²/°K/kW/hr. They all had a very similar stirrer speed, with a range of 103-110RPM; this is not a significant enough difference to have caused the differences in the fouling rate between the tests. Hence, there is no obvious explanation as to what caused

the differences between fouling tests. However if an average of the fouling rates is taken, it is likely to give a good representation of the actual fouling rate under these conditions.

9.6.6 The Effect of T_w on Fouling Rate: Summary and Arrhenius Plot

Table 10 below gives a summary of the tests conducted at each different T_w, and the average fouling rate of each. This is then plotted as a graph in Figure 63.

Table 10: A summary of the T_w fouling test data

T_w (°C)	Number of Tests	Average Fouling Rate (m^2/°K/kW/h)
340	1	0
345	1	0.0082
350	3	0.0101
355	2	0.0135
360	6	0.0154

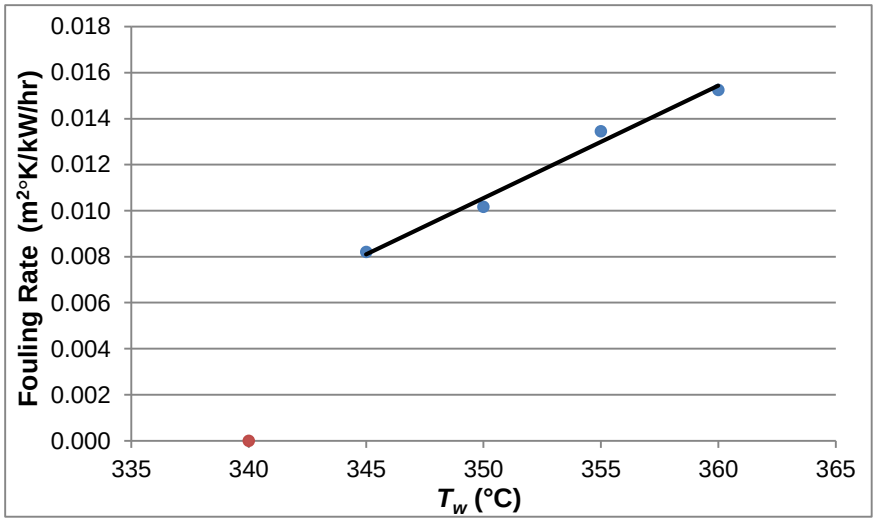

Figure 63: A graph to show the effect of T_w on fouling rate

These results show a linear correlation between T_w and fouling rate for crude 21; this is the same as has previously been found using the stirred batch cell rig with other crude oils. For example see the graph below (Figure 64) of data from the rig presented in Young *et al.* (2009).

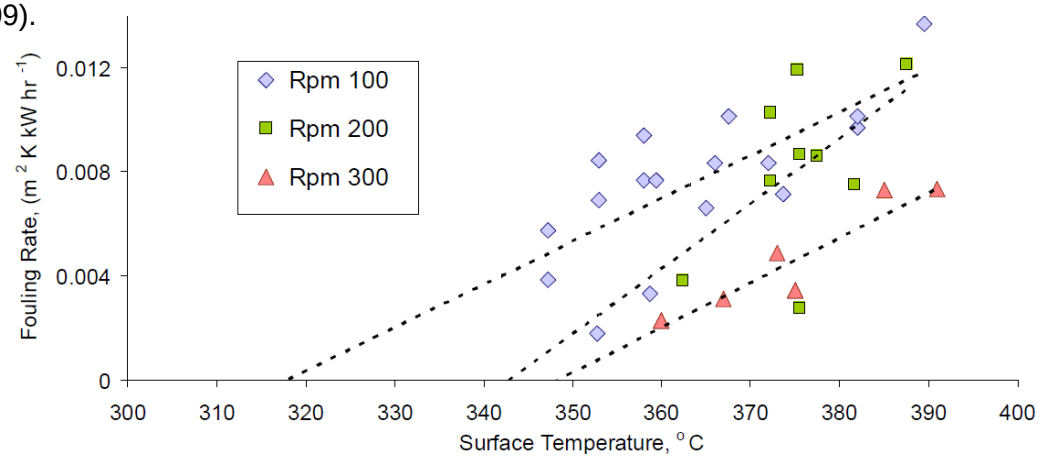

Figure 64: The increase in fouling rate at different T_w and stirrer speeds for a crude tested previously in the stirred batch cell (Young et al., 2009)

The fouling temperature threshold was found to be 340°C. This was a very clear threshold, in that as shown in Figure 49, the fouling graph was completely flat at this temperature. Two hours into this particular run, with no fouling occurring; 50W power was added, increasing the T_w by 5°C. The impact of this can be seen in Figure 50 which shows a clear fouling trend which started occurring as soon as the T_w was increased. The small increase in temperature pushed it past the temperature threshold.

As a linear trend was observed (note that the zero fouling point was not included in the trend line), an Arrhenius plot can therefore be applied to the data in order to estimate the activation energy of crude 21 at 100RPM stirrer speed. The Arrhenius plot of the data is shown below, where the log of the fouling rates are plotted versus 1/T in K.

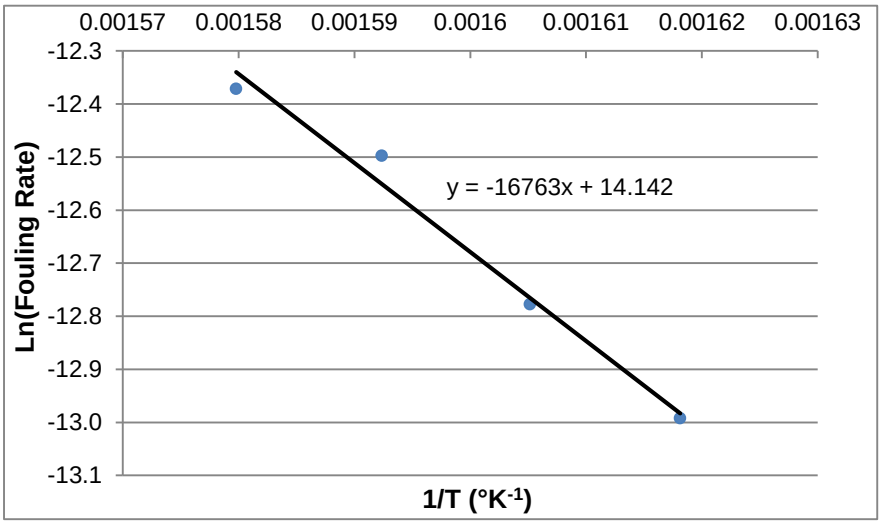

Figure 65: An Arrhenius plot for crude 21 at 100RPM

The gradient of this plot is $\frac{E_A}{R}$, therefore by multiplying it by R, the universal gas constant it gives E_A:

$$E_A = 8.314 \times 16763 = 139368 kJ/mol$$

$$E_A = 140 kJ/mol$$

This is comparable to the activation energy of other crudes previously tested in the rig, for example in Yang *et al*. (2011) the crude tested was found to have an activation energy of 122kJ/mol at a comparable agitator speed of 90RPM. The individual data points that made up the average fouling rates were also put together on an Arrhenius plot to see if this changed it much. This changed the measured activation energy to 111kJ/mol, which while it is different to that calculated from the averages, is also comparable to the 122 kJ/mol value so does not change the conclusion.

9.7 Crude 21 Fouling Removal Experiments: Test Information, Results and Analysis

As explained in Chapter 1.2, the aim of the fouling removal experiments was to see whether raising the stirrer speed high enough would cause fouling deposit to start to shear away producing a measurable negative fouling rate. In order to remove a deposit, one first has to be built up on the fouling surface and this was done in the tests described in Chapter 9.6. The methodology for these tests was similar to previous removal tests with the stirred batch cell as detailed in Yang *et al.* (2011). The rig is allowed to stabilise and start fouling at a low stirrer speed (100RPM), once a linear fouling rate has been observed for 2-4 hours the stirrer speed is increased to 400-600RPM and the removal test begins. The reason removal tests are not done by just starting the rig up at 500RPM is that the top layer of fouling is the weakest layer. It is often described as having a soft gel like consistency, below which deposit may have aged or even become coke (Coletti *et al*., 2010). Therefore, if deposit removal does occur, it is likely that the top layer will be easier to remove than the bottom one. Consequently, if a test is started at 500RPM, by the time the test conditions are stabilised the weak deposit may have already been removed, therefore affecting the results. Having fouling conditions already stable before stirrer speed is increased ensures effects on the deposit can be seen. Typically a large drop in T_w would be expected with stirrer speed increase. This, would lower the fouling deposition term in the Kern and Seaton model and thus the overall fouling rate resulting in an unfair test as stirrer speed tests should be done at a constant T_w. However, the findings of the heat transfer tests with crude 21 found that the T_w starts increasing after 200-300RPM and an increase in stirrer speed to 400-600RPM actually results in a T_w similar to at 100RPM, making the experiment fair.

Five removal tests were carried out. Each was conducted following several hours at 100RPM and 350-360°C T_w; 360°C T_w was the highest starting temperature. This high temperature enabled the greatest possible deposition rate on the metal finger each day before removal was attempted. Table 11 summarises the tests and Figures 66-70 display the data set plots; the red points are where the stirrer speed was raised to the higher level.

Table 11: A summary of the fouling removal tests

Test Date	T_b (°C)	T_w (°C)	Speed (RPM)	Removal Speed (RPM)	Power (W)
25th July 2013	260	360	108	500	541.5
30th July 2013	260	360	109	400	542.9
31st July 2013	260	360	109	500	539
20th August 2013	260	350	105	500	487.5
21st August 2013	250	350	106	600	495.1

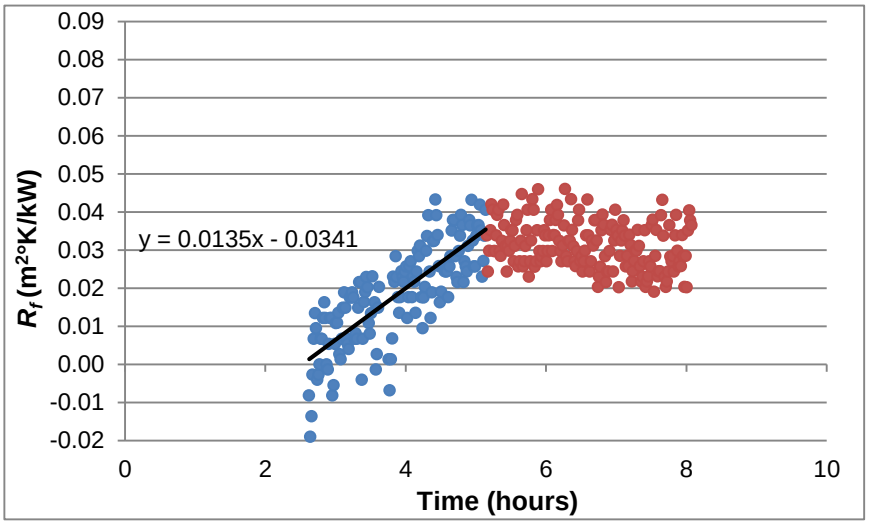

Figure 66: 25th July 2013, 260°C T_b, 360°C T_w, 100 and 500RPM, 550W

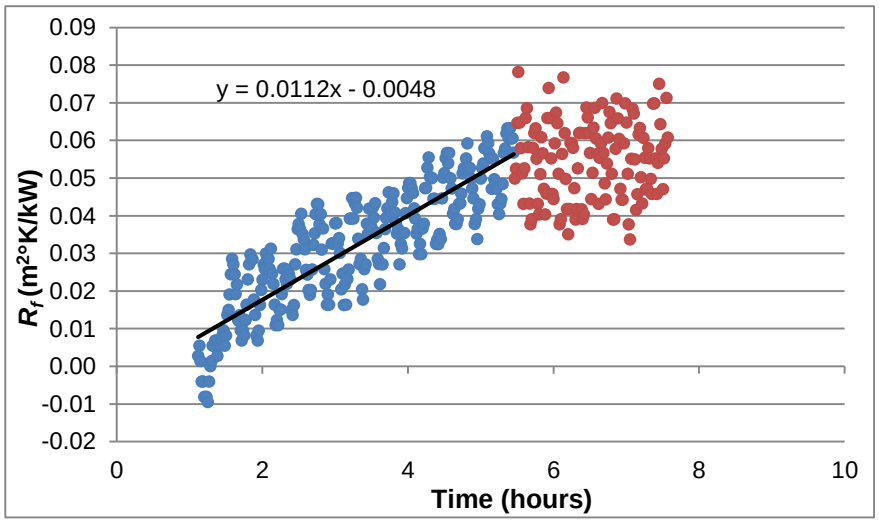

Figure 67: 30th July 2013, 260°C T_b, 360°C T_w, 100 and 400RPM, 550W

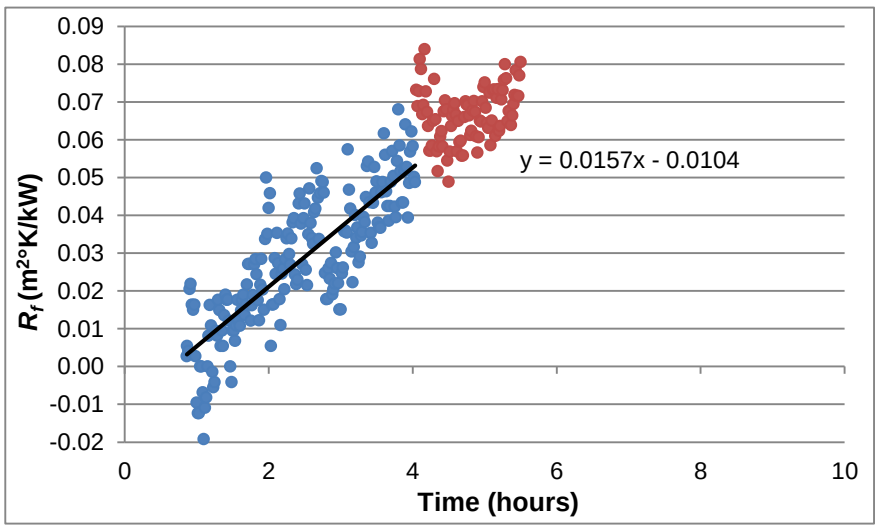

Figure 68: 31st July 2013, 260°C T_b, 360°C T_w, 100 and 500RPM, 550W

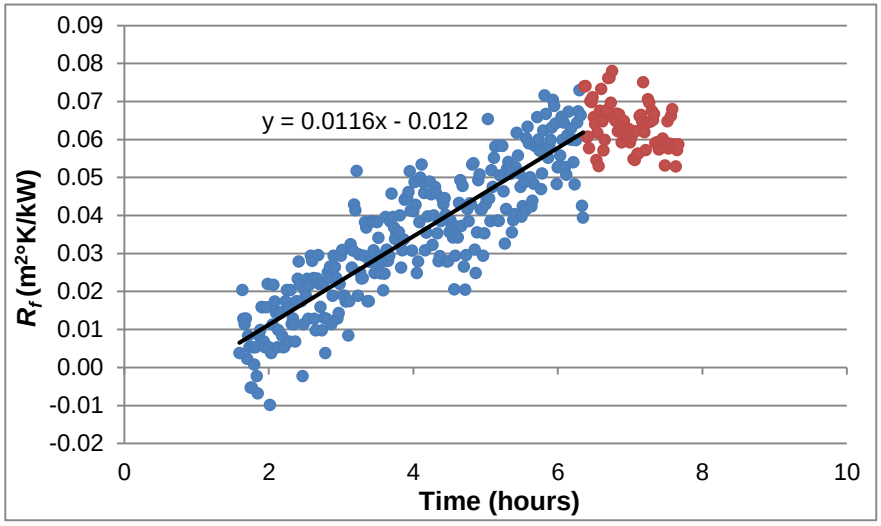

Figure 69: 20th August 2013, 260°C T_b, 350°C T_w, 100 and 500RPM, 500W

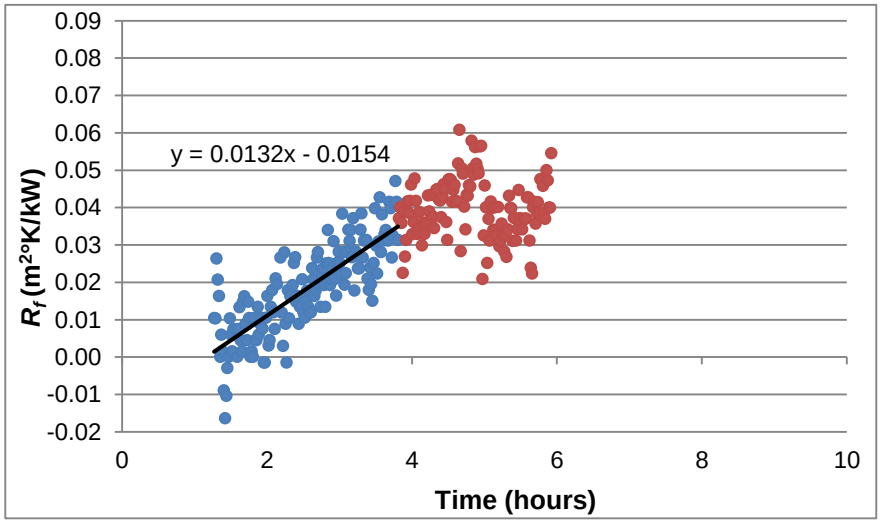

Figure 70: 21st August 2013, 260°C T_b, 350°C T_w, 100 and 600RPM, 500W

The results of these tests were mixed, with the 25th July 2013 (Figure 66) being the only time a small negative fouling removal trend could be seen. It is possible that fouling removal occurred on the 30th July (Figure 67), 20th August (Figure 69) and 21st August 2013 (Figure 70) as well. However, due to a large data spread it is not possible to conclude that fouling removal did occur and an equally valid conclusion from the graphs is that R_f remained roughly constant with time at the higher speed.

This is emphasised in Figure 71 which shows just the removal part of the experiment from the 21st August 2013.

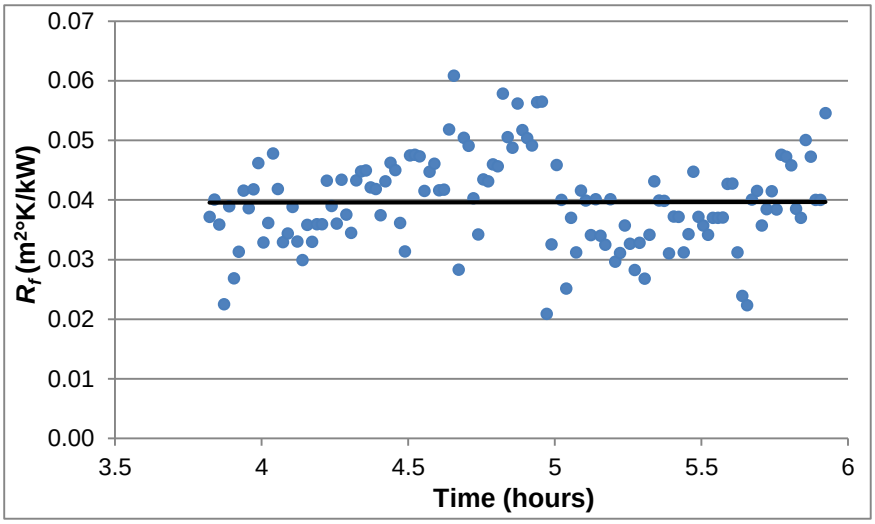

Figure 71: 21st August 2013 removal test with stirrer speed of 600RPM

When a trend line is fitted to the data in Figure 71, it gives an overall fouling rate of zero with no removal occurring. If, however, the last 30 minutes of the test are omitted, where it went up slightly, the overall trend would have been negative. This was at a 600RPM stirrer speed which was the highest used in the removal experiments, so if removal was occurring it would be expected to be fastest here. In the experiment on the 31st July 2013 (Figure 68) R_f actually increased instead of decreased, suggesting that fouling was actually still occurring at the increased stirrer speed, though it is more likely this was caused by variance in the operating conditions.

Unfortunately, due to time constraints of the working day, it was not possible to carry out the removal tests for longer than 2.5 hours. This is because it takes 1-2 hours to get the rig up to fouling temperatures from start-up and around 4 hours to build up a reasonable fouling layer and get conditions completely stable. Adding another 2.5 hours to these times for fouling removal gives a total experiment time of 8-9 hours: the limit of a working day. These time calculations assume that there are no major problems at the start of, or during the run. If removal was occurring as in Figure 66, it was at a very slow rate. Therefore to be completely conclusive as to whether removal was possible, the tests would have needed an extra 4-8 hours to study the overall trend and this was not possible with a single person running the rig.

The key cause of the large data spread during these tests (which largely contributed to their inconclusiveness) is that at higher stirrer speeds, the stirrer speed fluctuated a lot more, typically around +/-30-50RPM at 500RPM. The agitator speed also changed suddenly, dropping from its target speed quite regularly and therefore had to be manually reset on its control panel many times. The connection between stirrer speed variance and the T_w fluctuation is shown in Figure 72 for the removal test on the 21st August 2013.

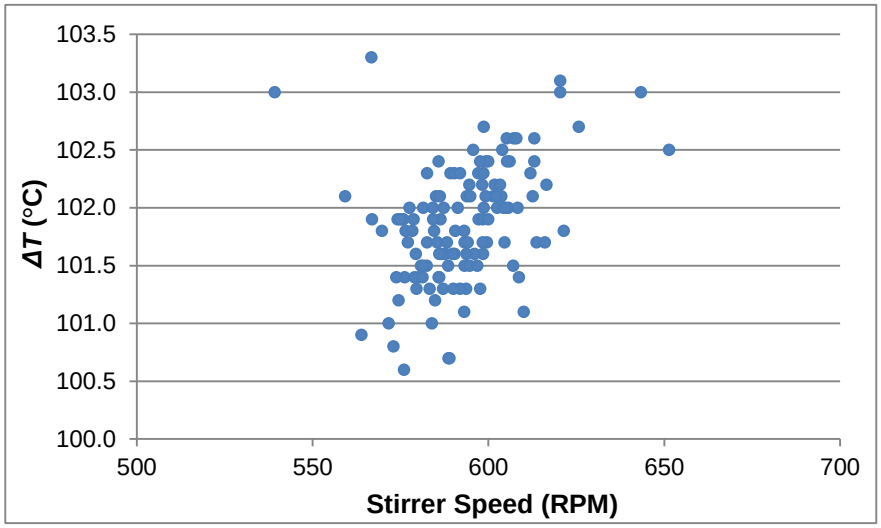

Figure 72: Stirrer speed versus ΔT for the 21st August 2013 removal test

As can be seen, there is an overall positive correlation between the two, suggesting that it is indeed the stirrer speed variance that is having a big effect on the T_w. There is a lot of scatter in the plot however, showing that there are other factors affecting the wide range in T_w, with the stirrer speed appearing to be the most dominant cause.

9.7.1 Crude 21 Fouling Removal Experiments: Inspection of the Deposit and Summary

Inspection of the metal finger itself after it was removed from the rig also yielded some potential evidence for fouling removal. This is shown in the photo below of one side of the metal finger after several days of removal tests had been attempted.

Figure 73: A photo of the fouled metal finger after the removal tests, August 2013

Small markings in the fouling deposit could be seen which had been made by the helical flow of fluid around the surface. This is clearly visible towards the top, centre of the photo in Figure 73 and shows that where the crude oil was flowing, there is very little deposit. It is possible that this occurred when the removal experiments were performed, and thus at these points the deposit was worn away by the shear stress exerted by the fluid flow.

Whilst several of these tests suggest a small amount of fouling removal, the graphs of fouling resistance against time are too scattered and inconclusive to measure a removal rate for use in estimating a threshold. Hence it can be concluded that possibly some removal of the fouling deposit occurred with crude 21, although it seems that if this process does happen then it happens slowly. This is probably because of the low viscosity of crude 21, which reduces its ability to exert shear stress on the surface of the metal finger in comparison to a more viscous crude oil. The fouling removal work that was carried out in 2011 used a heavier, higher viscosity oil and showed very clear fouling removal. Perhaps if work conditions allowed a removal experiment to run over a 24 hour+ period, then a measurable removal rate could be obtained, but for now this is not practicable.

9.8 Deposit Images Analysis

In addition to Figure 73, several other images of the fouling deposit on the surface of the metal finger were taken after it was removed from the rig. These are now presented.

Figure 74: A photo of the fouled metal finger, July 2013

Figure 75: A photo of the fouled metal finger, August 2013

The photo in Figure 74 was taken after the first set of fouling tests described in sections 9.5.1; the deposit only covered a small band at the bottom of the finger and was particularly tough, requiring sandpaper to remove properly. The location of the heaviest fouling at the bottom is similar to what has been observed on previous occasions in the rig (Young *et al.,* 2009). This area of the finger is shown by CFD simulations to be the hottest part, and thus is where fouling would be expected to occur. It is also the area of the finger where the thermocouples measure the T_w. This confirms that the fouling observed from the increase in T_w recorded by these thermocouples matches up with the physical observation of the deposit on the metal surface.

The photos in Figure 73 and Figure 75 were taken of both sides of the metal finger after the fouling tests described in sections 9.6 and 9.7. There were a larger amount of fouling experiments performed during these tests than the first set of tests, and therefore a greater proportion of the finger can be seen to be covered in deposit. The grain size of the deposit particles can also be seen to be larger in these photos, probably because the deposit has had longer to develop. As with the deposit on the finger in Figure 74, the deposit was concentrated around the bottom of the finger.

9.9 Error Analysis

In order to check the validity of the data presented in this thesis, an error analysis can be applied to it. This is performed by predicting the maximum effect variance of the key measurements has on the resultant calculated fouling resistances. The variables in the fouling resistance equation are the CH power, wall temperature and heat transfer area. The error margins for these are as follows:

- **Power error:** +/-5W
- **Wall temperature thermocouple error:** +/-0.05°C
- **Probe height error:** +/-0.0005m
- **Probe width error:** +/-0.00005m
- **Resultant area error:** +/-0.000045m^2

The data set from the 28th August 2013 is taken as an example fouling curve to carry out an error analysis; it had one of the lowest recorded fouling rates, so errors are more likely to have impacted it. An example of the calculations to find the upper and lower error limits for a single point is given below.

Recorded R_f calculation:

$$R_f = \frac{\Delta T}{Q/A} = \frac{2.3}{451.7/0.00506} = 0.0258 m^2°C/kW$$

Highest possible R_f upper margin for T and A, lower margin for Q:

$$R_f = \frac{2.3 + 0.05}{(451.7 - 5)/(0.00506 + 0.000045)} = 0.0269 m^2°C/kW$$

Difference = +0.0011m^2°C/kW or +4.35%

Lowest possible R_f upper margin for T and A, lower margin for Q:

$$R_f = \frac{0.5 - 0.05}{(444.9 + 5)/(0.00506 - 0.000045)} = 0.0247 m^2°C/kW$$

Difference = -0.0011m^2°C/kW or -4.35%

Several points from the end of the data set are taken, these error margins then calculated and applied to the fouling graph as error bars (Figure 76).

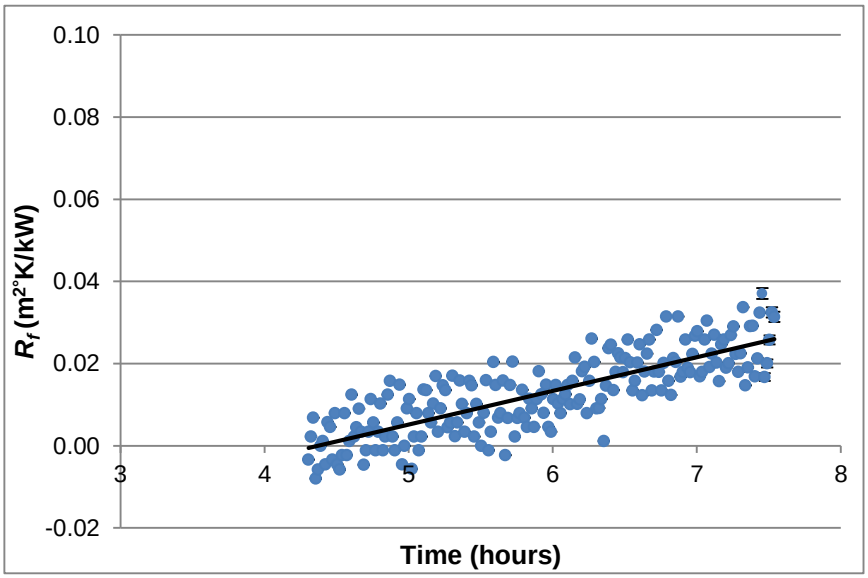

Figure 76: 28th August 2013 data with bars representing the error caused by variance of CH power, thermocouples and heat transfer area added

As can be seen in Figure 76, the scale of these error bars compared to the overall trend is very small, supporting the accuracy of the data and therefore the positive trend. However, it is clear that the fluctuations in the data were greater than the predicted maximum/minimum errors. This variation is because of the fluctuation in the stirrer speed, which affects the wall temperature as discussed previously. There is no term that directly represents the stirrer speed in the fouling resistance calculation, so it is difficult to account for this in it.

It is, however, possible to include the effect of the stirrer speed on R_f by calculating the average influence the stirrer speed has upon the wall temperature variation. This can be done by calculating the wall temperature standard deviation over a small time period (around 10 minutes) – not long enough for fouling to influence the temperature variance. This standard deviation is then added to the temperature part of the R_f calculation.

The standard deviation of the point chosen previously in the 28th August 2013 data was +/-0.64°C.

New maximum R_f = 0.0342 Difference = +0.0084m^2°C/kW or +32.7%

New minimum R_f = 0.0174 Difference = -0.0084m^2°C/kW or -32.7%

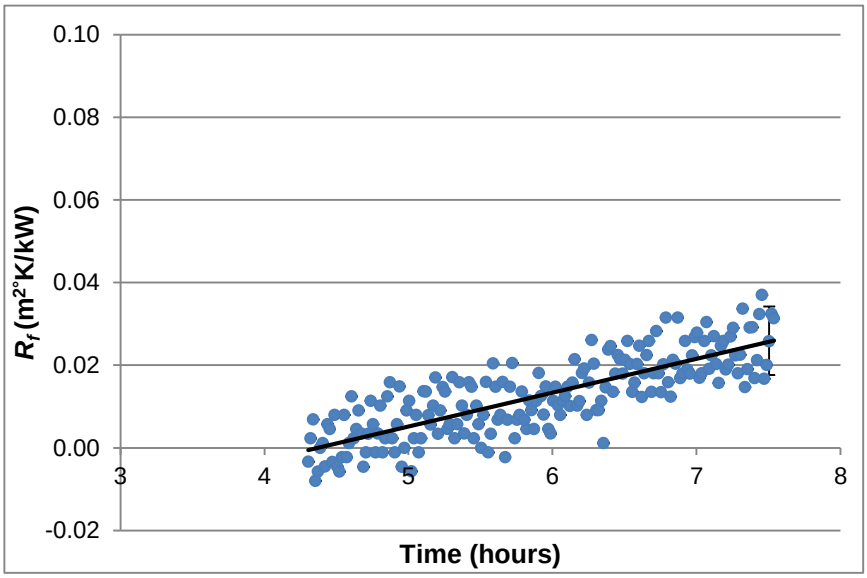

Figure 77: 28th August 2013 data with a bar representing the error caused by variance of CH power, thermocouples, heat transfer area and stirrer speed added

The new error bar in the above graph shows that accounting for the stirrer speed variation explains the spread in the data. The lower part of the error bar for the data at the end of the fouling curve is still higher than the highest measured R_f at the start of the test. This supports the validity of the positive fouling trend.

As the level of CH power, area and stirrer speed variation was the same for all tests, the above error analysis supports the conclusions and measurements of positive fouling rates in all of the tests. This is because as it has been proved that even at a very low fouling rate, accounting for variations in the conditions and measurement parameters does not change the overall conclusion.

There was only one test where it was possible there was a negative fouling rate observed in the removal tests, this was the test performed on the 25th July 2013. Therefore, it is a good idea to apply an error bar to this data to see if a more conclusive verdict can be made on whether removal did occur or not. The standard deviation of the wall temperature due to stirrer speed fluctuation was +/-0.41°C. This and the other standard errors were used to calculate the error bar for a single point at the start of the test (see Figure 78).

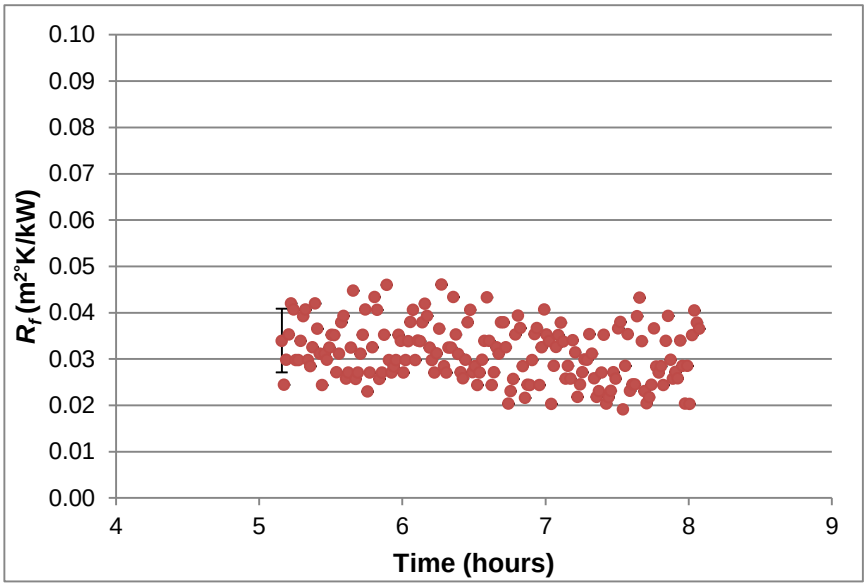

Figure 78: 25th July 2013 data with a bar representing the error caused by variance of CH power, thermocouples, heat transfer area and stirrer speed added

As can be seen, many of the data points at the end of the test are still within the limits of the error bar for the data at the start of the plot. This suggests that the slight negative overall trend is not statistically significant in comparison to the overall fluctuation of the data. Therefore, it cannot be decisively concluded that there was indeed any major fouling removal from this analysis.

9.10 Difference in Fouling Rates Between Oil Batches

As has been explained previously in Chapter 9.1 two different batches of crude 21 were used to collect the fouling data. The first batch was used to measure the effect of stirrer speed on the fouling rate in May 2013 and the second used to measure the effect of T_w on the fouling rate and carry out the removal tests in July-August 2013. These two test sets would be expected to show a similar fouling rate when operating conditions were set to be the same. However, this was not found to be the case. For the first batch, tests carried out at 345-350°C and with a stirrer speed of 100RPM had an average fouling rate of 0.032m²°K/kW/hr. Conversely, results from the second tests performed at the same stirrer speed and temperature range showed the average fouling rate was 0.001m²°K/kW/hr. This is a significant difference; the fouling rate for the first batch of oil was almost three times as fast as for the second batch.

There are two possible explanations for why this may have occurred:

- Firstly, it could be because a different amount of vapour was vented for each of the two crude 21 batches, and therefore the oil composition and rate of nucleate boiling was different in the two test sets. Therefore, if nucleate boiling is indeed inhibiting fouling, it would be expected that the lower the boiling rate, the higher the fouling rate would be. It is possible that more of the light ends were released in the tests for the

batch of oil that was used in May 2013, in comparison to the amount released in the July-August 2013 tests resulting in an overall increased fouling rate.

- Secondly, the CH was changed between these two sets of tests, from the batch 1, Watlow Firerod Design 1 CH, to the batch 4 Intertek CH respectively. As explained in Chapter 5.6, the batch 4 heaters had an approximately 30 micron smaller diameter than the batch 1 heaters and therefore there was an air gap between the heater and the metal finger. This resulted in a lower resultant T_w for the same CH power for the Intertek CH. This difference was counteracted in the tests by running the Intertek CH at 50W higher power, and increasing the T_b by 10°C. Due to this gap therefore it is likely that the heat flux through the vertical walls was slightly different and the end effect factor may also have been different because of the air gap. Whilst typically heat flux should not affect the fouling rate as it is T_w that controls it, the heat flux differences and energy wasted to overcome the air gap could have perhaps affected the heat getting to the metal finger surface, and therefore rate of fouling.

It may have been either of these explanations that caused the discrepancy in fouling rates between the experiment sets although it is more likely that it was a combination of the two.

9.11 Crude 21 Summary

The results from all of the fouling tests conducted with crude 21 have been presented, analysed and discussed in this chapter. Initially crude 21 would not foul in the rig, but eventually it was found that fouling would only commence once a proportion of the light ends had first been vented; nucleate boiling was thought to be inhibiting fouling deposition. Over a number of months the effects of both T_w and stirrer speed on the fouling rate were measured using the rig, and the results showed a linear correlation between the fouling rate and both of these variables. Fouling temperature and stirrer speed thresholds were also found for crude 21. Lastly, a number of fouling removal tests were carried out with mixed results; only one experiment showed some slight negative fouling, with the other four data sets being inconclusive due to a large amount of data spread. Inspection of the metal finger showed potential signs of fouling removal, and the fouling deposit was found to be most concentrated on the bottom part of the finger where it is hottest. Conclusions are now summarised and implications, limitations and future research presented in the next chapter.

CHAPTER 10

10 Conclusions

The stirred batch cell fouling rig has successfully been used over twelve months to generate a wide variety of fouling data in order to investigate the effect of stirrer speed on calcium carbonate fouling, the effect of stirrer speed and T_w on crude oil fouling and fouling removal by increased shear stress. A variety of heat transfer tests have also been carried out, which when supported by CFD simulation have provided new insights into what actually goes on inside the rig, especially when a lighter crude oil is tested. A number of modifications to the rig were also made to the stirred batch cell over the twelve months. These included removing a heavily degraded metal mesh that was wrapped around the cooling coil, removing and relocating the pressure relief valve, recalibrating the thermocouples, replacing all the main fittings on the rig to make it pressure tight, and replacing a number of parts including the band heaters, temperature controller and CHs.

Fouling experiments with calcium carbonate were conducted using a stainless steel sleeve fitted with a positive helical coil in order to see how the increased shear stress caused by the coil impacted on fouling. A negative correlation between stirrer speed and fouling rate for a fixed concentration of calcium carbonate solution was found, the fouling rate was observed to drop almost linearly with stirrer speed when plotted on a graph. This trend was similar to what was found previously with calcium carbonate fouling tests conducted in the rig using both a plain surfaced sleeve and a sleeve with a negative helical coil. The fouling threshold due to shear stress increase was found to occur at 500RPM. The stirrer speed threshold at which fouling stops had not been found for the other two sleeves, indicating the effect the increased shear stress due to the positive helical coil has on reducing fouling rate in the rig.

Crude oil tests using a crude named ‘crude 19’, which was provided by HTRI commenced in January 2013. It was a particularly light oil and in order to get it to reach typical test T_bs of around 240°C, some of the pressure and therefore crude oil vapour had to be released during tests. This oil was then tested in the rig at gradually increasing T_ws in an attempt to try and find the conditions under which it would foul. However, even at the very high T_w of 388°C, which was very close to the limit of temperatures that could safely be created in the rig, crude 19 still would not foul.

Following on from this a second crude named ‘crude 21’ was also provided by HTRI for fouling testing. It was also a light oil that created similar pressure problems in the rig to crude 19, whereby to reach test T_bs, some of the pressure and therefore crude oil vapour had to be released. Initial tests with the crude were problematic and it was difficult to get it to reach high T_ws, even with the CH at near maximum power. Therefore, it was decided that heat transfer tests should be conducted to see if there were any major problems occurring. These tests revealed that as the T_w of the metal finger increases, the effect increasing the

stirrer speed has on reducing the T_w drops. This disagreed with what CFD simulations predicted, which was that with stirrer speed increase, the T_w should always drop a similar amount at both high and low starting T_ws. This therefore suggested that something was happening inside the rig that was reducing the effect stirrer speed had on the HTC, and therefore T_w drop. The key cause is thought be nucleate boiling occurring on the surface of the metal finger, therefore forming a thermal barrier between the metal finger and the rotating fluid. This conclusion was further supported by simulated boiling point data, and the results of a SARA analysis of the crude showing that the C1-C9 fraction of the oil was as high as 27.53%. It was also observed that a sudden pressure increase inside the rig results in an instantaneous rise in T_w. This can only be explained by nucleate boiling bubbles being 'shocked' away for a few seconds by the pressure change, causing a rapid drop in the HTC. Lastly, the HTC was found to go up at an increasing rate as ΔT increases, matching up with the nucleate boiling part of the standard boiling regime plot.

Another cause of the reduced effect of stirrer speed at high temperatures was found to be the 'end effect'. This is where the proportion of the heat flux that travels through the vertical walls of the metal finger into the oil compared to through its base or top increases with stirrer speed. However as this is a proportional change, at higher CH powers the Δq over the stirrer speed change is larger than for lower CH powers. Therefore there is a greater amount of heat passing through the metal walls with increasing stirrer speeds at higher CH powers, resulting in an increase in T_w. This temperature increase works against the temperature decrease caused by the stirrer speed raising the HTC, resulting in an overall reduced T_w drop. It was also concluded that natural convection heat transfer could possibly be a more dominant mechanism at higher T_ws, and that this could also cause the reduced effect of stirrer speed on T_ws. It is believed that a combination of nucleate boiling, the end effect and natural convection are all contributing to the different way that T_w reacts to stirrer speed increase at high temperature, in comparison to at lower temperatures, though it is not possible to say which has the largest effect.

Fouling tests were carried out with crude 21 from May-August 2013 and initially the oil would not foul in the stirred batch cell. Eventually it was found that crude 21 would only start fouling if a sufficient amount of its light ends was first released. Nucleate boiling on the surface of the metal finger is believed to inhibit fouling through a combination of increasing turbulence around the wall, and forming an insulation layer between the crude oil and the heat transfer surface reducing the amount of it in contact with the wall. Only after the crude has been flashed and the nucleate boiling sufficiently reduced can a fouling deposit start to form on the metal finger. The impact of stirrer speed on the fouling rate for crude 21 at constant T_w was measured over six experiments, and a linear reduction in the fouling rate with stirrer speed was observed. The threshold stirrer speed at which the fouling rate was zero was observed to occur at around 400RPM. The impact of T_w on the fouling rate at constant stirrer

speed was also measured over a total of thirteen experiments. From these an Arrhenius plot was produced and crude 21 was calculated to have activation energy of 140kJ/mol at a stirrer speed of 100RPM. The fouling temperature threshold for crude 21 was found to occur at around 340°C.

Finally, five fouling removal experiments were undertaken in order to find out if a negative fouling rate could be observed. Results from these were mixed, and whilst a negative fouling rate was observed in one experiment, the other four were inconclusive. If fouling removal is possible with crude 21, it seems that it occurs at a very low rate, likely to be too low to be recorded in rig operation during a typical working day. This is probably because the crude oil has a low viscosity and therefore exerts quite a low shear stress on the fouling surface compared to heavier oils tested in the rig in the past. Therefore, it has not been possible to estimate the fouling threshold for the oil by interpolating between positive and negative fouling rates, as was the initial aim of the project.

10.1 Limitations and Further Research

Whilst the findings of this thesis, conducted using the stirred batch cell fouling rig have provided new insights into the effects nucleate boiling has on fouling formation, as well as the mechanisms of heat transfer inside the rig and the removal of fouling deposits, it is important to consider the limitations of this work. These limitations, as well as their potential impact on the conclusions and findings of the research, and how they could be addressed in future research work, are now discussed.

1. A fundamental limitation of conducting both heat transfer and fouling research in the rig is that whilst it is possible to make judgements based on the data it produces to predict what is going on inside, it will never be possible to see what is actually going on inside. Therefore whilst the data strongly suggest that nucleate boiling is having a large effect on both the heat transfer around the metal finger and on fouling, the only way it would be possible to conclude this with 100% certainty would be to see it happening, which is not possible.

2. Fouling began only after a certain amount of the light ends of crude 21 had first been released, which was observed for two different batches of oil. However the exact amount of oil that was vented is unknown, although is believed to equate to around 14-18% of the original 1 litre. It is assumed that it was the lightest fractions of the oil that were released, as they would have vaporised first. However, it is not possible to know exactly what was released without doing a full SARA analysis on the oil following an experiment. This could be done in future experiments to find out the exact composition of what was released.

3. If nucleate boiling affects the fouling rate, then fouling rate data from different batches of oil would be expected to have different fouling rates dependent on how much the oil is flashed before starting a fouling test. The greater the amount that had been released, the less severe the nucleate boiling and therefore the higher the fouling rate. Currently it is not possible to measure the volume of oil that is released through the valve, especially as it is a combination of both the nitrogen that is used to pressurise the rig and hydrocarbons that are released when the valve is opened. Repeatability between different batches of oil is therefore a potential issue when testing crude 21, although there is currently no way of fixing this issue. During all of the tests measuring the effect of T_w on the fouling rate, no extra vapour was released. Therefore, nucleate boiling rate did not affect the results of these tests. The same can be said for all of the tests measuring the effect of stirrer speed on the fouling rate. In many industrial refineries it is common for crude oil to be flashed before it reaches the hotter, higher fouling heat exchangers that these tests aimed to mimic the conditions of. Thus it was not unreasonable in this work to have recreated this by the flashing the crude before the fouling tests.

4. Part of the reason that the removal tests were inconclusive was that it was only possible to carry them out for around 2-3 hours. As removal (if it occurs) seems to happen at a very slow rate, there was not enough time to measure it accurately. Therefore, future removal tests would need to be carried out over a longer period of time. However, this would most likely require firstly several extra workers, and secondly the ability to run over night which is currently not possible due to safety and supervision requirements. Test length is also a limitation with fouling rate measurement tests, as having a longer test for each will always give a more accurate representation than a shorter test. However, for the same reasons as with the removal experiments, it is currently not possible to carry out tests overnight. The accuracy of these relatively short tests is supported by the fact that in nearly all of the recorded data sets, fouling increased at a constant rate throughout the whole test, suggesting that even if the test had been carried on, the measured rate would have been the same.

5. Variability and fluctuations in data are something that has already been discussed many times in this report. Variations in CH power and stirrer speed will always influence the T_w and thus fouling calculations. However, for almost all of the data plots in this thesis, these fluctuations seemed to have no effect on the overall trend of the graphs with regards to the rate that fouling was occurring. Therefore, it can be concluded that whilst these unpreventable fluctuations will have had an effect on the data, they have not altered it sufficiently to raise concern over the validity of the findings presented.

6. Due to the difficulties with getting crude 21 to foul in the first place and the time it took to carry out the heat transfer tests, there was only enough time to measure the effect of varying stirrer speed on the fouling rate at one T_w, and the effect of varying T_w on the fouling rate at one stirrer speed. It would, therefore, be beneficial to collect a full fouling data set for crude 21 over a variety of different T_ws and stirrer speeds. This would show if the trends observed for the conditions in which the tests were undertaken hold, or change with different conditions.

7. Whilst it is possible to release pressure and vapour in the stirred batch cell, it would not be possible to do this in a tubular rig. The methodology of releasing the light ends in order to start the oil fouling would be difficult to repeat in a tubular rig in order to see if the same occurs, though it is possible. It would be beneficial first, however, to see if a batch of fresh crude 21 will foul a tubular rig under similar T_w and shear stress conditions. If it would not foul, then the oil could perhaps be flashed and then a fouling run attempted. This would rely on a refinery providing a flashed sample of the crude which may not be possible.

8. It would be beneficial to investigate whether nucleate boiling occurs for crude 19 in the rig, as it too was a very light oil and had a similar viscosity to crude 21. It is, therefore, quite possible that nucleate boiling was occurring with it. Nucleate boiling could have also been the reason why it would not foul in any of the tests. The same procedure that was carried out with crude 21 could be repeated with crude 19, and a large amount of the oil's light ends released when it is tested, before carrying out a fouling test at around 340-350°C to see if this causes it to begin fouling. Heat transfer tests could also be carried out with crude 19 to see what is observed.

10.2 Research Implications

The largest implication of this work is the observed effect of nucleate boiling on the inhibition of fouling. There is very little information currently in the literature on the effect boiling has on crude oil fouling, and it is therefore perhaps an area of research that needs more attention. As explained in Chapter 10.1 it would first need investigation as to whether crude 21 would foul in a tubular fouling rig, and if not whether flashing would make it begin to start fouling. If this was found to happen, then it has implications for crude oil refineries, as they may be able to utilise boiling to reduce fouling levels in heat exchangers. Refineries typically process crude that has not been flashed, but there are times when they do process flashed crudes. Whilst a refinery may not be able to choose whether their crude source is flashed or not, if a flashed crude is being used, operators should be aware that it may be more likely to foul, and take steps to reduce fouling propensity, such as by increasing the shear stress forces by raising the flow velocity.

With regards to the implications of the findings of this thesis on future work using the stirred batch cell, it is the discovery of the contribution the end effect has on heat transfer in the cell that is particularly important. In the past fouling calculations have not taken into account the impact of the end effect on heat flux variance as stirrer speed increases; this is something that needs to be done in all future work. The effect of natural convection on overall heat transfer is also something that has not been greatly considered in the past and it is unknown if this has any major effects. CFD simulations in the future need to be utilised to better determine the effects of natural convection. As this thesis has found, there are often so many different heat transfer mechanisms and factors going on all at once in the rig, it is very difficult to work out which have bigger effects by experimental work alone.

CHAPTER 11

11 References

Albert, F., Augustin, W. and Scholl, S. (2011) Roughness and Constriction Effects on Heat Transfer in Crystallisation Fouling, *Chemical Engineering Science* 66 (3): 499–509.

Al-Faris, T.F. and Fakeeha, A.H. (1992) Viscosity Correlation for Non-Newtonian Waxy Oils, *Journal of King Abdulaziz University Engineering Science* 4: 91–100.

Andritsos, N. and Karabelas, A.J. (2003) Calcium Carbonate Scaling in a Plate Heat Exchanger in the Presence of Particles, *International Journal of Heat and Mass Transfer* 46 (24): 4613–4627.

Asomaning, S. (1997) *Heat Exchanger Fouling by Petroleum Asphaltenes*, PhD Thesis. Vancouver, Canada: University of British Colombia.

Asomaning, S., Panchal, C.B. and Liao, C.F. (2000) Correlating Field and Laboratory Data for Crude Oil Fouling, *Heat Transfer Engineering* 21 (3): 17–23.

Augustin, W. and Bohnet, M. (2001) Influence of Pulsating Flow on Fouling Behaviour on Heat Transfer Surfaces, *Chemie Ingenieur Technik* 73 (9): 1139–1144.

Bansal, B. and Müller-Steinhagen, H. (1993) Crystallisation Fouling in Plate Heat Exchangers, *Journal of Heat Transfer* 115 (3): 584–591.

Bennett, C.A., Kistler, R.S., Nangia, K., Al-Ghawas, W., Al-Hajji, N. and Al-Jemaz, A. (2009) Observation of an Isokinetic Temperature and Compensation Effect for High-Temperature Crude Oil Fouling, *Heat Transfer Engineering* 30 (10-11): 794–804.

Bories, M. and Patureaux, T. (2004) Preheat Train Crude Distillation Fouling Propensity Evaluation by the Ebert and Panchal Model, Heat Exchanger Fouling and Cleaning: Fundamentals and Applications 27: 200–210.

Bott, T.R., Melo, L.F., Panchal, C.B. and Somerscales, E.F.C. (Eds.) (1999) *Understanding Heat Exchanger Fouling and its Mitigation*. New York: Begell House.

Charaklis, W.G. (1981) “Microbial Fouling” Pages 251–281 in Somerscales, E.F.C. and Knudsen, J.G. (Eds.) *Fouling of Heat Transfer Equipment*. Washington D.C.: Hemisphere Publishing Company.

Churchill, S.W. (1988) Viscous Flows: The Practical Use of Theory. Boston, Massachusetts: Butterworths.

Coletti, F., Ishiyama, E.M., Paterson, W.R., Wilson, D.I. and Macchietto, S. (2010) Impact of Deposit Aging and Surface Roughness on Thermal Fouling: Distributed Model, *American Institute of Chemical Engineers* 56 (12): 3257–3273.

Costa, A.L.H., Tavares, V.B.G., Borges, J.L., Queiroz, E.M., Pessoa, F.L.P., Liporace, F.D.S. and de Oliveira, S.G. (2013) Parameter Estimation of Fouling Models in Crude Preheat Trains, *Heat Transfer Engineering* 34 (8-9): 683–691.

Coulson, J.M., Richardson, J.F., Backhurst, J.R. and Harker, J.H. (2007) *Coulson and Richardson’s Chemical Engineering: Volume 1 – Fluid Flow, Heat Transfer and Mass Transfer*, 6th Edition. Oxford: Elsevier.

Crittenden, B.D. and Kolaczkowski, S.T. (1979) “Mass Transfer and Chemical Kinetics in Hydrocarbon Fouling” Pages 169–187 in *Proceedings of the International Conference*

on Fouling: Science or Art. Guildford, Surrey: Institute of Corrections Science and Technology and Institute of Chemical Engineering.

Crittenden, B.D. and Kolaczkowski, S.T. (1987) Reducing Exchanger Fouling, *Hydrocarbon Processing* 66 (8): 45–46.

Crittenden, B.D., Kolaczkowski, S.T. and Downey, I.L. (1992) Fouling of Crude Oil Preheat Exchangers, *Chemical Engineering Research and Design* 70 (6): 547–557.

Crittenden, B.D., Kolaczkowski, S.T., Takemoto, T. and Phillips, D.Z. (2009) Crude Oil Fouling in a Pilot-Scale Parallel Tube Apparatus, *Heat Transfer Engineering* 30 (10-11): 777–785.

Crittenden, B.D., Kolaczkowski, S.T., Takemoto, T. (1993) The Use of In-Tube Inserts to Reduce Fouling From Crude Oils, *American Institute of Chemical Engineers Symposium Series* 89 (295): 300–307.

Crittenden, B.D., Yang, M., Dong, L., Hanson, R., Jones, J., Kundu, K., Harris, J., Klochok, O., Arsenyeva, O. and Kapustenko, P. (2013) "Crystallisation Fouling with an Enhanced Heat Transfer Surface" in *Proceedings of the International Conference on Heat Exchanger Fouling and* Cleaning. Budapest, Hungary: Heat Exchanger Fouling.

Deshannavar, U.B., Rafeen, M.S., Ramasamy, M. and Subbarao, D. (2010) Crude Oil Fouling: A Review, *Journal of Applied Sciences* 10 (24): 3167–3174.

Eaton, P. and Lux, R. (1984) Laboratory Fouling Test for Hydrocarbon Feed-Stocks, *ASME–HTD* 35: 33–42.

Eaton, P.E. (1983) *Fouling Test Apparatus*. United States Patent 4383438.

Ebert, W. and Panchal, C.B. (1997) "Analysis of Exxon Crude-Oil Slip Stream Coking Data" Pages 451–460 in Panchal, C.B., Bott, T.R., Somerscales, E.F.C. and Toyama, S. (Eds.) *Fouling Mitigation of Industrial Heat Exchange Equipment*. New York: Begell House.

Ebert, W.A. and Panchal, C.B. (1995) "Analysis of Exxon Crude-Oil Slip Stream Coking Data" Pages 451–460 in Panchal, C.B. and Kuru, W.C. (Eds.) *Fouling Mitigation of Industrial Heat-Exchange Equipment*. New York: Begell House.

Engineering Sciences Data Unit (2005) *Heat Exchanger Fouling in the Pre-Heat Train of a Crude Oil Distillation Unit*. London: IHS.

Epstein, N. (1983) Thinking About Heat Transfer Fouling: A 5x5 Matrix, *Heat Transfer Engineering* 4 (1): 43–56.

Epstein, N. (1994) "A Model of the Initial Chemical Reaction Fouling Rate for Flow Within a Heated Tube and its Verification" Pages 225–229 in Hewitt, G.F. (Ed.) *Proceedings of the 10th International Heat Transfer Conference*. Rugby: Institution of Chemical Engineers.

Escobedo, J. and Mansoori, G.A. (2010) Heavy Organic Particle Deposition From Petroleum Fluid Flow in Oil Wells and Pipe Lines, *Journal of Petroleum Science and Engineering* 7: 502–508.

Garrett-Price, B.A., Smith, S.A., Watts, R.L., Knudsen, J.G., Marner, W.J. and Suitor, J.W. (1985) *Fouling of Heat Exchangers: Characteristics, Costs, Prevention, Control, and Removal*. Park Ridge, New Jersey: Noyes Publications.

Gudmundson, J.S. (1981) "Particulate Fouling" Pages 357–387 in Somerscales, E.F.C. and Knudsen, J.G. (Eds.) *Fouling of Heat Transfer Equipment*. Washington D.C.: Hemisphere Publishing Company.

Hasan, B.O., Nathan, G.J., Ashman, P.J., Craig, R.A. and Kelso, R.M. (2012) The Use of Turbulence Generators to Mitigate Crystallisation Fouling Under Cross Flow Conditions, *Desalination* 288: 108-117.

Hasson, D. (1981) "Precipitation Fouling" Pages 527–568 in Somerscales, E.F.C. and Knudsen, J.G. (Eds.) *Fouling of Heat Transfer Equipment*. Washington D.C.: Hemisphere Publishing Company.

Hewitt, G.F. (Ed.) (1994) *Proceedings of the 10th International Heat Transfer Conference*. Rugby: Institution of Chemical Engineers.

Kern, D.Q. and Seaton, R.E. (1959) A Theoretical Analysis of Thermal Surface Fouling, *British Chemical Engineering* 4 (5): 258–262.

Knudsen, J.G., Lin, D. and Ebert, W.A. (1999) "The Determination of the Threshold Fouling Curve for a Crude Oil" Pages 265–272 in Bott, T.R., Melo, L.F., Panchal, C.B. and Somerscales, E.F.C. (Eds.) *Understanding Heat Exchanger Fouling and its Mitigation*. New York: Begell House.

Konak, A.R. (1974) A New Model for Surface Reaction-Controlled Growth of Crystals from Solution, *Chemical Engineering Science* 29 (7): 1537–1543.

Krause, S. (1993) Fouling of Heat-Transfer Surfaces by Crystallisation and Sedimentation, *International Chemical Engineering* 33 (3): 336–401.

Kuru, W.C. and Panchal, C.B. (1997) "High-Temperature Organic-Fluid Fouling Unit" in *American Institute of Chemical Engineers/American Society of Mechanical Engineers National Heat Transfer Conference: Current Developments in Numerical Simulation of Heat and Mass Transfer*. Baltimore, Maryland: American Institute of Chemical Engineers/American Society of Mechanical Engineers.

Lemke, H.K. (1999) "Fouling in Refinery Equipment: An Overview" Pages 375–382 in Wiehe, I.A. (Ed.) *Proceedings of the 1st International Conference on Petroleum Phase Behaviour and Fouling*. New York: American Institute of Chemical Engineers.

Malayeri, M.R., Müller-Steinhagen, H. and Watkinson, A.P. (Eds.) (2011) *Proceedings of International Conference of Heat Exchanger Fouling and Cleaning*. Crete, Greece: Heat Exchanger Fouling.

Müller-Steinhagen, H. (2000) *Heat Exchanger Fouling: Mitigation and Cleaning Technologies*. Rugby, Warwickshire: Institute of Chemical Engineers.

Müller-Steinhagen, H., Malayeri, M.R. and Watkinson, A.P. (Eds.) (2005) *Proceedings of 6th International Conference on Heat Exchanger Fouling and Cleaning: Challengers and Opportunities*. Irsee, Germany: Engineering Conferences International.

Müller-Steinhagen, H., Malayeri, M.R. and Watkinson, A.P. (Eds.) (2009) *Proceedings of the Eurotherm Conference on Fouling and Cleaning in Heat Exchangers*. Schladming, Austria: Heat Exchanger Fouling.

Mullin, J.W. (2001) *Crystallisation*, 4th Edition. Oxford: Butterworth-Heinemann.

Mullin, T., Lorenzen, A. and Pfister, G. (1983) Transition to Turbulence in a Non-Standard Rotating Flow, *Physics Letters A* 96 (5): 236–238.

Mwaba, M.G., Golriz, M.R. and Gu, J. (2006) A Semi-Empirical Correlation for Crystallisation Fouling on Heat Exchange Surfaces, *Applied Thermal Engineering* 26 (4): 440–447.

Nelson, W.L. (1934) Fouling of Heat Exchangers, *Refining and Natural Gasoline Manufacturer*. 13 (7): 271-276

Nasr, J.M.R. and Givi, M.M. (2006) Application of Threshold Model with Various Tube Wall Temperatures for Crude Oil Preheat Train Fouling, *Iranian Journal of Chemistry and Chemical Engineering* 25 (3): 49–58.

Pääkkönen, T.M., Riihimäki, M., Simonson, C.J., Muurinen, E. and Keiski, R.L. (2012) Crystallisation Fouling of $CaCO_3$ – Analysis of Experimental Thermal Resistance and its Uncertainty, *International Journal of Heat and Mass Transfer* 55 (23-24): 6927–6937.

Panchal, C.B. and Huangfu, E-P. (2000) Effects of Mitigating Fouling on the Energy Efficiency of Crude-Oil Distillation, *Heat Transfer Engineering* 21 (3): 3–9.

Panchal, C.B. and Kuru, W.C. (Eds.) (1995) *Fouling Mitigation of Industrial Heat-Exchange Equipment*. New York: Begell House.

Panchal, C.B. and Somerscales, E.F.C. (Eds.) (1999) *Understanding Heat Exchanger Fouling and its Mitigation: Proceedings of an International Conference on Understanding Heat Exchanger Fouling and its Mitigation*. New York: Begell House.

Panchal, C.B., Bott, T.R., Somerscales, E.F.C. and Toyama, S. (Eds.) (1997) *Fouling Mitigation of Industrial Heat Exchange Equipment*. New York: Begell House.

Panchal, C.B., Kuru, W.C., Liao, C.F., Ebert, W.A. and Palen, J.W. (1999) "Threshold Conditions for Crude Oil Fouling" Pages 273–279 in Panchal, C.B. and Somerscales, E.F.C. (Eds.) *Understanding Heat Exchanger Fouling and its Mitigation: Proceedings of an International Conference on Understanding Heat Exchanger Fouling and its Mitigation*. New York: Begell House.

Petitjean, E., Aquino, B. and Polley, G.T. (2007) Observations on the Use of Tube Inserts to Suppress Fouling in Heat Exchangers, *Hydrocarbon World*: 42–46.

Petroval (2013) "Tube Inserts" [www.petroval.fr/thermal-tube-inserts.asp; Accessed 1st June 2013].

Polley, G.T., Wilson, D.I., Yeap, B.L. and Pugh, S.J. (2002) Evaluation of Laboratory Crude Oil Fouling Data for Application to Refinery Pre-Heat Trains, *Applied Thermal Engineering* 22 (7): 777–788.

Poncet, S., Haddadi, I. and Viazzo, S. (2011) Numerical Modeling of Fluid Flow and Heat Transfer in a Narrow Taylor-Couette-Poiseuille System, *International Journal of Heat and Fluid Flow* 32 (1): 128–144.

Pugh, S.J., Hewitt, G.F. and Müller-Steinhagen, H. (2009) Fouling During the Use of 'Fresh' Water as Coolant – The Development of a 'User Guide', *Heat Transfer Engineering* 30 (10-11): 851–858.

Reeder, R.J. (Ed.) (1983) *Carbonates: Mineralogy and Chemistry*, Volume 11. Stony Brook, New York: USA Mineralogical Society of America.

Ritchie, J.M., Droegenmueller, P. and Simmons, M.J.H. (2009) HiTrain Wire Matrix Inserts in Fouling Applications, *Heat Transfer Engineering* 30 (10-11): 876–884.

Saleh, Z.S., Sheikholeslami, R. and Watkinson, A.P. (2005) Fouling Characteristics of a Light Australian Crude Oil, *Heat Transfer Engineering* 26 (1): 15–22.

Scarborough, C.E., Cherrington, D.C., Diener, R. and Golan, L.P. (1979) Coking of Crude Oil at High Heat Flux Levels, *Chemical Engineering Progress* 75 (7): 41–46.

Sheikholeslami, R. (2000) Composite Fouling of Heat Transfer Equipment in Aqueous Media – A Review, *Heat Transfer Engineering* 21 (3): 34–42.

Sheikholeslami, R. and Watkinson, A.P. (2013) "Composite Fouling: Fundamentals and Mechanisms", *Desware* [www.desware.net/Physical-Chemical-Biological-Properties-Water.aspx; Accessed 1st June 2013].

Silva, C.D.S., Liporace, F.S. and Queiroz, E.M. (2005) Fouling Models for Real Time Heat Exchanger Fouling Detection, *2nd Mercosur Congress on Chemical Engineering/4th Mercosur Congress on Process Systems Engineering* 14: 1–9.

Sinnott, R.K., Coulson, J.M. and Richardson, J.F. (2005) *Coulson and Richardson's Chemical Engineering: Volume 6 – Chemical Engineering Design*, 4th Edition. Oxford: Elsevier.

Smith, G.P. and Townsend, A.A. (1982) Turbulent Couette Flow Between Concentric Cylinders at Large Taylor Numbers, *Journal of Fluid Mechanics* 123: 187–217.

Somerscales, E.F.C. (1981) "Corrosion Fouling" Pages 17–27 in Somerscales, E.F.C. and Knudsen, J.G. (Eds.) *Fouling of Heat Transfer Equipment*. Washington D.C.: Hemisphere Publishing Company.

Somerscales, E.F.C. and Knudsen, J.G. (Eds.) (1981) *Fouling of Heat Transfer Equipment*. Washington D.C.: Hemisphere Publishing Company.

Srinivasan, M. and Watkinson, A.P. (2005) Fouling of Some Canadian Crude Oils, *Heat Transfer Engineering* 26 (1): 7–14.

MERUS Oil and Gas (2013) "Hydrocarbon Fouling, Image 5" [www.merusoilandgas.com/fouling-in-hydrocarbon-heat-processes; Accessed 1st April 2013].

Stephan, K. and Laesecke, A. (1985) The Thermal Conductivity of Fluid Air, *Journal of Physical and Chemical Reference Data* 14 (1): 227–234.

Storm, D.A., Barresi, R.J. and Sheu, E.Y. (1996) Flocculation of Asphaltenes in Heavy Oil at Elevated Temperatures, *Fuel Science and Technology International* 14 (1-2): 243–260.

Tai, C.Y. and Chen, F-B. (1998) Polymorphism of $CaCO_3$ Precipitated in a Constant Composition Environment, *American Institute of Chemical Engineers* 44 (8): 1790–1798.

Watkinson, A.P. and Wilson, D.I. (1997) Chemical Reaction Fouling: A Review, *Experimental Thermal and Fluid Science* 14 (4): 361–374.

Watkinson, A.P., Navaneetha-Sundaram, B. and Posarac, D. (2000) Fouling of a Sweet Crude Oil Under Inert and Oxygenated Conditions, *Energy and Fuels* 14 (1): 64–69.

Wiehe I.A. (1997) *The Role of Phase Equilibria in Coke and Sediment Formation*. Houston, Texas: American Institute of Chemical Engineers.

Wiehe, I.A. (2006) *Petroleum Fouling: Causes, Tools and Mitigation Methods*. Gladstone, New Jersey: Soluble Solutions.

Wiehe, I.A. (Ed.) (1999) *Proceedings of the 1st International Conference on Petroleum Phase Behaviour and Fouling*. New York: American Institute of Chemical Engineers.

Wilson, D.I., Polley, G.T. and Pugh, S.J. (2005) "Ten Years of Ebert, Panchal and the 'Threshold Fouling' Concept" Pages 25–36 in Müller-Steinhagen, H., Malayeri, M.R. and Watkinson, A.P. (Eds.) *Proceedings of 6th International Conference on Heat Exchanger Fouling and Cleaning: Challengers and Opportunities*. Irsee, Germany: Engineering Conferences International.

Wray, J.L. and Daniels, F. (1957) Precipitation of Calcite and Aragonite, *Journal of the American Chemical Society* 79 (9): 2031–2034.

Yang, M., O'Meara, A. and Crittenden, B.D. (2011) "Determination of Crude Oil Fouling Thresholds" Pages 309–314 in Malayeri, M.R., Müller-Steinhagen, H. and Watkinson, A.P. (Eds.) *Proceedings of International Conference of Heat Exchanger Fouling and Cleaning*. Crete, Greece: Heat Exchanger Fouling.

Yang, M., Young, A. and Crittenden, B.D. (2009) "Use of CFD to Correlate Crude Oil Fouling Against Surface Temperature and Surface Shear Stress in a Stirred Fouling Apparatus" Pages 272–280 in Müller-Steinhagen, H., Malayeri, M.R. and Watkinson, A.P. (Eds.) *Proceedings of the Eurotherm Conference on Fouling and Cleaning in Heat Exchangers*. Schladming, Austria: Heat Exchanger Fouling.

Yang, Q., Liu, Y., Gu, A., Ding, J. and Shen, Z. (2002) Investigation of Induction Period and Morphology of $CaCO_3$ Fouling on Heated Surface, *Chemical Engineering Science* 57 (6): 921–931.

Yeap, B.L., Wilson, D.I., Polley, G.T. and Pugh, S.J. (2004) Mitigation of Crude Oil Refinery Heat Exchanger Fouling Through Retrofits Bases on Thermo-Hydraulic Fouling Models, *Chemical Engineering Research and Design* 82 (1): 53–71.

Yépez, O. (2005) Influence of Different Sulfur Compounds on Corrosion Due to Naphthenic Acid, *Fuel* 84 (1): 97–104.

Young, A., Venditti, S., Berrueco, C., Yang, M., Waters, A., Davies, H., Hill, S., Millan, M. and Crittenden, B. (2011) Characterisation of Crude Oils and their Fouling Deposits Using a Batch Stirred Cell System, *Heat Transfer Engineering* 32 (3-4): 216–227.

Zhao, X. and Chen, X.D. (2013) A Critical Review of Basic Crystallography to Salt Crystallisation Fouling in Heat Exchangers, *Heat Transfer Engineering* 34 (8-9): 719–732.

APPENDICIES

Appendix 1: Crittenden *et al.* (2013) Fouling Removal Conference Paper

CRYSTALLIZATION FOULING WITH ENHANCED HEAT TRANSFER SURFACES

[1]B.D. Crittenden, [1]M. Yang, [1]L. Dong,[1]R. Hanson, [1]J. Jones, [1]K. Kundu, [1]J. Harris,
[2]Oleksandr Klochok, [2]Olga Arsenyeva, [2]Petro Kapustenko

[1]Department of Chemical Engineering,
University of Bath, Bath, BA2 7AY, UK
Tel: 01225 386501
Email: cesbdc@bath.ac.uk

[2]Spivdruzhnist-T JSC
Kharkiv, Ukraine

ABSTRACT

The main aim of this paper is to demonstrate that a simple stirred batch cell can be used to study the effects of surface shear stress (amongst other process parameters) on fouling from saturated calcium sulphate and calcium carbonate solutions. Fouling tests have been conducted using heated probes fitted with both smooth and enhanced surfaces. For otherwise identical operating conditions, the overall fouling rate on a mild steel surface was found to be reduced when either fine wires were attached to it or when helical threads were incorporated into the surface, either in the form of a continuous helical groove or in the form of a raised helix. The raised helical surface was more effective in reducing fouling than the helical groove. The results confirm the general effect that fouling rates can be reduced by increasing the surface shear stress through surface enhancement. The potential weakness of the stirred batch cell compared with a continuous flow loop apparatus is that the former cannot be operated at steady state conditions. Hence a simple mathematical model has been developed to take into account the dynamic change in bulk concentration as crystallization fouling occurs. In all cases, the overall fouling resistance increased asymptotically towards a constant value and could easily and accurately be described quantitatively by the new analytical model. The variations of shear stresses on the various surfaces were determined from CFD simulations using the commercial package Comsol 4.2.

INTRODUCTION

Crystallization fouling on heat exchanger surfaces can create chronic operational problems in a broad range of processing applications that include cooling water systems, desalination, steam generation, etc. Energy losses, additional power consumption and the costs of cleaning all make this practical operational problem a significant challenge in the progression towards sustainable development.

Several researchers have investigated crystallization fouling of calcium sulphate and calcium carbonate using recirculating tubular flow type devices (eg Malayeri et al., 2007, Fahiminia et al., 2007, Albert et al., 2009, and Esawy et al., 2009). The effects of a number of operational parameters such as velocity, temperature, calcium concentration, and surface geometry on the fouling rate have been studied. In the research presented in this paper, a different approach has been adopted. The simple stirred batch cell which was originally designed to study fouling from crude oils (Young et al., 2011) has now been used for the first time to study the effects of surface shear stress and surface temperature on fouling from saturated calcium salt solutions. The principal advantage of the batch cell over its continuous flow counterpart is that different surface configurations that enhance turbulence and heat transfer can easily be studied. The effects of enhancements such as wires, dimples, helical threads, etc, on fouling can then be interpreted to assist prediction of the effects of surface enhancements on fouling in, for example, plate heat exchangers and tubes fitted with inserts such as hiTRAN. A disadvantage of the stirred batch cell, given that the volume of solution is small (about 1 litre), is that the concentration of calcium salt may not be considered to be constant due to the formation of crystallization deposits on the heated surface. The fouling rate is therefore dynamically related to the change in bulk concentration with time. This clearly sets a challenge when interpreting the experimental data, but on the other hand, initial fouling rates arise at the known initial bulk concentration and of course the data may provide an excellent opportunity to discover the effect of bulk concentration on fouling rate in a single simple experiment.

Apart from determining fouling resistances through interpretation of the heat transfer data, the actual fouling layer profiles have also been studied using a ProScan laser micro-scanning technology. In addition, the experimental data are complemented by CFD simulations of the fluid flow in the stirred cell in the manner described elsewhere (Yang et al., 2009). The CFD studies have been made for

test probes with and without surface enhancements using the commercial package Comsol 4.2. The resulting velocity, shear stress and temperature fields are able to show clearly how the experimental effects of temperature and surface shear stress on the fouling are well correlated by the CFD simulations.

EXPERIMENTS

The stirred cell and probes

Details of the stirred cell system and the heated test probe shown in Figure 1a are provided by Young et al. (2011). The cell comprises a pressure vessel made in-house from a block of 304 stainless steel and is fitted with a top flange. The base of the vessel houses an upwards pointing test probe heated internally by a cartridge heater. The heat flux is controlled electrically. A batch of about 1.0 litres of aqueous solution is agitated by a downwards facing cylindrical stirrer mounted co-axially with the test probe and driven by an electric motor. External band heaters are incorporated to provide initial heating to the vessel and its contents. An internal cooling coil uses a non-fouling fluid (Paratherm) to remove heat at the rate that it is put in via the cartridge heater during the fouling run. The vessel is fitted with a pressure relief valve and there is a single thermocouple to measure the bulk solution temperature. The mechanisms for the control of bulk temperature and stirring speed are described elsewhere (Young et al., 2011). The surface temperature of the test probe can be changed by altering the heat flux by adjusting the input power to the cartridge heater.

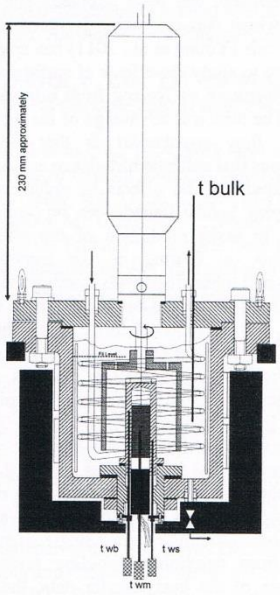

Fig. 1a The stirred batch cell
twb, twm, and tws are thermocouples

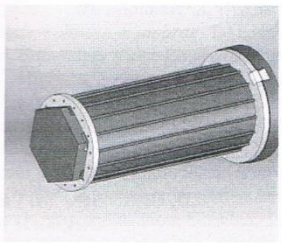

Fig. 1b The fouling probe fitted with a nest of wires (Yang et al., 2013)

Details of the plain mild steel probe and the one fitted with a nest of wires, as shown in Figure 1b, respectively, have been reported elsewhere (Yang et. al., 2013). The probe has, additionally, been modified by attaching sleeves with helical threads incorporated into their surface, either in the form of a continuous helical groove or in the form of a raised helix. Figures 2a and 2b show the two helically enhanced sleeves with negative and positive helices, respectively, and Figure 2c shows, as a reference, a plain sleeve of the same diameter as the two helically enhanced ones.

a b c

Fig. 2 Probe sleeves
a: Sleeve with negative helical thread
b: Sleeve with positive helical thread
c: Plain sleeve

Materials and experimental method

The purpose of this paper is to confirm that the stirred batch cell can be used to study the effects of enhanced surfaces on fouling from aqueous solutions. For this purpose, simple standard solutions of calcium sulphate and calcium carbonate have been used. This study is not concerned with studying the effects of water chemistry on the fouling process. The standard solution of $CaSO_4$ is prepared by dissolving 4.1g of $Ca(NO_3)_2$ and 8.0 g of $Na_2SO_4(H_20)_{10}$ (both from Sigma-Aldrich) in 500 ml of deionized water, and then mixing the two solutions to form a 1 litre working solution containing 3400 ppm of $CaSO_4$ at pH=5.6. The standard solution of $CaCO_3$ is prepared by dissolving 1.68 g of $NaHCO_3$ and 1.44 g of $CaCl_2(H_20)_2$ (both from Sigma-Aldrich) in 500 ml of deionized water, and then mixing the two solutions to form a 1 litre working solution containing 1000 ppm of $CaCO_3$ at pH=5.2. For working solutions at other concentrations, the mass of each chemical is adjusted proportionately. All chemicals are reagent grade. The working solution is transferred to the stirred batch cell and brought up to the desired bulk operating temperature by means of the external band heaters

uniform over the probe surface when it is not enhanced (Yang et al., 2009). The local heat flux data were then used to calculate the fouling resistance using the temperature difference data such as that shown in Figure 3. Typical fouling curves in terms of how the fouling resistance varies with time are shown in Figures 7a and 7b for $CaSO_4$ and $CaCO_3$, respectively.

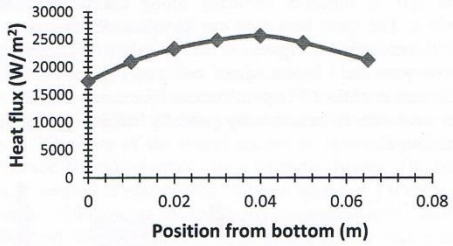

Fig. 6 Heat flux profile over the probe surface (stainless steel probe)
Heating power: 130W; stirrer speed: 310 rpm; bulk temperature: 55°C

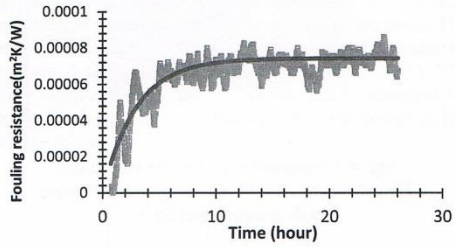

Fig. 7a Fouling resistance data of $CaSO_4$ and model fit (stainless steel probe)
Symbols: experimental data derived from twb;
Line: model fitting
Stirrer speed: 150 rpm; bulk temperature: 55°C;
average heat flux: 32 kW m^{-2}

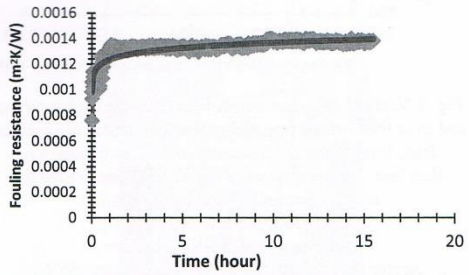

Fig. 7b Fouling resistance data of $CaCO_3$ and model fit (stainless steel probe)
Symbols: experimental data derived from twb;
Line: model fitting
Stirrer speed: 150 rpm; bulk temperature: 55°C;
average heat flux: 33 kW m^{-2}

Effect of bulk concentration

Figures 7a and 7b show that the fouling resistances seem to reach asymptotic values relatively quickly. On the one hand, the net fouling rate which many consider to be the difference between a deposition rate and a removal rate can be considered to be reducing gradually towards zero up to the asymptote. On the other hand, further analysis reveals that this asymptotic situation could be caused by the gradual reduction in the driving force for crystallization as time progresses in the batch system. That is, as deposition progresses then the degree of super-saturation, due to the calcium salt leaving the bulk solution and depositing on the heated surface, causes a reduction in the bulk concentration. As an example of the potential magnitude of this concentration depletion effect, the dry mass of deposit after one fouling run was found to be 0.97 g, accounting for about 30% of the original salt mass in the bulk solution. If this is the cause of the asymptotic curves shown, for example, in Figures 7a and 7b, then traditional asymptotic models may not be applicable and the dynamic change in bulk solution must, accordingly, be taken into account. Fahiminia et al. (2007) developed a fouling rate model after Konak (1974) and Krause (1993) that gives a relationship between the initial fouling rate and the difference in concentration between super-saturation in the bulk and in normal saturation:

$$\emptyset = \frac{\Delta C}{\frac{1}{k_m} + \frac{1}{k_a^{1/n}} \emptyset^{(n-1)/n}} \quad (1)$$

Here Φ is the crystallization deposition rate, $\Delta C = C_b - C_s$ is the difference in concentration between the super-saturation in the bulk, C_b, and the normal saturation, C_s. Additionally, k_m, k_a, and n are the mass transfer coefficient, reaction rate constant, and reaction order, respectively. The fouling rate is related to Φ after Fahiminia et al. (2007), as follows:

$$\frac{dR_f}{dt} = \frac{\emptyset}{\lambda_f \rho_f} \quad (2)$$

Here, λ_f and ρ_f are the thermal conductivity and density of the fouling deposit, respectively. Assuming that the bulk concentration reduction caused by fouling is proportional to the fouling resistance, then the change in bulk concentration is given by:

$$C_b = C_{b0} - \alpha R_f \quad (3)$$

In equation (3), C_{b0} is the initial bulk concentration and α is a constant. Given that $\Delta C_0 = C_{b0} - C_s$, then by combining equations (1), (2), and (3), by assuming that $n = 1$, and by taking into account a deposit removal term, as proposed by Crittenden et al. (1987), equation (4) is obtained:

$$\frac{dR_f}{dt} = \frac{\frac{\Delta C_0}{\lambda_f \rho_f} - \frac{\alpha}{\lambda_f \rho_f} R_f}{\frac{1}{k_m} + \frac{1}{k_a}} - \gamma R_f \quad (4)$$

Here γ is the rate constant of any deposit removal process which would depend critically on both temperature and velocity (or surface shear stress). The equation is broadly similar to that developed for a model organic fluid system by Crittenden et al. (1987). Integration of equation (4) yields:

$$R_f = \frac{\Delta C_0}{\alpha + \frac{k_m - k_a}{k_m k_a}\gamma \lambda_f \rho_f}\left[(1 - \exp\left(-\left(\frac{\alpha}{\lambda_f \rho_f}\frac{k_m k_a}{(k_m - k_a)} + \gamma\right)t\right)\right] \quad (5)$$

As shown in Figures 7a and 7b, the calcium salt fouling curves obtained using the stirred cell are correlated well using equation (5). The equation shows correctly that R_f is zero at $t = 0$, and that the fouling resistance tends towards a constant value when the running time is sufficient, appearing to give a fouling curve of the asymptotic type. The maximum value of R_f is proportional to the difference in concentration between the initial bulk super-saturation and the normal saturation. The initial fouling rate can be obtained by differentiation of equation (5), setting $t = 0$, or simply using equation (4) and setting $R_f = 0$, at $t = 0$:

$$\frac{dR_f}{dt} = \frac{\Delta C_0}{\lambda_f \rho_f}\frac{k_m - k_a}{k_m k_a} \quad (6)$$

According to equation (6), the initial fouling rate is proportional to the initial difference in concentration between the initial super-saturation and the normal saturation. Figure 8 shows four initial fouling rates for $CaSO_4$ at different initial concentrations, keeping all other operating parameters constant. Figure 8 indeed shows that the initial fouling rate is linearly dependent on the difference in concentration between the initial super-saturation and the normal saturation, as given by equation (6).

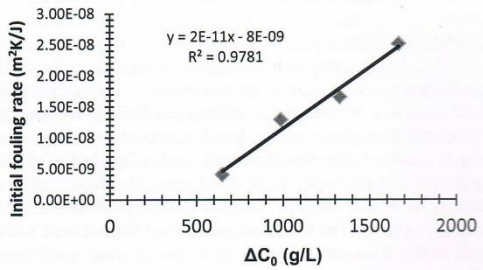

Fig. 8 Linear dependency of initial fouling rate on the difference in concentration between initial super-saturation and normal saturation
$\Delta C_0 = C_{b0} - C_s$
with $C_s = 2.070$ kg m^{-3} (Calmanovici et al., 1993)

Effect of temperature

In general, fouling is more intensive when the surface temperature is higher. As shown in Figures 4 and 5, the surface temperature of the heated probe is higher in the middle and lower towards its two ends. This variation arises as a result of the complex fluid flow patterns within the inner boundary of the batch cell's stirrer.

Figure 9a shows a photograph of the probe with a scaling deposit, and Figure 9b shows the deposit thickness profile along the vertical length obtained using ProScan 2000. It can be seen that the fouling layer thickness profile over the probe surface is strikingly similar in form to the temperature profile shown in Figure 5, with maxima in both deposit thickness and temperature occurring near to the middle of the heated probe surface. As reported previously (Yang et al., 2009), the shear stress over the probe surface where the fouling zone is located is relatively constant. Hence the profile of the fouling behaviour is determined solely by the surface temperature and not the shear stress. Accordingly, the similarity of the temperature and the fouling layer thickness profiles can be used to explain qualitatively the fouling rate behaviour in the experiment as a function of surface temperature.

Fig. 9a Mild steel probe with $CaSO_4$ deposit

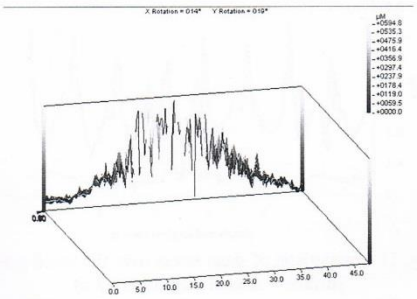

Fig. 9b ProScan deposit thickness profile

Effect of surface enhancements on fouling

The overall fouling rate on a mild steel surface was found to be reduced when fine wires were attached to it. Under the same operational conditions of bulk temperature (55°C), initial surface temperature (88°C) and stirrer speed (300 rpm), the fouling rates on the wired probe and the bare probe were 2.9 x 10^{-5} m^2 K J^{-1}, and 4.2 x 10^{-5} m^2 K J^{-1}, respectively. Furthermore, as shown in Figure 10, the fouling rates on the probes fitted with helical surfaces (both negative and positive) were found to be lower than on the

smooth surface. Moreover, the fouling rates on the positive helical surface were found to be the lowest. These reductions in fouling rate with enhanced surfaces are caused by the enhanced turbulence created either by the attached wires or by the incorporated helical threads. As shown in Figure 11, the shear stress is higher over the surface of the wired probe than over the bare probe. In the cases of probes fitted with sleeves, the average shear stress was found to increase in the order of smooth surface, negative helical groove, and positive helical surface, as shown in Figure 12. The difference in fouling rate on the different surface configurations can therefore be explained using the shear stress data obtained by CFD simulation.

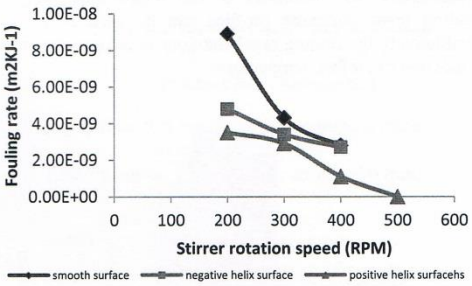

Fig. 10 Fouling rates of CaCO3 on smooth, negative and positive helical surfaces
Stirrer speed: 200 rpm; Bulk temperature: 55°C
▲: positive helix surface; ■: Negative helix surface; ♦: smooth surface

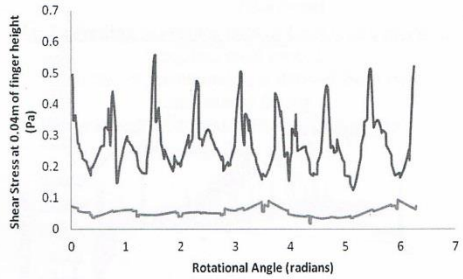

Fig. 11 Comparison of shear stress over the wired probe surface – around a circle (0 - 2 π)
Stirrer speed: 200 rpm; bulk temperature: 55°C

It can be seen from Figure 13 that when wires are present the distribution of fouling is non-uniform. Indeed, the greatest amount of fouling appears downstream of the wires where the surface shear stress is the lowest (Figure 11) and the least amount appears just upstream of the wires where the surface shear stress is the highest. Given the clockwise flow direction, the shear stress is higher in front of a wire than behind it. This may suggest that fouling is more likely behind the wire, and this is confirmed by Figure 13.

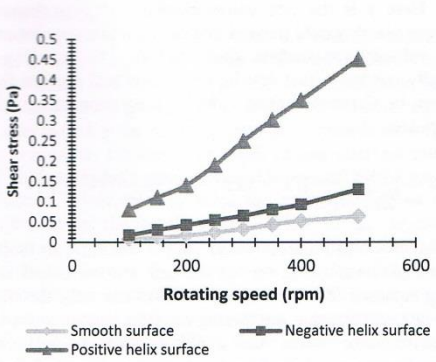

Fig. 12 Average shear stress on smooth surface, negative and positive helical surfaces

Fig. 13 Photograph of the wired probe after $CaSO_4$ fouling test; fluid flows clockwise when viewed from the top

CONCLUSION

The stirred batch cell fouling has been used to make preliminary investigations of the effects of surface shear stress, surface temperature, and starting bulk concentration on calcium sulphate and calcium carbonate fouling. The paper demonstrates the flexibility and adaptability of the cell over its continuous flow counterpart, thereby offering a facility in which ways to mitigate fouling problems can be studied quickly. The potential weakness of the stirred batch cell is that it cannot be operated at steady state conditions. Hence, a model has been developed to take into account the dynamic change in bulk concentration as scaling occurs. The experimental results show that calcium salt scaling can be mitigated to some extent by changing the turbulence structure by means of attaching wires or incorporating helical threads into the heat transfer surface. This augurs well for mitigation of scaling by adding inserts into tubular flow systems or by surface corrugation. The scaling behaviour can only be interpreted properly with the help of CFD simulation since it is essential that an understanding of the effect of shear stress is available. Given that the work reported in this paper focuses only on developing a

methodology for interpreting fouling data in a stirred batch cell as well as on the effects of enhanced surfaces, the effect of the chemistry of calcium salt solutions has not been addressed here, but could be the subject for further research.

AKNOWLEDGEMENT

The authors are grateful the European Commission for the award of research grant FP7-SME-2010-1-262205-INTHEAT to study intensified heat transfer technologies for enhanced heat recovery. The authors are also grateful to their project partners at the University of Manchester, and to Cal Gavin Ltd for their support, advice and provision of the probe with wires attached.

NOMENCLATURE

C $CaSO_4$ concentration, g/L or kg m^{-3}
C_b $CaSO_4$ bulk concentration, kg m^{-3}
C_{b0} $CaSO_4$ initial bulk concentration, kg m^{-3}
C_s $CaSO_4$ saturation concentration, kg m^{-3}
ΔC $C_b - C_s$, kg m^{-3}
ΔC_0 $C_{b0} - C_s$, kg m^{-3}
k_a surface reaction/attachment rate constant, $m^4 kg^{-1} s^{-1}$
k_m mass transfer coefficient, m s^{-1}
n reaction order
R_f fouling resistance, $m^2 k W^{-1}$
t time, s and hour

Greek symbols

α model constant, kg $m^{-5} K^{-1} W$
ρ_f fouling deposit density, kg m^{-3}
λ_f fouling deposit thermal conductivity, W $m^{-2} K^{-1}$
γ deposit removal rate coefficient, s^{-1}
Φ deposition flux, kg $m^{-2} s^{-1}$

REFERENCES

Albert, F., Augustin, W. and Scholl, S., 2009, Enhancement of heat transfer in crystallization fouling due to surface roughness, *Proc. Eurotherm Conference on Fouling and Cleaning in Heat Exchangers*, Schladming, Austria, June 14-19, pp. 303-310.

Calmanovici, C. E., Gabas, N. and Laguerle, C., 1993, Solubility measurement for calcium sulfate dehydrate in acid solution at 20, 50, and 70°C, *J. Chem. Eng. Data*, Vol. 38, pp. 534-536.

Crittenden, B.D., Kolaczkowski, S. T. and Hout, S. A., Modelling hydrocarbon fouling, 1987, *TransIChemE*, Vol. 65, pp. 171-179.

Esawy, M., Malayeri, M. R. and Müller-Steinhagen, H., 2009, Crystallization fouling of finned tubes during pool boiling: effect of fin density, *Proc. Eurotherm Conference on Fouling and Cleaning in Heat Exchangers*, Schladming, Austria, June 14-19, pp. 311-318.

Fahiminia, F., Watkinson, A. P. and Epstein, N., 2007, Calcium sulfate scaling delay times under sensible heating conditions, *Proc. 6th International Conference on Fouling and Cleaning in Heat Exchangers*. Tomar, Portugal, July 1-6, ECI Symposium Series, Vol. RP2, pp. 176-184.

Konak, A. R., 1974, A new model for surface reaction controlled growth of crystals from solution, *Chem. Eng. Sci.,* Vol 29, pp. 1537-1543.

Krause, S., 1993, Fouling of heat transfer surface by crystallization and sedimentation, *International Chemical Engineering,* Vol. 33, pp. 355-401.

Malayeri, M. R. and Müller-Steinhagen, H., 2007, Initiation of $CaSO_4$ scale formation on heat transfer surface under pool boiling conditions, *Heat Transfer Engineering*, Vol. 28(3), pp. 240- 247.

Yang, M., Young, A. and Crittenden, B. D., 2009, Use of CFD to correlate crude oil fouling against surface temperature and surface shear stress in a stirred fouling apparatus, *Proc. Eurotherm Conference on Fouling and Cleaning in Heat Exchangers*, Schladming, Austria, June 14-19, pp. 272 – 280.

Yang, M., Wood, Z., Rickard, B., Crittenden, B., Martin , G., Droegemueller, P. and Higley, T., 2013, Mitigation of crude oil fouling by turbulence enhancement in a batch stirred cell, *Applied Thermal Engineering*, Vol. 54, pp. 516-520.

Young, A., Venditti, S., Berrueco, C., Yang, M., Waters, A., Davies, H., Hill, S., Millan, M., and Crittenden, B. D., 2011, Characterisation of crude oils and their fouling deposits using a batch stirred cell system, *Heat Transfer Engineering*, Vol. 32 (3-4), pp. 216-227.

Appendix 2: CFD Simulation Data of the Nu-Re Index

200°C T_b

μ = 0.00036Pa/s

k = 0.1w/m°K

c = 2717j/kg°K

ρ = 629.01kg/m^3

Power = 500W

k = 0.012W/m^{2o}K

D = 0.07m

	100 RPM	200 RPM	300 RPM	400 RPM
T_w (°K)	569	555	546	537
T_b (°K)	473	473	473	473
Heat Flux (W/m²)	65899	70965	76186	82977
h (W/m^2K)	686.45	865.42	1043.66	1296.52
Nu	480.51	605.8	730.56	907.56
Ln(Nu)	6.163	6.406	6.594	6.811
Re	4985.78	7128.11	13165.58	21306.43
Ln(Re)	8.514	8.872	9.485	9.967
Liquid Linear v (m/s) at Cap Edge by CFD	0.128	0.183	0.338	0.547
Equivalent RPS	0.582	0.833	1.538	2.489

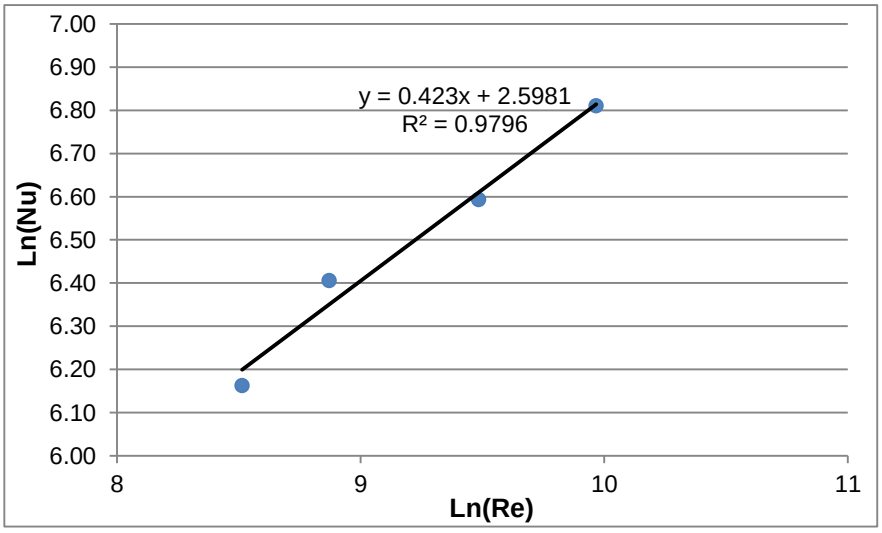

100°C T_b

μ = 0.000933Pa/s

k = 0.12w/m°K

c = 2291j/kg°K

ρ = 757.69kg/m^3

Power = 500W

k = 0.012W/m^2°K

D = 0.07m

	100 RPM	200 RPM	300 RPM	400 RPM
T_w (°K)	479	468	460	452
T_b (°K)	373	373	373	373
Heat Flux (W/m^2)	60863	68274	76958	82533
h (W/m^2K)	574.18	718.67	884.57	1044.72
Nu	334.93	419.23	516	609.42
Ln(Nu)	5.813	6.038	6.246	6.413
Re	5102.64	7439.72	13594.05	21734.9
Ln(Re)	8.538	8.915	9.517	9.987
Liquid Linear v (m/s) at Cap Edge by CFD	0.131	0.191	0.349	0.588
Equivalent RPS	0.596	0.869	1.588	2.539

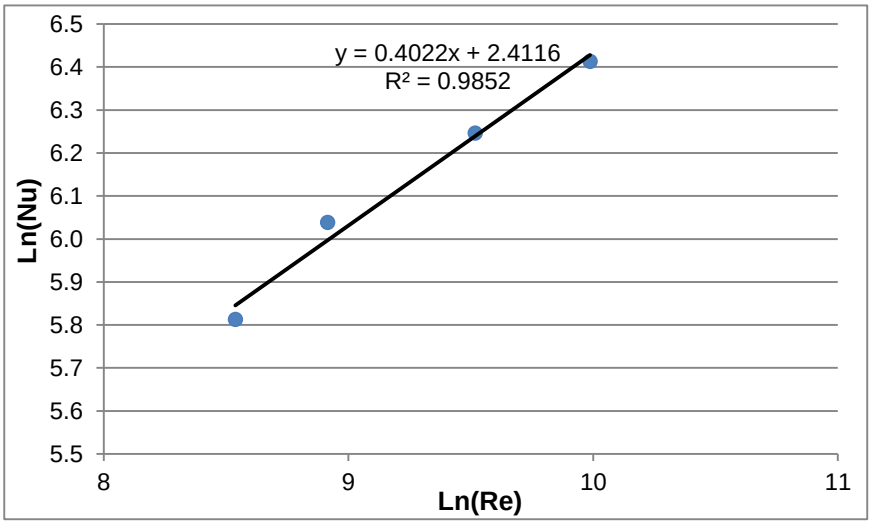

37°C T_b

μ = 0.0003653Pa/s

k = 0.12w/m°K

c = 2014.97j/kg°K

ρ = 818.12kg/m^3

Power = 500W

k = 0.012W/m^2°K

D = 0.07m

	100 RPM	200 RPM	300 RPM	400 RPM
T_w (°K)	433	423	408	396
T_b (°K)	313.5	313.5	313.5	313.5
Heat Flux (W/m^2)	60100	66200	74300	82120
h (W/m^2K)	502.93	604.56	786.24	995.39
Nu	293.38	352.66	458.64	580.66
Ln(Nu)	5.68	5.86	6.13	6.36
Re	5102.64	7439.72	13594.05	21734.9
Ln(Re)	6.834	7.49	7.908	8.358
Liquid Linear v (m/s) at Cap Edge by CFD	0.135	0.26	0.395	0.62
Equivalent RPS	0.614	1.183	1.797	2.821